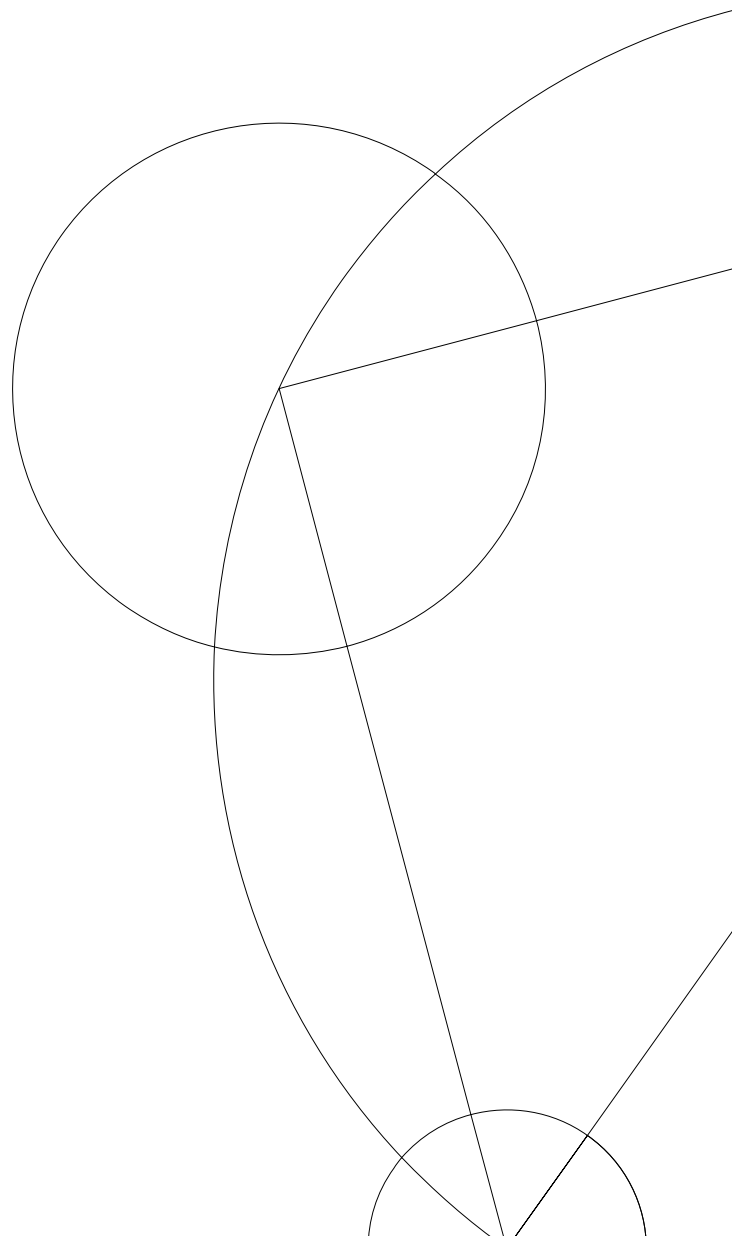**PhD Thesis**

Kim Georg Lind Pedersen

Theoretical Investigations Regarding Single Molecules

Neoclassical Valence Bond Theory,
Quantum Transport,
Quantum Interference,
Kondo Effect, and
Electron Pumping.

Prof. Per Hedegård

Tuesday 5th November, 2013

Contents

Acknowledgements

Publications

During my PhD the following manuscripts have been published.

[1] Kim G. L. Pedersen et al. "Inducing spin-dependent tunneling to probe magnetic correlations in optical lattices" in: *Physical Review A* 85 (Mar. 2012), p. 043642 DOI: 10.1103/PhysRevA.85.053642.

[2] Kim G. L. Pedersen et al. "Measuring spin correlations in optical lattices using superlattice potentials" in: *Physical Review A - Rapid* 84.4 (2011), p. 41603 DOI: 10.1103/PhysRevA.84.041603.

Chapter 1

Introduction

This thesis is concerned with a corner of nanotechnology which is the result of a very age-inappropriate marriage between two scientific disciplines: The old and renowned field of *organic chemistry*, and the young bride of *quantum transport*. In order to understand the spirit of this thesis, it is imperative that we begin with a short introduction to the interdisciplinary field of *molecular electronics*.

The realization of molecular electronics have been made possible by a series of technological innovations which allows for precise engineering on the nanoscale. Several experimental techniques like the mechanical break junction,[65,66] electromigration,[40,120] and the scanning electron microscope,[47] have made it possible to create single molecule junctions, where *one* chemically synthesized molecule is trapped between to metallic electrodes. Additionally, innovations in cooling techniques and electronic engineering have made it possible to create a small bias voltage across the molecular junction and measure the current response even at temperature close to absolute zero.[20]

Molecular electronics presents the possibility for merging semiconductor electronics with precisely engineered molecules synthesized by the multitude of methods available to contemporary chemistry. The meticulous control over the quantum behavior of molecular junctions, can then improve technologies such as solar cells,[118] thermoelectrics[49] and possibly numerical computing.[108]

Generally speaking molecular electronics is part of broader field of quantum transport. This field also encompasses transport through doped semiconductor structures. By clever engineering it is possible to construct nanometer-sized confinements called *quantum dots*, which effectively behave like artificial atoms.[2,38] While these artificial atoms could be used to construct artificial molecules, at the moment only double or triple quantum dots have been produced. Molecules on the other hand, are usually much larger. However, experimentally it has so far proved difficult to control or determine the binding geometry in molecular junctions. This could possibly be improved, e.g. by constructing the electrodes from graphene.[85]

Historically speaking, theoretical chemistry have improved on their molecular models since the early 1920'es. Today there exists a range of sophisticated software methods, which are constructed as reasonable compromises between computational complexity and calculational accuracy. Here we will rely on a somewhat simplified approach pioneered by Pariser,[76] Parr and Pople[83] modeling the π-system of planar organic molecules. This Pariser-Parr-Pople model is in fact an extended Hubbard model, and the results, we obtain, can easily be transferred to other transport systems (like the multiple quantum dots), which can be described by such models.

It quickly becomes complicated to keep track of the many electrons and their possible configurations, this problem usually lends itself to a numerical approach. However, we dedicate a whole chapter (and a bit more) to a mostly analytical approach to the many-body problem, known as *neoclassical valence bond theory*. This treatment covers: the basic ideas of the theory, shows how many-body calculations can be performed easily, and introduces a controlled way of approximating the many-body properties of the underlying Hubbard model. However, there is much more to neoclassical valence bond theory, than there is room for a in a single chapter, and we are currently preparing a manuscript with the full story.

In addition to the neoclassical valence bond theory, this work contains three projects related to molecular electronic quantum transport. Here we will present a quick technical overview of the topics, and reserve the general introduction to the corresponding chapters.

Chapter 4 considers the investigation of quantum interference in the off-resonant transport through single-molecule junctions. The chapter on quantum interference contain several interesting results, and most importantly the interference features of a molecular junction can be classified according to a "topological" classification scheme. For neutral hydrocarbon molecule this classification can be evaluated using simple coloring rules even a child could apply (cf. Figure 1.1). The findings are also part of manuscript being prepared for publication in collaboration with M. Leijnse, M. Strange, G. Solomon and J. Paaske.

Interference due to molecular structure have been found in the off-resonant transport. However, very few have considered the interplay between destructive interference and the enhanced zero-bias conductance mediated by the Kondo effect. In **chapter 5**, we show how interference may suppress the Kondo enhanced conductance, and also show how molecular structure can create an anti-ferromagnetic Kondo effect in only part of the transport spectrum, hence creating "holes" in the Kondo enhanced conductance. In this project we acknowledge the help of J. Paaske.

Chapter 6 considers electron pumping in quantum transport junctions. In principle the chapter tries to answer a simple question: What is the difference between a classical pump and quantum pump? We develop a straightforward transfer-matrix method for calculating the quantum pumped current, when ignoring electron-electron interactions all-together. The semi-classical pumping model is solved analytically allowing for a direct comparison of
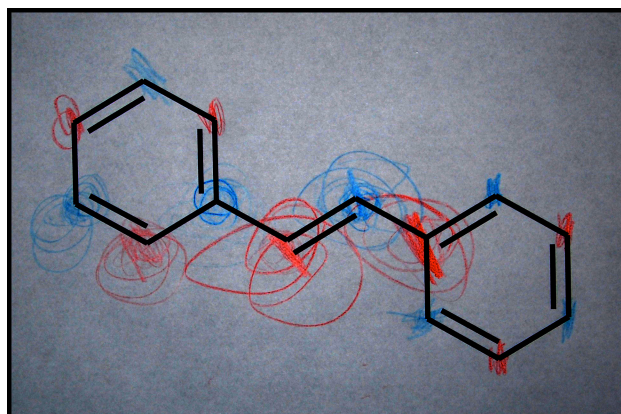
Figure 1.1: **Childs play**: Quantum interference classification of the neutral stilbene molecule performed by a child.

the two models. To find the answer you must consult the chapter. Part of this work is inspired by discussions with J. Thijssen and J. Seldenthuis regarding their proposal for a an all electric molecular motor.[96]

Enjoy.

Chapter 2

On the Constitution of Atoms and Molecules

> In order to explain the results of experiments on scattering of α rays by matter Prof. Rutherford has given a theory of the structure of atoms. According to this theory the atoms consists of a positively charged nucleus surrounded by a system of electrons kept together by attractive forces from the nucleus; the total negative charge of the electrons is equal to the positive charge of the nucleus.
>
> N. Bohr[11]

So begins the famous paper on the quantum theory of atoms published by Niels Bohr exactly a century ago this year. Bohr asserted that the atom was constituted of electrons and a nucleus, with the electrons moving in *quantized* classical orbits around the stationary nucleus. For hydrogen, consisting of a single electron orbiting the nucleus, the electron orbits are now known as *shells* each numbered by their principal quantum number $n = 1, 2, \ldots$.

This was the first hint, about how to understand the wonderful world of atoms and molecules. However, while Bohr took the first quantum leap towards understanding the atom, we now know that the Bohr model is wrong. It was a good guess which correctly explained the optical excitation spectra of hydrogen, but struggled to predict the spectra of larger atoms. While Bohr also tried to explain diatomic molecules with his model, he failed.

However the model did encourage the new *quantum physics* and thirteen years later in 1926 Schrödinger[93] was the first to discover that the electronic states of hydrogen were in fact solutions to the complex wave-equation,

$$\hat{H}(\mathbf{r})\psi(\mathbf{r}) = \left(\hat{T} + \hat{H}_V(\mathbf{r})\right)\psi(\mathbf{r}) = \left(-\frac{\hbar^2}{2m_e}\nabla^2 - V_e(\mathbf{r})\right)\psi(\mathbf{r}) = E\psi(\mathbf{r}). \tag{2.1}$$

Here $\hat{H}(\mathbf{r})$ is the Hamiltonian describing the system, $\hbar = 1.05 \cdot 10^{-34}$ Js is Plancks famous constant, $e = 1.602 \cdot 10^{-19}$ C is the elementary charge and $m_e = 9.109 \cdot 10^{-31}$ kg is the electron mass. For the electron in hydrogen the potential V_{e-i} is the electromagnetic attractive Coulomb potential between the nucleus and the electron,

$$V_{n-e}(\mathbf{r}_e) = \frac{1}{4\pi\varepsilon_0}\frac{e^2}{|\mathbf{r}_e|}. \tag{2.2}$$

Schrödinger's stationary wave equation is an eigenvalue problem, which can be solved by a set of *eigenenergies* E_{nlm} and corresponding *eigenfunctions* $\psi_{nlm}(\mathbf{r})$. The eigenfunctions are labeled by the three integer quantum numbers: the principal quantum number n, and the orbital quantum numbers l and m. For the hydrogen atom the such eigenfunctions $\psi_{nlm}(\mathbf{r})$ with the lowest eigenenergies are shown in Table 2.1,

| E_n | $l = 0$ | $l = 1$ | | |
| | | $m = 0$ | $m = \pm 1$ | |

		$1s$			
n=1	-13.6 eV				
		$2s$	$2p_z$	$2p_x$	$2p_y$
n=2	-3.4 eV				
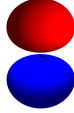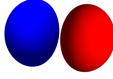
Table 2.1: The hydrogen orbitals $\psi_{nlm}(\mathbf{r})$ shown as constant absolute value surfaces. Blue and red colors distinguish between positive and negative values of the orbitals. The wavefunction is indexed by the principal quantum number n and the orbital quantum numbers l and m.

2.0.1 Many-Body Physics

However, for larger atoms with more than one electron, Pauli[77] showed that one must take into account an additional quantum parameter called *spin*. The total spin is $S = \frac{\hbar}{2}$ meaning that the electron can have a *spin projection* of either spin up $\uparrow$ or spin down $\downarrow$.

By introducing this spin degree of freedom, Pauli showed that the electrons instead of piling up in the lowest energy state obey an exclusion principle meaning that no two particles can exist in the same quantum state. This realization is a consequence of the *anti-symmetry* of the electrons, where the exchange of two electrons (located at $\mathbf{r}_1$ and $\mathbf{r}_2$) adds an overall minus to their many-body wavefunction, $\Psi(\mathbf{r}_1, \mathbf{r}_2) = -\Psi(\mathbf{r}_2, \mathbf{r}_1)$.

Starting from single-particle orbitals, χ_i, many-body states can be built by filling up the orbitals with electrons. The proper anti-symmetrised many-body wavefunction is given by the Slater determinant,[101]

$$\Psi(\mathbf{x}_1, \mathbf{x}_2, \ldots, \mathbf{x}_N) = \frac{1}{\sqrt{N!}} \begin{vmatrix} \chi_1(\mathbf{x}_1) & \chi_2(\mathbf{x}_1) & \cdots & \chi_N(\mathbf{x}_1) \\ \chi_1(\mathbf{x}_2) & \chi_2(\mathbf{x}_2) & \cdots & \chi_N(\mathbf{x}_2) \\ \vdots & \vdots & \ddots & \vdots \\ \chi_1(\mathbf{x}_N) & \chi_2(\mathbf{x}_N) & \cdots & \chi_N(\mathbf{x}_N) \end{vmatrix} \equiv \begin{vmatrix} \chi_1 & \chi_2 & \cdots & \chi_N \end{vmatrix}, \quad (2.3)$$

In second quantization one introduce field operators which create $\hat{c}_\nu^\dagger$ and annihilates $\hat{c}_\nu$ an electron in the quantum state ν.[14] The anti-symmetrization is incorporated through anti-commutation relations valid for orthonormal basis states ν_i,

$$\{\hat{c}_{\nu_i}^\dagger, \hat{c}_{\nu_j}\} = \hat{c}_{\nu_i}^\dagger \hat{c}_{\nu_j} + \hat{c}_{\nu_j} \hat{c}_{\nu_i}^\dagger = \delta_{i,j}. \quad (2.4)$$

However, while the antisymmetry of the many-body electron wavefunction can be taken into account, one must also include the Coulomb repulsion between the negatively charged

electrons in the equation. The eigenvalue problem has now turned into a complicated *many-body problem*, and in that case one must often resort to solving Schrödinger's equation numerically.

However, the most closely bound electrons can *screen* the nuclear charge, and the more loosely bound electrons will then still inhabit hydrogen-like orbitals for an atom with a slightly reduced nuclear charge. This screening combined with spherical symmetry assures that the angular part of the the single particle hydrogen-like orbitals still comprise a fairly good single-particle basis *even* for the many-electron atoms.[63]

2.1 The Nature of the Chemical Bond

Lewis[58] was the first to offer a descent explanation of the chemical bond, an explanation which was quickly formalized by Heitler and London[42].

Here we will seek to give a brief example elucidating the nature of the chemical bond using the simplest of molecules: hydrogen H_2 composed of two hydrogen atoms bound together by a single chemical bond.

As a starting point consider two hydrogen atoms each with one electron in their *1s*-shell. The atoms are located at $\mathbf{r}_1$ and $\mathbf{r}_2$ and their wavefunctions overlap with the Hamiltonian $\hat{H}$ like,

$$t = \int d\mathbf{r}\, \psi_{100}^*(\mathbf{r} - \mathbf{r}_1) \hat{H} \psi_{100}(\mathbf{r} - \mathbf{r}_2). \tag{2.5}$$

Ignoring the movement of the nuclei the relevant Hamiltonian consists of just two terms,

$$\hat{H} = \hat{H}_t + \hat{H}_U. \tag{2.6}$$

In second quantization the creation operator $\hat{c}_{i\sigma}^\dagger$ creates an electron in the orbital $i \in (1,2)$ with spin $\sigma \in (\uparrow, \downarrow)$, and the conjugate $\hat{c}_{i\sigma}$ annihilates that same electronic state.

The hopping can in second quantization be written like,

$$\hat{H}_t = \sum_{i \neq j} \sum_\sigma t_{ij} \hat{c}_{i\sigma}^\dagger \hat{c}_{j\sigma}, \tag{2.7a}$$

while the effective Coulomb potential 'penalty' for having two electrons in the same 1s orbitals (as opposed to different orbitals), is captured by the term,

$$\hat{H}_U = U \sum_i \hat{n}_{i\uparrow} \hat{n}_{i\downarrow}. \tag{2.7b}$$

The constant U expresses the severity of the Coulomb penalty, and should be compared in size to the hopping energy t in order to find out which of the two dominates the contribution to the total energy.

When the spin projection of the two electrons are parallel $|\uparrow\uparrow\rangle$ any hopping is blockaded by the Pauli exclusion principle, and Schrödinger's equation is trivially $\hat{H}|\uparrow\uparrow\rangle = 0$.

However for two electrons with opposite spin projections the problem becomes harder. Diagonalizing the Hamiltonian gives the (unnormalized) ground state

$$|\Psi\rangle \propto \left(\frac{U}{4t} + \frac{\sqrt{16t^2 + U^2}}{4t} \right) (\hat{c}_{2\uparrow}^\dagger \hat{c}_{1\downarrow}^\dagger - \hat{c}_{2\downarrow}^\dagger \hat{c}_{1\uparrow}^\dagger)|vac\rangle + (\hat{c}_{1\uparrow}^\dagger \hat{c}_{1\downarrow}^\dagger + \hat{c}_{2\uparrow}^\dagger \hat{c}_{2\downarrow}^\dagger)|vac\rangle, \tag{2.8}$$

with the corresponding eigenenergy

$$E = U\left(\tfrac{1}{2} - \sqrt{\tfrac{4t^2}{U^2} + \tfrac{1}{4}}\right). \tag{2.9}$$

This is indeed the electronic ground state of the hydrogen atom, and because $E < 0$ it is always favorable for the hydrogen atom to bond together to form a molecule. Examining this bonding wavefunction in different limits of U of t can then tell us something interesting about the nature of chemical bonding.

In the limit of a vanishing Coulomb interaction $|U| \ll |t|$, the result is the product of two so called *bonding* molecular orbitals occupied by electrons of opposite spin,

$$|\Psi\rangle_{U=0} \propto (\hat{c}_{1\uparrow}^{\dagger} + \hat{c}_{2\uparrow}^{\dagger})(\hat{c}_{1\downarrow}^{\dagger} + \hat{c}_{2\downarrow}^{\dagger})|vac\rangle, \tag{2.10}$$

with an energy $E = -2|t|$. This ground state could also have been found by diagonalizing the hopping $\hat{H}_t$ and forming the Slater determinant of the *single particle* bonding orbital for each spin specie.

In this case the bonding arises solely from the *delocalization* of the electrons over the entire molecule and the corresponding lowering of the electronic kinetic energy.

In the opposite limit an infinitely large Coulomb energy dominates, $|U| \gg |t|$, and the ground state instead approximates

$$|\Psi\rangle_{t\approx0} \propto (\hat{c}_{1\uparrow}^{\dagger}\hat{c}_{2\downarrow}^{\dagger} - \hat{c}_{1\downarrow}^{\dagger}\hat{c}_{2\uparrow}^{\dagger})|vac\rangle. \tag{2.11}$$

In this case the ground state energy is close to (but smaller than) zero, i.e. $E = 0^-$. It is obvious that the large U has almost prohibited the electron from occupying the same orbital. The result is a *singlet* ground state, where the (virtual) exchange of electrons lowers the energy. This state represents the extreme version of a *covalent* bond.

Usually the nature of an actual bond is found in-between those two extremes, and the closeness to either the single-particle bonding orbital picture or the singlet picture is determined by the value of U/t. The overlap of the actual ground state with either extreme is shown in Figure 2.1.

2.2 Organic Molecules

Pauling[79] was the first to offer a decent explanation of bonding in a wide variety of molecules. However with many atoms bonding together, the full many-body problem quickly becomes intractable. Instead of following in the footsteps of Pauling, we shall leap-frog his explanation, and derive an approximate many-body model, which effectively describes a wide class of organic molecules.

In the most general description a molecular system consists of positively charged nuclei located at space coordinates $\{\mathbf{R}_a\}$ and negatively charged electrons located at space coordinates $\{\mathbf{r}_i\}$.

The Hamiltonian describing the total energy of the system consists of several parts. The kinetic energy of the nuclei, T^n, and electrons respectively, T^e. The Coulomb repulsion between the nuclei, V^{n-n}, and between the electrons, V^{e-e}, along with the attractive Coulomb interaction between the electrons and the nuclei, V^{e-n}.

The full Hamiltonian then takes the form,[9]

$$\hat{H} = T^n_{\{\mathbf{R}_a\}} + T^e_{\{\mathbf{r}_i\}} + V^{n-n}_{\{\mathbf{R}_a\}} + V^{e-n}_{\{\mathbf{r}_i\},\{\mathbf{R}_a\}} + V^{e-e}_{\{\mathbf{r}_i\}}. \tag{2.12}$$
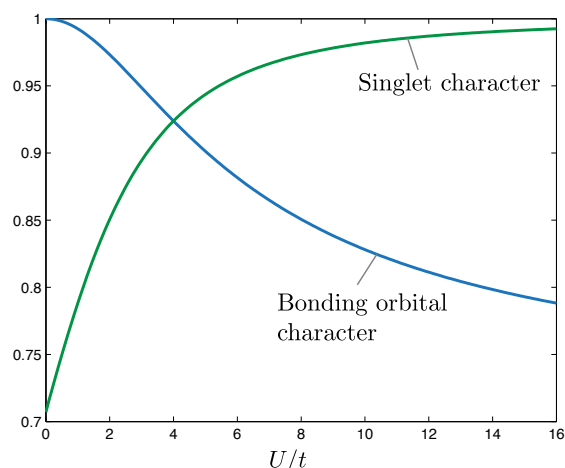
Figure 2.1: Overlap of the actual ground state with either the single particle bonding orbital ground state ($U = 0$), or the singlet ground state ($U \gg |t|$) here presented as a function of U/t.

As was the case for the H_2 example, the large Coulomb repulsion V^{n-n} and V^{e-e} penalizes the atoms for being bound closely together in a molecule, while the delocalization of the electrons over a larger space lowers the collective kinetic energy T^e. Additionally rearranging the electronic charge can also potentially lower the total electro-static energy of the system, $V^{e-n} + V^{e-e}$.

When the energy gain from electron delocalization overcomes the Coulomb penalty the atoms are bound together in a molecule. While the general Hamiltonian perfectly describes the molecule, it is simply too complicated to deal with the full $6(N_e + N_n)$ continuous degrees of freedom for any practical calculations. Hence we wish to reduce the complexity by performing a series of well founded approximations.

The first step is to notice the nuclei are vastly more massive than the electrons[a]. This means that for comparable kinetic energies of the nuclei and electrons $T_n \sim T_e$, the velocity of the nucleons are negligible when compared to the velocity of the electrons. This gives rise to the Born-Oppenheimer approximation where all nuclear coordinates are assumed to be constant $\mathbf{R}_a$.[12,14]

The hydrogen orbitals exhibit a strong hierarchy with well separated energy levels. For many-electron atoms, this means that orbital energies are well separated, and it is safe to assume that the electrons in the inner shells are closely bound to the nuclei, while electrons in the outer (valence) shell are free to delocalize. The effect of the core electrons are then to screen the electric charge of the nuclei from the valence electrons.

The hydrocarbons composed of only hydrogen and carbon constitutes a major part of all organic molecules. Including molecules containing the close carbon relatives like nitrogen, oxygen and sulfur makes it possible to cover almost all of organic chemistry.

Carbon has six electrons, with two core electrons occupying the inner shell ($n = 1$) and four valence electrons ($n = 2$). Pauling[79] was the first to notice that in order to understand the bonding in carbon compounds one would have to consider linear combinations of the occupied $2s$ and $2p$ orbitals and the unoccupied $2p$ orbitals. Those new linear combinations

---

[a]The proportion between the mass of a single nucleon and the electron mass is approximately $m_n/m_e \approx 1836$.

Figure 2.2: The periodic table of the elements. Highlighted: The carbon relatives boron, nitrogen, oxygen and sulfur.

are known as sp-*hybridized orbitals*. For sp^2-hybridized orbitals the 2s orbital is combined with two of the three p orbitals to form the three sp^2-hybridized orbitals which together resembles a Mercedes star as shown in Figure 2.3.

$$sp^2 = \frac{1}{\sqrt{6}} \begin{pmatrix} \sqrt{2} & 1 & \sqrt{3} \\ \sqrt{2} & 1 & -\sqrt{3} \\ -\sqrt{2} & 2 & 0 \end{pmatrix} \begin{pmatrix} |2s\rangle \\ |2p_x\rangle \\ |2p_y\rangle \end{pmatrix}. \tag{2.13}$$

For planar molecules the overlap between e.g. carbon sp^2 hybridized orbitals or hydrogen 1s orbitals can become rather large and form a strong σ-bond.
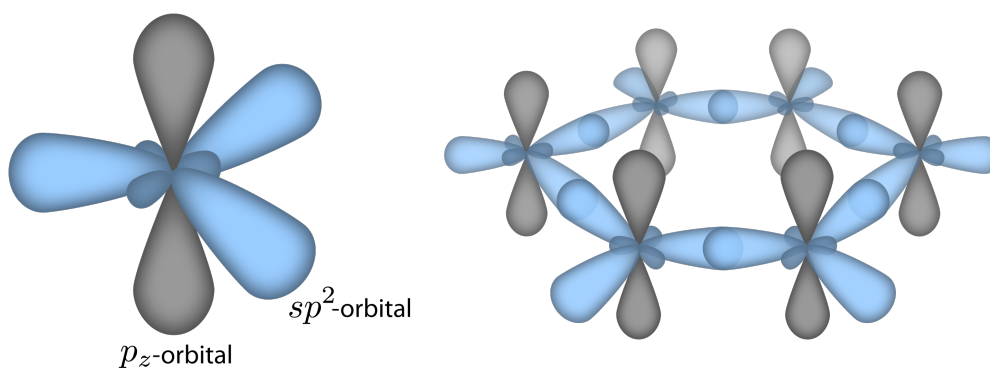
Figure 2.3: Simple illustration of sp^2 hybridized orbitals and a six-ring molecule of atoms with hybridized orbitals. When all remaining sp^2-orbitals is bonded with hydrogen, the ring models the benzene molecule having carbon at every site. With alternating boron and nitrogen atoms, the ring models the borazine molecule.

Because the overlaps between the sp^2 hybridized orbitals are much larger than between the p_z-orbitals the electronic states occupying σ-orbitals are much lower in energy. Because of this separation of energy scales, one can construct an effective low-energy theory for the isolated system of p_z-orbitals commonly known as the π-system.

2.2.1 The Pariser-Parr-Pople Model

Restricting our model to the π-system formed of overlapping p_z orbitals in planar organic molecules, and by considering the positions of the ions and the location of the π-system electrons as the only free parameters, heavily reduces the complexity of Schrödinger's equation. The equation becomes

$$\left(T^{\pi} + V^{\pi-\pi} + V^{\pi-\text{ion}} + V^{\text{ion}-\text{ion}}\right)\varphi(\{\mathbf{R}_a\}, \{\mathbf{r}_i\}) = E\varphi(\{\mathbf{R}_a\}, \{\mathbf{r}_i\}). \tag{2.14}$$

Here $V^{\pi-\pi}$, $V^{\pi-\text{ion}}$ and $V^{\text{ion}-\text{ion}}$ together represent the effective Coulomb potential between the ions and the π-system electrons.

This effective model for the π-system electrons was originally proposed in 1953 by Pariser,[76] Parr and Pople.[83] When expressed in second quantized form the Pariser-Parr-Pople Hamiltonian takes the guise of an extended Hubbard model:

$$\hat{H}_{\text{PPP}} = \hat{T} + \hat{H}_{\mu} + \hat{H}_U + \hat{H}_V. \tag{2.15}$$

The kinetic term $\hat{T}$ captures hopping between different p_z orbitals and is expressed in terms of the orbital overlaps t_{ij}.

$$\hat{T} = \sum_{\langle i,j \rangle} \sum_{\sigma=\uparrow,\downarrow} \left(t_{ij}\hat{c}_{i,\sigma}^{\dagger}\hat{c}_{j,\sigma} + t_{ji}\hat{c}_{j,\sigma}^{\dagger}\hat{c}_{i,\sigma}\right). \tag{2.16}$$

Here $\langle i,j \rangle$ is short for all nearest neighbor orbital pairs i and j. The on-site chemical potential term $\hat{H}_{\mu}$ captures the local electrostatic potential from the ions. For brevity the chemical potential for carbon is normally chosen such that $\mu_C = 0$, while hetero-atomic p_z orbitals have a small offset $\mu_i \neq 0$.

$$\hat{H}_{\mu} = \sum_i \mu_i \hat{n}_i. \tag{2.17}$$

Here we have introduced the counting operator $\hat{n}_i = \hat{n}_{i\uparrow} + \hat{n}_{i\downarrow}$, where $\hat{n}_{i\sigma} = \hat{c}_{i\sigma}^{\dagger}\hat{c}_{i\sigma}$ counts the number of electrons on site i with spin σ. The interaction $\hat{H}_U + \hat{H}_V$ captures both the Coulomb repulsion between the π-electrons as well as part of the Coulomb attraction from the screened ionic charge,

$$\hat{H}_U + \hat{H}_V = \sum_i U_i(\hat{n}_{i\uparrow} - \tfrac{1}{2})(\hat{n}_{i\downarrow} - \tfrac{1}{2}) + \frac{1}{2}\sum_{i \neq j} V_{ij}(\hat{n}_i - z_i)(\hat{n}_j - z_j). \tag{2.18}$$

Here we have introduced the unshielded residual charge z_i on site i, where e.g. a carbon atom usually donates a single electron to the π-system leaving a single unshielded charge, $z_C = 1$.

The contribution to the on-site Coulomb repulsion $\hat{H}_U$ at a specific site i, takes a minimum value of $-U_i/4$ when occupied by a single electron, and a maximum $U_i/4$ when occupied by either zero or two electrons, hence favoring the single occupied case. The intra-orbital Coulomb interaction $\hat{H}_V$ has been written on a form, which ensures that any

contribution from an orbital i to the long distance Coulomb interaction vanishes, when the residual ionic charge is completely shielded.

The interaction can also be written on the simpler form,

$$\hat{H}_U + \hat{H}_V = \sum_i U_i \hat{n}_{i\uparrow} \hat{n}_{i\downarrow} + \frac{1}{2} \sum_{i \neq j} V_{ij} \hat{n}_i \hat{n}_j - \sum_i \tilde{\mu}_i \hat{n}_i, \tag{2.19}$$

where we have removed a the constant term $\sum_i (U_i/2 + \sum_{j(\neq i)} z_i z_j V_{ij})/2$, and introduced the local potential offset $\tilde{\mu}_i = \frac{1}{2} U_i + \sum_{j(\neq i)} V_{ij} z_j$.

While the PPP model parameters can (in principle) be calculated from complicated orbital overlap integrals, the parameter values are instead found by fitting the predictions of the PPP model directly to measurement data of e.g. optical excitation spectra or ionization energies.

In order to reduce the number of free parameters and perform a satisfactory fit, the intra-orbital Coulomb integrals V_{ij} are usually described using the semi-empirical *Ohno parametrization*[73] [b]

$$V_{ij} = \frac{U_{ij}}{\sqrt{1 + |\alpha \mathbf{r}_{ij}|^2}} \tag{2.20}$$

Here the average Coulomb potential strength $U_{ij} = (U_i + U_j)/2$, and $\mathbf{r}_{ij}$ is the inter-orbital distance between p_z orbitals labeled i and j. To give you an idea of the length scales involved, the carbon-carbon bond length is roughly $r_{C-C} \approx 1.3$ Å. The constant $\alpha = 4\pi\epsilon_0 U/e^2$, is chosen such that the V_{ij} approaches the on-site Coulomb interaction U at small distances, while it approaches the vacuum Coulomb interaction $V_{ij} \approx e^2/(4\pi\epsilon_0 |\mathbf{r}_{ij}|^2)$ at large distances.[c]

2.2.2 Spin

This is a good place to introduce the total spin operator, $\mathbf{S} = \sum_i \mathbf{S}_i$, here written in terms of the local spin operator,

$$\mathbf{S}_i = \frac{\hbar}{2} \sum_{\sigma\gamma} \hat{c}_{i\sigma}^\dagger \boldsymbol{\tau}_{\sigma\gamma} \hat{c}_{i\gamma}. \tag{2.21}$$

Here we introduced the three-dimensional Pauli tensor $\boldsymbol{\tau} = (\tau_i^x, \tau_i^y, \tau_i^z)$ defined in terms of the Pauli matrices,

$$\tau^x = \begin{pmatrix} 0 & 1 \\ 1 & 0 \end{pmatrix}, \quad \tau^y = \begin{pmatrix} 0 & -i \\ i & 0 \end{pmatrix}, \quad \tau^z = \begin{pmatrix} 1 & 0 \\ 0 & -1 \end{pmatrix}. \tag{2.22a}$$

The total spin length $\mathbf{S}^2$ and the spin projection $\mathbf{S}^z$ both commute with the PPP (extended Hubbard) Hamiltonian. Hence their eigenvalues are good quantum numbers of the PPP eigenstates. Eigenstates with an even (odd) number of electrons have integer (half-integer) total spin S and spin projection $m \in -S, -S + 1, \ldots, S$ (setting $\hbar = 1$). The lowest total spin eigenvalues are the singlet ($S = 0$), doublet ($S = \frac{1}{2}$), triplet ($S = 1$) and quadruplet ($S = \frac{3}{2}$).

---

[b]or alternatively the Nataga-Nishmoto representation[67] given by $V_{ij} = U_{ij}/(1 + \alpha U_{ij}|\mathbf{r}_{ij}|)$.

[c]By directly inserting the numerical value of α, and taking $\tilde{r}_{ij}$ to be the p_z orbital distance measured in Angstrom, the Ohno parametrization gives $V_{ij} = 28.794\,\text{eV}/(\sqrt{\tilde{r}_{ij}^2 + (U_{ij}/28.794\,\text{eV})^2}$.

X	z_X	μ_X [eV]	U_X [eV]
C	1	0	10.06
Ȯ	1	-9.78 (-3)	18.89 (14)
Ṅ	1	-3.4 (-2.72)	14.97
N̈	2	-18.43	15
Ṡ	1	-10.36	9.85
S̈	2	-7.8	5.0

X	t_{C-X} [eV]	$t_{C=X}$ [eV]
C (benzene)	-2.539	
C	-2.22	-2.684
O	-1.5	-2.4
N	-2.05	-2.05
Ṡ	-3.0	-3.0
S̈	-1.37	

Table 2.2: Parameter values for common π system hetero-atoms taken from the literature. While the underlying model and calculational approach differs, the table still offers a sense of the involved parameters and their relative size. The parameter values have been found by e.g. fitting models to optical excitation spectra, giving carbon data from benzene and biphenyl,[15] oxygen from carbonyl[46] or benzo-quinones [d], nitrogen from pyridine[29] (from pyrrole[31]) and sulfur from thiophene.[27,99]

While we have chosen to quantize spin along the $\hat{z}$-direction, we can just as well choose any other direction. The spin quantization axis can be rotated an angle θ around any direction $\hat{n}$ by the operator $\mathcal{R}_\theta^{\hat{n}}$, which in a doublet spin space takes the form,

$$\mathcal{R}_\theta^{\hat{n}} = e^{i\theta\hat{n}\cdot\mathbf{S}/\hbar} = \cos(\theta)\hat{I} + i\sin(\theta)\hat{n}\cdot\boldsymbol{\tau}. \tag{2.23}$$

2.2.3 PPP Model Parameters

We will take special interest in the *hydrocarbons* where any free carbon sp^2-orbitals are bonded to hydrogen. Each carbon atom contributes a single electron to the π system, and the local chemical potential is equal for all sites, allowing us to choose the zero-point of energy such that $\mu_C = 0$. Hydrocarbons can dimerize into a compound with alternating σ-bond lengths because of the Peierls instability,[82] giving rise to three different values of the transfer integrals between neighbor orbitals. Counting also the on-site Coulomb interaction U this gives a total of four parameter values modeling all hydrocarbon molecules.

Many organic molecules are similar in structure to hydrocarbons but with few carbon atoms replaced with hetero-atoms like oxygen, nitrogen and sulfur. These elements are close relatives of carbon but have one (or more) additional electrons which must then be accommodated in *lone pairs* completely occupying a single sp^2-orbital. This means that the lone pair only partially shields their nuclear charge, resulting in an attractive potential incorporated as a lowering of the local chemical potential $\mu_X < \mu_C$. However this effect is often compensated for by a larger on-site Coulomb repulsion $U_X > U_C$, entailing that configurations with one electron per orbital are <u>still</u> energetically favorable.

In addition to forming lone pairs, nitrogen and sulfur can also donate an additional electron to the π-system. In this case the unshielded nuclear charge is larger $z_N = z_S = 2$, and the local chemical potential and the on-site Coulomb repulsion must also be changed accordingly.

Reasonable parameter values for carbon, oxygen, sulfur and nitrogen can be found in the chemistry literature, and some common results for different atoms are presented in Table 2.2.

---

[d]These values are partly based on DFT, and an exact diagonalization PPP simulation of the benzo-quinone experimental data published by Fu, Yang, and Wang[32].

For some molecules the distinction between double and single bonds can become somewhat problematic, and instead one employs the semi-empirical formula,[29] $t_{C-C} = t + 3.2(r_{C-C} - 1.397)$, for calculating the transfer integrals between two carbon atoms separated by a distance r_{C-C}. While we have devoted this section to the numerical values of the PPP parameters, we would argue against putting too much effort into obtaining exact numerical results.

One should remember that the PPP model, only considers the π-system and ignores any effects arising from the σ-system, and additionally the model relies heavily on more-or-less correct semi-empirical formulas for some parameter values. So already several approximations have been made, making it unlikely to have *exact* agreement with experimental data. So while the PPP model captures a wide range of interesting molecular physics, one should not pursue or be put off by slight disagreements with experimental measurements.

2.3   Numerical Solution of the PPP Hamiltonian

For an N_a orbital π-system containing N electrons there is a total of

$$C(2N_a, N) = \frac{(2N_a)!}{N!(2N_a - N)!} \tag{2.24}$$

many body basis Fock states. At half-filling $N = N_a$ and the number of many-body states grows at least exponentially with $n = C(2N, N) \geq N^{-1/2} 2^{2N-1}$.

Analytical solution is of course impossible when considering anything but the very simplest systems. The computation time of direct numerical diagonalization scales like matrix size cubed $O(n^3)$. However, the memory cost of storing the Hamiltonian or the eigenvectors as double precision numbers grows at least like n^2, hitting 1.3 GB for systems of size $N = 8$ and a staggering 58.5 TB at $N = 12$.

It is straightforward to show that the PPP Hamiltonian commutes with the total number of both spin species $\hat{N}_\sigma = \sum_i \hat{n}_{i\sigma}$. Hence the Hamiltonian is block-diagonal in the Fock space of many-body states with blocks characterized by the $(N_\uparrow, N_\downarrow)$ quantum numbers. Each Fock space block can be solved separately in order to find the total ground state of the system.

In the balanced half-filled case $N_a = N = 2N_\uparrow = 2N_\downarrow$, and the basis in the $(N/2, N/2)$ is of the size $C(N, N/2)^2 = N!^2/(N/2)!^4 \geq N^{-1} 2^{2N-1}$, hence reducing the basis size with at least a factor of $\sqrt{N}$.

When constructing the PPP Hamiltonian in the $(N_\uparrow, N_\downarrow)$ Fock subspace, Lin and Gubernatis[61] proposed a clever method, where the Fock states are written as the product of a spin up and a spin down component,

$$|s\rangle = |011\ldots010\rangle_\uparrow |011\ldots101\rangle_\downarrow \tag{2.25}$$

Focusing on one spin component, the state labels the occupied orbitals using binary representation. For each spin component all relevant states can be generated as an ordered lookup table I_σ of binary indices. In the case of four orbitals occupied by two particles the list is generated like,

s_σ	state	index $I_\sigma(s_\sigma)$
1	$\lvert 0011 \rangle$	3
2	$\lvert 0101 \rangle$	5
3	$\lvert 0110 \rangle$	6
4	$\lvert 1001 \rangle$	9
5	$\lvert 1010 \rangle$	10
6	$\lvert 1100 \rangle$	12

The full $(N_\downarrow, N_\uparrow)$ basis is then the direct product space of each spin component basis. Technically speaking each full basis vector $\lvert s \rangle$ can be assigned an unique index based on the Lin table indices of the two spin components,

$$I(s) = 2^N I_\downarrow(s_\downarrow) + I_\uparrow(s_\uparrow). \tag{2.26}$$

Usually it is difficult to perform the reverse lookup where an index is matched with the corresponding Fock state, but using the Lin table method this is actually a simple decimal to binary conversion.

The PPP Hamiltonian then have a matrix representation in each Fock subspace. The interaction terms are the simplest because they are both diagonal in the Fock basis, meaning that

$$\langle s_i \rvert (\hat{H}_U + \hat{H}_V) \lvert s_j \rangle = \begin{cases} \text{non-zero} & i = j \\ \text{zero} & i \neq j \end{cases} \tag{2.27}$$

The kinetic term $\hat{T}$ can be calculated for each spin component $\hat{T}_\sigma$. The kinetic term is iteratively applied to each state $\lvert s_\sigma \rangle$, and by performing the reverse lookup the resulting states are converted to indices I_σ in order to fill the corresponding matrix elements of $\hat{T}_\sigma$. The Lin index of equation (2.26) have the additional advantage that the the full hopping matrix is simply the Kronecker product matrix $\hat{T} = \hat{T}_\downarrow \otimes \hat{T}_\uparrow$.

The Hamiltonian matrix is naturally sparse, hence reducing the storage limits on the matrix. However for large systems (~ 16 orbitals) even storing the Hamiltonian in persistent memory becomes a problem. Instead the action of the Hamiltonian on relevant states $H\lvert \Psi \rangle$ can be calculated on the fly from the components of each spin subspace $\hat{T}_\downarrow$, $\hat{T}_\uparrow$.[98]

2.3.1 The Recursion Method

Because the PPP model is an effective low-energy model we are mostly interested in finding the low energy eigenstates. Instead of applying common diagonalization techniques which maps the whole eigenspectrum, the Lanczos method[55] iteratively generates a small subset of the eigenstates while also limiting the memory footprint of the algorithm.

The starting step of the Lanczos algorithm is some relevant state $\lvert \Psi_0 \rangle$. From this state one calculates the new orthogonal state,

$$b_1 \lvert \Psi_1 \rangle = \hat{H} \lvert \Psi_0 \rangle - a_0 \lvert \Psi_0 \rangle \tag{2.28}$$

Here the coefficients a_0 and b_1 are chosen in order to ensure orthogonality,

$$a_0 = \frac{\langle \Psi_0 \rvert \hat{H} \lvert \Psi_0 \rangle}{\langle \Psi_0 \vert \Psi_0 \rangle}, \qquad b_1 = \frac{\langle \Psi_1 \rvert \hat{H} \lvert \Psi_0 \rangle}{\langle \Psi_1 \vert \Psi_1 \rangle}. \tag{2.29}$$

A new state is then constructed such that it is orthogonal to both $\lvert \Psi_0 \rangle$ and $\lvert \Psi_1 \rangle$,

$$b_2 \lvert \Psi_2 \rangle = \hat{H} \lvert \Psi_1 \rangle - a_1 \lvert \Psi_1 \rangle - b_1 \lvert \Psi_0 \rangle \tag{2.30}$$

with coefficients given by,

$$a_1 = \frac{\langle \Psi_1 | H | \Psi_1 \rangle}{\langle \Psi_1 | \Psi_1 \rangle}, \qquad b_2 = \frac{\langle \Psi_1 | H | \Psi_2 \rangle}{\langle \Psi_2 | \Psi_2 \rangle}. \tag{2.31}$$

Generally a complete series of relevant orthogonal states can be iteratively generated by use of

$$b_{n+1} | \Psi_{n+1} \rangle = \hat{H} | \Psi_n \rangle - a_n | \Psi_n \rangle - b_n | \Psi_{n-1} \rangle \tag{2.32}$$

with

$$a_n = \frac{\langle \Psi_n | \hat{H} | \Psi_n \rangle}{\langle \Psi_n | \Psi_n \rangle}, \qquad b_{n+1} = \frac{\langle \Psi_n | \hat{H} | \Psi_{n+1} \rangle}{\langle \Psi_{n+1} | \Psi_{n+1} \rangle} \tag{2.33}$$

In fact, by applying this procedure we have transformed the Hamiltonian into a tridiagonal matrix T with the a_i coefficients on the main diagonal and the b_i coefficients along the two neighbor diagonals. The transformation is formally given by,

$$HQ = QT, \tag{2.34}$$

Here $Q \in U(dim(H))$ is a unitary operator consisting of the generated orthogonal basis $Q = (|\Psi_0\rangle, |\Psi_1\rangle, \ldots)$, and T is the mentioned tridiagonal matrix

$$T = \begin{pmatrix} a_0 & b_1 & & & \cdots \\ b_1 & a_1 & b_2 & & \\ & b_2 & a_2 & b_3 & \\ & & b_3 & & \\ \vdots & & & & \ddots \end{pmatrix} \tag{2.35}$$

The space spanned by the basis Q is known as a *Krylov subspace* of the full Hilbert space. The major advantage of the Lanczos algorithm, is that starting from some relevant state $|\Psi_0\rangle$ one immediately constructs the most relevant perturbations $|\Psi_1\rangle, |\Psi_2\rangle, \ldots$. Hence even when terminating the algorithm quite quickly all the features relevant to $|\Psi_0\rangle$ are still captured.

The Actual Algorithm

The actual algorithm only needs to store two state vectors at a time, and a pseudo code version based on Golub and Loan[36] is presented in algorithm 1.

The tridiagonalization can be terminated after very few iterations – normally less than 200. Simply diagonalizing the tridiagonal Hamiltonian gives a set of eigenstates expressed in the Krylov subspace basis. Because the basis is not saved during the algorithm, the Lanczos tridiagonalization must be repeated once more in order to construct the full Fock space eigenstates.

The Lanczos recursive algorithm is prone to loss of orthogonality of the Lanczos vectors [26]. The causes and consequences of this orthogonality loss has been extensively investigated by Paige[75]. In order to avoid the many problems related to the loss of orthogonality of the Krylov subspace basis, the Lanczos method can instead be terminated before the loss occurs. The resulting relevant eigenstate (e.g. the calculated ground state) is then simply used as the starting point for a new Lanczos procedure which is also quickly terminated. This process is then repeated until the eigenstate converges, and it is commonly known as the restarted Lanczos algorithm.

```
initialize ψ₁
b₁ ← 0
a₁ ← 0
for j ← 1 to N do
    rⱼ ← Hψⱼ − bⱼψⱼ₋₁
    aⱼ ← rⱼ†ψⱼ
    rⱼ ← rⱼ − aⱼψⱼ
    bⱼ₊₁ ← ‖rⱼ‖
    ψⱼ₊₁ ← rⱼ/bⱼ₊₁
end
```

Algorithm 1: Minimal pseudocode showing the Lanczos algorithm.

2.3.2 Resolvents

The Lanczos algorithm also lends itself beautifully to the calculation of resolvents of the type,

$$\mathcal{R}_{ba}(\omega) = \langle \Psi_a | \frac{1}{\omega - \hat{H} + i0^+} | \Psi_b \rangle \tag{2.36}$$

Where usually $|\Psi_{a/b}\rangle$ are not eigenfunctions of the Hamiltonian $\hat{H}$. The simplest case involves resolvents between two identical states $|\Psi_a\rangle = |\Psi_b\rangle$ (normally related to the spectral function).

Initializing the Lanczos tridiagonalization algorithm using the $|\Psi_0\rangle = |\Psi_a\rangle$, the same state resolvent can be found

$$\mathcal{R}_{aa}(\omega) = \langle \Psi_0 | \frac{1}{\omega - \hat{H} + i0^+} | \Psi_0 \rangle \tag{2.37}$$

$$= \langle \Psi_0 | Q \frac{1}{\omega - T + i0^+} Q^\dagger | \Psi_0 \rangle \tag{2.38}$$

$$= \left(\frac{1}{\omega - T + i0^+} \right)_{11} \langle \Psi_0 | \Psi_0 \rangle^2 \tag{2.39}$$

The last line follows from the fact that

$$Q^\dagger | \Psi_0 \rangle = \begin{pmatrix} 1 \\ 0 \\ \vdots \end{pmatrix} \langle \Psi_0 | \Psi_0 \rangle \tag{2.40}$$

This leaves us almost out of harms way. All we need to do, is to calculate the $(1,1)$ component of the inverse of a tridiagonal matrix. Calculating the inverse by use of Appendix A, we can directly write

$$\left(\frac{1}{\omega - \hat{H} + +i0^+} \right)_{11} = \cfrac{1}{\omega - a_0 - \cfrac{b_1^2}{\omega - a_1 - \cfrac{b_2^2}{\omega - a_2 - \cdots}}} \tag{2.41}$$

Here the continued fraction representation is naturally terminated by setting $b_N = 0$ for a sufficiently large N as discussed by Haydock and Te[39].

If dealing with off-state resolvents, one can form the odd and even combinations,

$$|\Psi_+\rangle = |\Psi_a\rangle + |\Psi_b\rangle, \qquad |\Psi_-\rangle = |\Psi_a\rangle - |\Psi_b\rangle. \tag{2.42}$$

Then the corresponding odd and even resolvents are given by,

$$\mathcal{R}_\pm(\omega) = \langle\Psi_\pm|\frac{1}{\omega - \hat{H} + i0^+}|\Psi_\pm\rangle = \mathcal{R}_{aa}(\omega) + \mathcal{R}_{bb}(\omega) \pm \mathcal{R}_{ab}(\omega) \pm \mathcal{R}_{ba}(\omega).$$

Hence the real part of the resolvent, can be calculated from,

$$\mathcal{R}_+(\omega) - \mathcal{R}_-(\omega) = 2\{\mathcal{R}_{ab}(\omega) + \mathcal{R}_{ba}(\omega)\}. \tag{2.43}$$

When the resolvents are real, $\mathcal{R}_{ab}(\omega) = \mathcal{R}_{ba}(\omega)$, and the relevant off-state $a \neq b$ resolvent is then simply expressed in terms of two same state resolvents, $\mathcal{R}_{ab}(\omega) = \frac{1}{4}(\mathcal{R}_+(\omega) - \mathcal{R}_-(\omega))$.

2.4   Approximations

2.4.1   The Hubbard Approximation

The Pariser-Parr-Pople model can be approximated by a simple Hubbard model with only an effective on-site interaction U^*, given by

$$\mathcal{H} = \hat{T} + \sum_i U_i^*(\hat{n}_{i\uparrow} - \tfrac{1}{2})(\hat{n}_{i\downarrow} - \tfrac{1}{2}) + \sum_i \mu_i \hat{n}_i + \Delta\hat{N}_a \tag{2.44}$$

Note the introduction of the energy offset $\Delta\hat{N}_a$, which is required in order to match the eigenenergies of the PPP model exactly.

To demonstrate the adequateness of this approximation, we calculate the ground state of simple half-filled Hubbard chains of varying lengths N_a varying the effective U^*. The ground states are then compared with the 'exact' groundstates calculated using the full PPP Hamiltonian of equation (2.15). The principle of replacing the PPP model with an effective U^* Hubbard model have also recently been investigated for benzene and graphene using a Peierls-Feynman-Bogoliubov variational theory,[94] where they found $U^*/t = 1.6 \pm 2$ for a benzene π-system. From the calculated results in Figure 2.4 one sees that the ground state of a $U^* \approx 1.9|t|$ Hubbard model is almost identical to the groundstate of the full PPP model. We will return to the Hubbard approximation already in the next chapter when confronting valence bond theory.

There is in general also quite good agreement between the low energy eigenspectrum of the two models. However the ordering in the eigenenergy spectrum can mix up unpredictably for chains $N_a > 4$. This is understandable, because excited state wacefunctions will have a higher degree of ionized sites, hence enhancing the role of the off-site $\mathcal{V}$ operator.

2.4.2   The Hückel/Tight-Binding Approximation

The complexity of the many-body Hubbard model prohibits the exact numerical solution of general systems with more than ~ 16 sites. Inspired by the partial success of the single-particle picture in Fig. 2.1 the tight-binding approximation deals with this problem by ignoring the Coulomb repulsion altogether . The tight-binding Hamiltonian only contains the hopping and the onsite chemical potential

$$\hat{H}_{tb} = \hat{T} + \hat{H}_\mu = \sum_{\langle i,j \rangle} \sum_{\sigma=\uparrow,\downarrow} \left(t_{ij}\hat{c}^\dagger_{i,\sigma}\hat{c}_{j,\sigma} + t_{ji}\hat{c}^\dagger_{j,\sigma}\hat{c}_{i,\sigma} \right) + \sum_i \mu_i \hat{n}_i \tag{2.45}$$
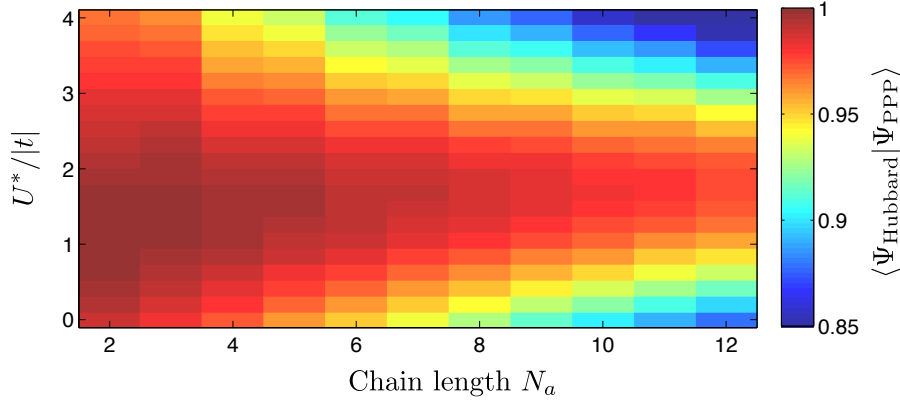
Figure 2.4: Wavefunction overlap between the ground state in a PPP model of a (non-dimerized) carbon chain of length N_a and the similar Hubbard model with a renormalized local Coulomb repulsion U^*. The optimal choice for the effective Hubbard model appears to be $U^*/|t| = 1.9$.

In the chemistry literature this is known as a simple *Hückel model*. The eigenfunction of the tight-binding Hamiltonian are simple *molecular orbitals*. Slater determinants of these molecular orbitals then constitutes many-body eigenstates.

Because the tight-binding model is a non-interacting model the full many-body wavefunctions are single Slater determinants of the relevant single-particle wavefunctions. The size of the single particle basis scales linearly with system size N_a and hence the numerical solution of single-particle problems is immensely more feasible than the full many-body treatment.

2.4.3   The Hartree Self-Consistent Field Approximation

The Hartree approximation deals with this problem by letting each electron move in the *average* Coulomb potential of the other electrons, hence effectively reducing the calculation to a one-body problem.

The Hartree Hamiltonian can easily be expressed in terms of the average electron densities $\langle \hat{n}_{i\sigma} \rangle$,

$$\hat{H}_{\text{Hartree}}(\langle \hat{n} \rangle) = \mathcal{T} + \hat{H}_U^{\text{Hartree}} + \hat{H}_V^{\text{Hartree}} \tag{2.46}$$

with

$$\hat{H}_U^{\text{Hartree}}(\langle \hat{n} \rangle) = \sum_{i\sigma} U_i \left(\langle \hat{n}_{i\sigma} \rangle - \tfrac{1}{2} \right) \hat{n}_{i\bar{\sigma}} - \sum_i U_i \left(\langle \hat{n}_{i\uparrow} \rangle \langle \hat{n}_{i\downarrow} \rangle + \tfrac{1}{4} \right) \tag{2.47a}$$

$$\hat{H}_V^{\text{Hartree}}(\langle \hat{n} \rangle) = \sum_{ij} V_{ij} \left(\langle \hat{n}_i \rangle - 1 \right) \left(\hat{n}_j - 1 \right) - \sum_{ij} V_{ij} \langle \hat{n}_i \rangle \langle \hat{n}_j \rangle. \tag{2.47b}$$

The many-body ground state is then constructed as a Slater determinant of the N lowest single particle eigenfunctions. Because the Hamiltonian depends parametrically on the wavefunction averages $\langle \hat{n}_{i\sigma} \rangle$, the solution to Schrödinger's equation $H_{\text{Hartree}}(\langle n \rangle)|\psi\rangle = E|\psi\rangle$ must then be found self-consistently.

Starting from eigenstates of the barebones hopping Hamiltonian $\mathcal{T}$, the averages $\langle \hat{n}_{i\sigma} \rangle$ are calculated and inserted into the expression of the mean field Hamiltonian. The process of

diagonalization and recalculation of the averages inserted into the Hamiltonian is repeated until the solutions converge. As was the case for the non-interacting tight binding model, the single-particle eigenstates of the Hartree Hamiltonian delocalize over the molecule π-system and behave like large *molecular orbitals*.

2.5   Conclusions

In this chapter we introduced the concept of chemical bonding, and discussed the Pariser-Parr-Pople (PPP) Hamiltonian describing the p_z-bonding in planar organic molecules. The PPP model is the starting point for the theoretical investigations in the rest of the thesis.

We also explained the exact diagonalization procedure based on the iterative Lanczos procedure, and showed how to calculate resolvents numerically. In the end we also discussed some popular approximations to the PPP model, most notably the non-interacting Hückel model, which we also will return to in the coming work.

Chapter 3

Neoclassical Valence Bond Theory

> Starting from the discovery by Rumer that the eigenfunctions corresponding to different distributions of valence bonds in a molecule can be represented by plane diagrams which provide information regarding their mutual linear independence, a very simple graphical method is developed for calculating the coefficients of the integrals occurring in the matrix elements involved in Slater's treatment of the electronic structure of molecules.
>
> L. Pauling[78]

Let us begin this chapter in the heyday of molecular bonding theory during the late 1920s and 1930s. Heitler and London[42] had proposed a solution for the chemical bonding in the Hydrogen molecule. Naively speaking larger molecules could probably be described as a patchwork of such bonds between the electrons of the constituent atoms. However, actual derivation is hard because the mathematical tools for dealing with many-body problems are still scarce.

In 1933 Pauling and Wheland[80] performed the analytical calculation of bonding in larger molecules by extending the work of Slater[100]. Pauling[78] extended Slaters many-body calculation by a graphical representation of the bonded valence electrons in the molecule, and this revelation was the first serious *valence bond (VB) theory*. The hallmark of the theory is the single page derivation of the benzene π-system ground state previously investigated by Hückel in a series of papers.[45]

However, almost simultaneously Slater, Mulliken, Lennard-Jones, and others developed the molecular orbital (MO) theory based on single particle orbitals delocalized over the entire molecule. And like Betamax in the seventies videotape format war, valence bond theory was left out in the cold, while molecular orbital theory became the preferred tool of computational chemistry through the middle of the century.[63,97] Klein and Trinasjstic[51] have delivered a detailed historical account of the evolution of valence bond theory and its applications in chemistry.

Our intention is to solve the semi-emperical Pariser-Parr-Pople model analytically by using a graphical valence bond theory. The starting point is to project out most of the (very large) Hilbert space of the PPP model. This was first done by Spałek[106] in 1977, and the effective Hamiltonian for the projected subspace is commonly known as the t-J model. The t-J model can then be solved graphically by representing the basis in terms of valence bond states.

This have been employed for bulk materials to investigate quantum phase transitions and superconductivity.[5] Here we will follow the prodigal son, when he returns home to his father. We will describe the mathematical derivation of the t-J model, the valence bond

basis and the related graphical rules. We will then apply them to some example molecules, compare to the exact results derived for the PPP model, and discuss the various pros and cons of this *neoclassical*[a] valence bond theory.

3.1   Derivation of the t-J Model Hamiltonian

The basic idea is to consider only a small subspace of the full many-body Hilbert space of the Pariser-Parr-Pople model. When the Coulomb interaction U is larger than the hopping amplitude t this can be done accurately by projecting out the high energy many-body states containing (many) doubly occupied sites. At half-filling the low energy many-body states have exactly one electron per site, and the effective Hamiltonian for the electronic spins is the well-known Quantum Heisenberg Hamiltonian.[41]

he full PPP model can perfectly well be solved in neoclassical valence bond theory, but for brevity we will not consider the full implementation here. In order to keep the derivation as approachable as possible, we ignore any variation in the local chemical potential μ_i, or any Coulomb interaction between electrons on different orbitals. This is similar to the simple Hubbard approximation of the PPP model (cf. section 2.4.1).

The Hubbard model is one of the simplest Hamiltonians describing interacting electrons on any lattice. The electrons hop between connected orbitals i and j with an amplitude t_{ij}, and two electrons of opposite spin can occupy the same orbital i at a cost of the Coulomb energy U_i. In second quantization the Hubbard Hamiltonian looks like,

$$\hat{H} = \mathcal{T} + \mathcal{U} = -\sum_{ij\sigma} t_{ij}\hat{c}^{\dagger}_{i\sigma}\hat{c}_{j\sigma} + U\sum_{ij}\hat{n}_{i\downarrow}\hat{n}_{j\uparrow}, \tag{3.1}$$

where $\mathcal{T}$ is the kinetic term (assuming $t_{ij} = t^*_{ij}$), and $\mathcal{U}$ is the Coulomb interaction. Note that the Hubbard model conserves the number of particles, the total spin $\mathbf{S}$, and the total spin projection $\hat{S}_z$.

Hence, consider a system of N_a sites occupied by $N_e < N_a$ electrons. Following Auerbach[5] we partition the Hilbert space of the many-body electronic system into a subspace S containing all the states with no doubly occupied sites, and another subspace D containing states with at least one doubly occupied site.

$$S = |n_{1\downarrow}, n_{1\uparrow}, n_{2\downarrow}, \ldots, n_{N_e\uparrow}\rangle \qquad \forall i : n_{i\uparrow} + n_{i\downarrow} \leq 1, \tag{3.2a}$$

$$D = |n_{1\downarrow}, n_{1\uparrow}, n_{2\downarrow}, \ldots, n_{N_e\uparrow}\rangle \qquad \exists i : n_{i\uparrow} + n_{i\downarrow} = 2. \tag{3.2b}$$

The S Hilbert space is actually the null space of the Coulomb operator $\mathcal{U}$, and it is quite easy to redefine,

$$S = \left\{\text{states } |\psi\rangle \,\middle|\, \mathcal{U}|\psi\rangle = 0\right\}, \quad \text{and} \quad D = \left\{\text{states } |\psi\rangle \,\middle|\, \mathcal{U}|\psi\rangle \neq 0\right\}. \tag{3.3}$$

Hence the states in the two subspaces are only connected to each other through the kinetic term $\mathcal{T}$. Then introduce the projection $\mathcal{P}$ onto the subspace S, and the projection $\mathcal{Q}$ onto the subspace D. These projection operators are idempotent $\mathcal{P}^2 = \mathcal{P}$ and $\mathcal{Q}^2 = \mathcal{Q}$, mutually orthogonal $\mathcal{QP} = 0$, and because S and D constitutes a partition of the original Hilbert space, $\mathcal{P} + \mathcal{Q} = \mathcal{I}$, where $\mathcal{I}$ is the identity operator.

---

[a]*Neoclassical* is here chosen as facetious juxtaposition to many of the adjectives, which have been added to valence bond theory over the years: Especially the *modern* valence bond theory[23] and *post-modern* valence bond theory.[102]

Having introduced the projection operators, our objective is to find an effective Hamiltonian for the projected eigenstates $|\psi_P\rangle = \mathcal{P}|\psi\rangle$, and the first step is a dissection of Schrödinger's equation on the full Hilbert space,

$$\hat{H}(\mathcal{P}+\mathcal{Q})|\psi\rangle = E(\mathcal{P}+\mathcal{Q})|\psi\rangle \quad \Rightarrow \quad \hat{H}\mathcal{P}|\psi_P\rangle + \hat{H}\mathcal{Q}|\psi_Q\rangle = E|\psi_P\rangle + E|\psi_Q\rangle. \tag{3.4}$$

Applying the projection operator $\mathcal{Q}$ gives us the following equation for $|\psi_Q\rangle$,

$$|\psi_Q\rangle = \frac{1}{E - \mathcal{Q}\hat{H}\mathcal{Q}}\mathcal{Q}\hat{H}\mathcal{P}|\psi_P\rangle. \tag{3.5}$$

If we instead apply the projection $\mathcal{P}$ to equation (3.4) and insert the result for $|\psi_Q\rangle$, we obtain the effective Schrödinger's equation,

$$\left(\mathcal{P}\hat{H}\mathcal{P} + \mathcal{P}\hat{H}\mathcal{Q}\frac{1}{E - \mathcal{Q}\hat{H}\mathcal{Q}}\mathcal{Q}\hat{H}\mathcal{P}\right)|\psi_P\rangle = E|\psi_P\rangle. \tag{3.6}$$

Because S contains no doubly occupied sites, one must have $\mathcal{P}\mathcal{U}\mathcal{P} = 0$, and since $\mathcal{U}$ does not change the distribution of electrons, $\mathcal{Q}\hat{H}\mathcal{P} = \mathcal{Q}\mathcal{T}\mathcal{P}$. Inserting these results, yields

$$\left(\mathcal{P}\mathcal{T}\mathcal{P} + \mathcal{P}\mathcal{T}\mathcal{Q}\frac{1}{E - \mathcal{Q}\hat{H}\mathcal{Q}}\mathcal{Q}\mathcal{T}\mathcal{P}\right)|\psi_P\rangle = E|\psi_P\rangle. \tag{3.7}$$

Note that no approximations have been carried out yet. Equation (3.7) is an exact projection of the original Hubbard model to the subspace of singly occupied sites S, and e.g. the eigenspectrum E of both models must be identical. All we have achieved so far, is to reduce size of the Hilbert space at the cost of a more complicated Schrödinger's equation.

In order to simplify the effective Hamiltonian, we expand $(E - \mathcal{Q}\hat{H}\mathcal{Q})^{-1}$ in powers of $t/(E - U)$,

$$\frac{1}{E - \mathcal{Q}\hat{H}\mathcal{Q}} = \frac{1}{E - \mathcal{Q}\mathcal{U}\mathcal{Q}} + \frac{1}{E - \mathcal{Q}\mathcal{U}\mathcal{Q}}\mathcal{Q}\mathcal{T}\mathcal{Q}\frac{1}{E - \mathcal{Q}\mathcal{U}\mathcal{Q}} + \ldots \tag{3.8}$$

Assuming that $|t| \ll |E - U|$, our effective Hamiltonian restricted to the S space, takes the final form,

$$\hat{H}_{\text{eff}}(E) = \mathcal{P}\mathcal{T}\mathcal{P} + +\mathcal{P}\mathcal{T}\mathcal{Q}\frac{1}{E - (\mathcal{U} + \mathcal{T})}\mathcal{Q}\mathcal{T}\mathcal{P} \tag{3.9}$$

$$= \mathcal{P}\left(\mathcal{T} - \frac{1}{U}\sum_{ijk}\sum_{\sigma\gamma} t_{ij}t_{jk}\hat{c}_{i\sigma}^{\dagger}\hat{c}_{j\sigma}\hat{n}_{j\uparrow}\hat{n}_{j\downarrow}\hat{c}_{j\gamma}^{\dagger}\hat{c}_{k\gamma}\right)\mathcal{P}. \tag{3.10}$$

Note that $\hat{H}_{\text{eff}}$ depends parametrically on the energy, which means that Schrödinger's equation $\hat{H}_{\text{eff}}(E)\psi = E\psi$ must now be solved *self-consistently*.

This result is exactly what you would expect. The projected Hamiltonian allows both direct hopping between S states, and (to first order in t^2/U) transitions involving one virtual visit to the D subspace.

The expression of equation (3.10) can be simplified. When the initial and final site is the same, i.e $i = k$, the following derivation yields a familiar result,

$$\sum_{ij}^{i \neq j} \sum_{\sigma\gamma} t_{ij} t_{ji} \hat{c}_{i\sigma}^\dagger \hat{c}_{j\sigma} \hat{n}_{j\uparrow} \hat{n}_{j\downarrow} \hat{c}_{j\gamma}^\dagger \hat{c}_{i\gamma}$$

$$= \sum_{ij} t_{ij} t_{ji} \sum_\sigma \left(\hat{c}_{i\sigma}^\dagger \hat{c}_{j\sigma} \hat{n}_{j\sigma} \hat{c}_{j\bar{\sigma}}^\dagger \hat{c}_{i\bar{\sigma}} + \hat{c}_{i\sigma}^\dagger \hat{c}_{j\sigma} \hat{n}_{j\bar{\sigma}} \hat{c}_{j\sigma}^\dagger \hat{c}_{i\sigma} \right)$$

$$= \sum_{ij} t_{ij} t_{ji} \sum_\sigma \left(-\hat{c}_{i\sigma}^\dagger \hat{c}_{i\bar{\sigma}} \hat{c}_{j\bar{\sigma}}^\dagger \hat{c}_{j\sigma} + \hat{n}_{i\sigma} \hat{n}_{j\bar{\sigma}} + \tfrac{1}{2}(\hat{n}_{i\sigma} \hat{n}_{j\sigma} - \hat{n}_{i\sigma} \hat{n}_{j\sigma}) \right)$$

$$= -\sum_{ij} t_{ij} t_{ji} \left(2(S_i^x S_j^x + S_i^y S_j^y) + 2 S_i^z S_j^z - \tfrac{1}{2} \sum_s (\hat{n}_{i\sigma} \hat{n}_{j\sigma} + \hat{n}_{i\sigma} \hat{n}_{j\bar{\sigma}}) \right)$$

$$= -\frac{1}{2} \sum_{ij} 4 \left| t_{ij} \right|^2 \left(\hat{\mathbf{S}}_i \cdot \hat{\mathbf{S}}_j - \frac{\hat{n}_i \hat{n}_j}{4} \right). \tag{3.11}$$

This is the quantum Heisenberg Hamiltonian for spins on a lattice.

When, $i \neq k$, the derivation is quite similar,

$$\sum_{ijk}^{i \neq k} t_{ij} t_{jk} \sum_{\sigma\gamma} \hat{c}_{i\sigma}^\dagger \hat{c}_{j\sigma} \hat{n}_{j\uparrow} \hat{n}_{j\downarrow} \hat{c}_{j\gamma}^\dagger \hat{c}_{k\gamma}$$

$$= \sum_{ijk}^{i \neq k} t_{ij} t_{jk} \sum_\sigma \left(\hat{c}_{i\sigma}^\dagger \hat{c}_{j\sigma} \hat{n}_{j\sigma} \hat{c}_{j\bar{\sigma}}^\dagger \hat{c}_{k\bar{\sigma}} + \hat{c}_{i\sigma}^\dagger \hat{c}_{j\sigma} \hat{n}_{j\bar{\sigma}} \hat{c}_{j\sigma}^\dagger \hat{c}_{k\sigma} \right)$$

$$= \sum_{ijk}^{i \neq k} t_{ij} t_{jk} \sum_\sigma \left(\tfrac{1}{2} \hat{c}_{i\sigma}^\dagger \hat{c}_{k\sigma} \hat{n}_j - \hat{c}_{i\sigma}^\dagger \hat{c}_{k\bar{\sigma}} \hat{c}_{j\bar{\sigma}}^\dagger \hat{c}_{j\sigma} + \tfrac{1}{2} \hat{c}_{i\sigma}^\dagger \hat{c}_{k\sigma} \hat{n}_{j\bar{\sigma}} - \tfrac{1}{2} \hat{c}_{i\sigma}^\dagger \hat{c}_{k\sigma} \hat{n}_{j\sigma} \right)$$

$$= \frac{1}{2} \sum_{ijk}^{i \neq k} t_{ij} t_{jk} \left(\sum_s \hat{c}_{i\sigma}^\dagger \hat{c}_{k\sigma} \hat{n}_j - \sum_{s\gamma} \hat{c}_{i\sigma}^\dagger \boldsymbol{\tau}_{\sigma\gamma} \hat{c}_{k\gamma} \cdot \sum_{\sigma\gamma} \hat{c}_{j\bar{\sigma}}^\dagger \boldsymbol{\tau}_{\sigma\gamma} \hat{c}_{j\gamma} \right)$$

$$= -\frac{1}{2} \sum_{ijk}^{i \neq k} t_{ij} t_{jk} \left(\hat{\mathbf{S}}_{ik} \cdot \hat{\mathbf{S}}_j - \frac{\sum_\sigma \hat{c}_{i\sigma}^\dagger \hat{c}_{k\sigma} \hat{n}_j}{4} \right). \tag{3.12}$$

Here $\boldsymbol{\tau} = (\tau_i^x, \tau_i^y, \tau_i^z)$ is the Pauli tensor defined in equation (2.22) , and the local spin operators (setting $\hbar = 1$),

$$\mathbf{S}_i = \sum_{\sigma\gamma} \hat{c}_{i\sigma}^\dagger \boldsymbol{\tau}_{\sigma\gamma} \hat{c}_{i\gamma}, \tag{3.13a}$$

$$\mathbf{S}_{ij} = \sum_{\sigma\gamma} \hat{c}_{i\sigma}^\dagger \boldsymbol{\tau}_{\sigma\gamma} \hat{c}_{j\gamma}. \tag{3.13b}$$

Hence the effective Hamiltonian governing the projected subspace, can be written like,

$$H_{\text{t-J}} = \mathcal{P}(\mathcal{T} + \mathcal{K} + \mathcal{J})\mathcal{P}. \tag{3.14a}$$

This is the *t-J* Hamiltonian with the three terms generally defined as,

$$\mathcal{T} = -\sum_{ij}\left(t_{ij}\sum_{\sigma}\hat{c}_{i\sigma}^{\dagger}\hat{c}_{j\sigma} + h.c.\right), \tag{3.14b}$$

$$\mathcal{K} = \frac{1}{2}\sum_{ij}^{i\neq j}J_{ij}(E)\left(\hat{\mathbf{S}}_i\cdot\hat{\mathbf{S}}_j - \frac{\hat{n}_i\hat{n}_j}{4}\right), \tag{3.14c}$$

$$\mathcal{J} = \frac{1}{2}\sum_{ijk}^{i\neq k}\tilde{J}_{ijk}(E)\left(\hat{\mathbf{S}}_{ik}\cdot\hat{\mathbf{S}}_j - \frac{\sum_{\sigma}\hat{c}_{i\sigma}^{\dagger}\hat{c}_{k\sigma}\hat{n}_j}{4}\right). \tag{3.14d}$$

Here the two exchange couplings are defined as functions of the energy in the following way:

$$\begin{aligned} J_{ij}(E) &= -\frac{4|t_{ij}|^2}{E-U},\\ \tilde{J}_{ijk}(E) &= -\frac{4t_{ij}t_{jk}}{E-U}. \end{aligned} \tag{3.15}$$

One can even expand the energy in terms of $\beta = 4|t|^2/U$,[44] so

$$E = E^{(0)} + \beta E^{(1)} + \beta^2 E^{(2)} + \cdots \tag{3.16}$$

And assuming $E^{(0)} = 0$ the two coupling strengths takes their usual form:

$$J_{ij} = \lim_{E\to 0}J_{ij}(E) = \frac{4|t_{ij}|^2}{U}, \qquad \tilde{J}_{ijk} = \lim_{E\to 0}\tilde{J}_{ijk}(E) = \frac{4t_{ij}t_{jk}}{U}. \tag{3.17}$$

At half-filling all sites are occupied by an electron, which means that $\mathcal{P}(\mathcal{T}+\mathcal{J})\mathcal{P} = 0$, and the *t-J* model reduces to the quantum Heisenberg model with an anti-ferromagnetic coupling.

When the Coulomb energy is much larger than the hopping amplitudes $4U \gg t$, the coupling constants orders hierarchically $t \gg J \approx \tilde{J}$. Because t is the major contributor to the hopping of holes (or electrons) rather than $\tilde{J}$ the $\mathcal{J}$ is usually dropped from the Hamiltonian,[5] giving us the well-known *t-J* model,

$$H_{t\text{-}J} = \mathcal{P}\left\{-\sum_{ij}\left(t_{ij}\sum_{\sigma}\hat{c}_{i\sigma}^{\dagger}\hat{c}_{j\sigma} + h.c.\right) + \frac{1}{2}\sum_{ij}^{i\neq j}J_{ij}\left(\hat{\mathbf{S}}_i\cdot\hat{\mathbf{S}}_j - \frac{\hat{n}_i\hat{n}_j}{4}\right)\right\}\mathcal{P}. \tag{3.18}$$

However, typical values for the interaction and hopping integrals in organic molecule π-systems have $U \sim |2t|$, so in general one should *not* drop the $\mathcal{J}$ term.

3.1.1 Above Half-Filling

The derivation of the *t-J* Hamiltonian can trivially be generalized to include systems above half-filling. Here, the Hilbert space contains states with one or more doubly occupied sites.

Consider a system with N_a orbitals occupied by $N_e > N_a$ electrons. It is obvious that at least $n = N_e - N_a$ of the orbitals must be doubly occupied. Let the states with exactly n doubly occupied sites belong to a subspace D_n, while states with more than n doubly occupied sites belong to $D_{>n}$. Again the two subspaces can be defined using the $\mathcal{U}$ operator

$$D_n = \left\{\text{states }|\psi\rangle\,\big|\,\mathcal{U}|\psi\rangle = nU|\psi\rangle\right\}, \text{ and } D_{>n} = \left\{\text{states }|\psi\rangle\,\big|\,\mathcal{U}|\psi\rangle \neq nU|\psi\rangle\right\}. \tag{3.19}$$

It is trivial to introduce the projection $\mathcal{P}$ onto the D_n subspace, and the projection $\mathcal{Q}$ onto the $D_{>n}$ subspace. By removing the constant offset nU to the Coulomb energy, one reproduces the t-J Hamiltonian of equation (3.14), so that the effective Hamiltonian becomes $H_{eff} = H_{t\text{-}J} + nU$.

3.2 The Dimer Example

As a warm up exercise consider the already scrutinized dimer (cf. section 2.1), consisting of two orbitals hybridized by a hopping t and with on-site Coulomb repulsive energy U. At half-filling the t-J Hamiltonian for the Hilbert subspace S of singly occupied sites is,

$$H_{t\text{-}J} = \mathcal{P}\mathcal{K}\mathcal{P} = \mathcal{P}\left\{ J\left(\hat{\mathbf{S}}_1 \cdot \hat{\mathbf{S}}_2 - \frac{\hat{n}_1 \hat{n}_2}{4} \right)\right\}\mathcal{P}. \tag{3.20}$$

In this case the S subspace contains four different many-body states $|\uparrow_1\uparrow_2\rangle$, $|\downarrow_1\downarrow_2\rangle$, $|\uparrow_1\downarrow_2\rangle$ and $|\downarrow_1\uparrow_2\rangle$. Only the quantum Heisenberg part of the t-J Hamiltonian contributes, and it follows directly from the definition in equation (3.14c) that,

$$\mathcal{K}|\uparrow\uparrow\rangle = 0,$$
$$\mathcal{K}|\downarrow\downarrow\rangle = 0,$$
$$\mathcal{K}|\uparrow\downarrow\rangle = \tfrac{1}{2}J(|\downarrow\uparrow\rangle - |\uparrow\downarrow\rangle),$$
$$\mathcal{K}|\downarrow\uparrow\rangle = \tfrac{1}{2}J(|\uparrow\downarrow\rangle - |\downarrow\uparrow\rangle).$$

When subtracting the last two equations one finds that the ground state is a singlet. The eigenenergy can be found directly using the approximate expression for J of equation (3.17),

$$|s\rangle = \frac{1}{\sqrt{2}}(|\uparrow\downarrow\rangle - |\downarrow\uparrow\rangle), \qquad E_s = -J = -4t^2/U. \tag{3.21}$$

With an energy $E_t = 0$ the excited state is the triplet,

$$|t_1\rangle = |\downarrow\downarrow\rangle,$$
$$|t_2\rangle = \frac{1}{\sqrt{2}}(|\uparrow\downarrow\rangle + |\downarrow\uparrow\rangle),$$
$$|t_3\rangle = |\uparrow\uparrow\rangle.$$

The Heisenberg Hamiltonian $\mathcal{K}$ commutes with the total spin $\hat{S}$, and so $\mathcal{K}$ can be diagonalized in the singlet space and the triplet space separately.

If you looked up section 2.1, you have probably noticed that the ground state energy of the singlet E_s differ from the one we derived directly from the Hubbard model. If we instead use the full self-consistent expression for the exchange coupling J of equation (3.15), we find the familiar

$$E = -\frac{4t^2}{U - E} \Rightarrow E = \tfrac{1}{2}(U \pm \sqrt{U^2 + 16t^2}).$$

3.3 Ground States and Spin

Let us take a closer look at the quantum Heisenberg model, which describes the effective interactions between the electronic spins in different orbitals. At half-filling this becomes the only surviving contribution to the t-J Hamiltonian, and the many-body states become

pure spin states. For both the quantum Heisenberg model and the parent Hubbard model on bipartite lattices (also knwon as alternant lattices), there exists strong constraints on the total spin of the system ground state.

A bipartite lattice contains two sublattices A and B, such that lattice points in A are only connected to lattice points in B and vice versa. For the quantum Heisenberg model, if S_A and S_B denotes the maximum value of the spin projection on the A and B sublattices respectively, the Lieb-Mattis theorem[60] states that the ground state has a total spin $S_0 \leq |S_A - S_B|$, and the eigenenergy spectrum is ordered according to spin S such that $E(S+1) > E(S)$ for all states with a total spin $S \geq |S_A - S_B|$.

In the t-J model at half-filling each orbital is occupied with a single electron of spin $\frac{1}{2}$, and for a bipartite lattice with sublattices of equal size, $S_A - S_B = 0$, and hence by the Lieb-Mattis theorem, the ground state *must* be a singlet $S_0 = 0$. On the other hand, when one sublattice contains just one more orbital than the other, then $S_A - S_B = \frac{1}{2}$, and the ground state must be a doublet $S_0 = \frac{1}{2}$. However, when the number of orbitals in each sublattice differ by more than one, then $S_A - S_B > \frac{1}{2}$, and the Lieb-Mattis theorem cannot precisely predict the spin of the ground state.

Lieb[59] later investigated the repulsive Hubbard model on a bipartite lattice with N_A orbitals belonging to the lattice A and N_B orbitals belonging to the lattice B. At half-filling the total spin of the ground state is given by $S = \frac{1}{2}|N_A - N_B|$. This means that a bipartite lattice with an equal number of sublattice sites $N_A = N_B$ has a singlet ground state, while a bipartite lattice with $N_A = N_B \pm 1$ has a doublet ground state etc.

Due to the Lieb theorem and the Lieb-Mattis theorem many systems have low spin ground states, and because the t-J Hamiltonian conserves the total spin, we can simplify our calculations by limiting them to this low spin Hilbert subspaces.

3.3.1 Rules for Addition of Angular Momentum

According to the addition rules of angular momentum, two systems with angular momentum j_1 and j_2 repsectively, will have a total angular momentum eigenvalue j fulfilling the relation, $|j_1 - j_2| \leq j \leq j_1 + j_2$.

Applying this logic to the combination of two spin $\frac{1}{2}$ systems we find a singlet and a triplet.

$$\frac{1}{2} \otimes \frac{1}{2} = \{0, 1\}. \tag{3.22}$$

Similarly the combination of two singlets will produce a spin singlet, adding a spin $\frac{1}{2}$ system to a singlet gives a doublet, and adding a triplet gives a triplet. Extending this logic, the number of different spin multiplets when combining any number n of spin $\frac{1}{2}$ systems can be computed. Table 3.1 shows the result of such a computation up till $n = 15$.

Hence low spin systems can be built up from the combination of singlet states,

$$0 \otimes 0 \otimes \cdots \otimes 0 = 0,$$
$$\frac{1}{2} \otimes 0 \otimes \cdots \otimes 0 = \frac{1}{2},$$
$$1 \otimes 0 \otimes \cdots \otimes 0 = 1.$$

$n\backslash S$	0	$\frac{1}{2}$	1	$1\frac{1}{2}$	2	$2\frac{1}{2}$	3	$3\frac{1}{2}$	4	$4\frac{1}{2}$	$\dots$
1		1									
2	1		1								
3		2		1							
4	2		3		1						
5		5		4		1					
6	5		9		5		1				
7		14		14		6		1			
8	14		28		20		7		1		
9		42		48		27		8		1	
10	42		90		75		35		9		$\ddots$
11		132		165		110		44		10	
12	132		297		275		154		54		
13		429		572		429		208		65	
14	429		1001		1001		637		273		
15		1430		2002		1638		910		350	$\dots$

Table 3.1: **The number of spin S multiplets when adding n spin $\frac{1}{2}$ particles**. E.g. a system of $n = 4$ electrons, has 2 spin singlets, 3 spin triplets and one spin $S = 2$ quintuplet.

3.4   Valence Bonds

The absolutely simplest singlet state is the maximally entangled state of two electrons,

$$|s\rangle = \frac{1}{\sqrt{2}}\left\{\hat{c}_{1,\uparrow}^{\dagger}\hat{c}_{2,\downarrow}^{\dagger} - \hat{c}_{1,\downarrow}^{\dagger}\hat{c}_{2,\uparrow}^{\dagger}\right\}|vac\rangle. \tag{3.23}$$

Each state consists of a number of singlet pairings between different sites. Adopting the notation of Beach and Sandvik[8] we introduce the valence bond creation operator,

$$\hat{\chi}_{ij}^{0\dagger} = \frac{1}{\sqrt{2}}\left(\hat{c}_{i\uparrow}^{\dagger}\hat{c}_{j\downarrow}^{\dagger} - \hat{c}_{i\downarrow}^{\dagger}\hat{c}_{j\uparrow}^{\dagger}\right). \tag{3.24}$$

It is readily seen that this operator representation of the singlet is *undirected*, because

$$\hat{\chi}_{ij}^{0\dagger} = \frac{1}{\sqrt{2}}\left(\hat{c}_{i\uparrow}^{\dagger}\hat{c}_{j\downarrow}^{\dagger} - \hat{c}_{i\downarrow}^{\dagger}\hat{c}_{j\uparrow}^{\dagger}\right) = \frac{1}{\sqrt{2}}\left(-\hat{c}_{j\downarrow}^{\dagger}\hat{c}_{i\uparrow}^{\dagger} + \hat{c}_{j\uparrow}^{\dagger}\hat{c}_{i\downarrow}^{\dagger}\right) = \hat{\chi}_{ji}^{0\dagger}. \tag{3.25}$$

The singlet – being composed of two fermionic operators – is itself bosonic and obeys the usual commutation relation $[\hat{\chi}_{ij}^{0}, \hat{\chi}_{ij}^{0\dagger}] = 1$. When the valence bond operators share only one site index a bit of algebra shows that,

$$\left[\hat{\chi}_{ij}^{0}, \hat{\chi}_{kj}^{0\dagger}\hat{\chi}_{il}^{0\dagger}\right]|vac\rangle = -\frac{1}{2}\hat{\chi}_{kl}^{0\dagger}|vac\rangle. \tag{3.26}$$

Likewise a set of triplet valence bond creation operators can be introduced:

$$\hat{\chi}_{ij}^{1\dagger}|vac\rangle = \hat{c}_{i\downarrow}^{\dagger}\hat{c}_{j\downarrow}^{\dagger}|vac\rangle, \tag{3.27a}$$

$$\hat{\chi}_{ij}^{2\dagger}|vac\rangle = \frac{1}{\sqrt{2}}\left(\hat{c}_{i\uparrow}^{\dagger}\hat{c}_{j\downarrow}^{\dagger} + \hat{c}_{i\downarrow}^{\dagger}\hat{c}_{j\uparrow}^{\dagger}\right)|vac\rangle, \tag{3.27b}$$

$$\hat{\chi}_{ij}^{3\dagger}|vac\rangle = \hat{c}_{i\uparrow}^{\dagger}\hat{c}_{j\uparrow}^{\dagger}|vac\rangle. \tag{3.27c}$$

A notable difference to the singlets is that all triplet operators are directed, so $\hat{\chi}_{ij}^{l\dagger} = -\hat{\chi}_{ji}^{l\dagger}$ for $l = 1, 2, 3$. The commutation relation in equation (3.26) can be generalized to include any combination of singlet and triplet states,[8]

$$\left[\hat{\chi}_{ij}^{\rho}, \hat{\chi}_{kj}^{\mu\dagger} \hat{\chi}_{il}^{\nu\dagger} \right] |vac\rangle = \frac{1}{2} T^{\lambda\mu\rho\nu} \hat{\chi}_{kl}^{\lambda\dagger} |vac\rangle, \tag{3.28}$$

where $T^{\lambda\mu\rho\nu} = \frac{1}{2}\mathrm{tr}(\tau^{\lambda\dagger}\tau^{\mu}\tau^{\rho\dagger}\tau^{\nu})$.

Having quarried our building blocks in the form of valence bond operators, a valence bond state can be built up by adding valence bonds to the vacuum state.

But there is a lot of freedom in writing down the valence bond states, and several papers[8,105] have been dedicated to investigating different ways of efficiently representing these states. Apart from valence bonds, states pertaining to the t-J model can also contain empty sites (*holons*), doubly occupied sites (*doublons*) and the occasional un-bonded electron (*spinon/free radical*). We will choose the following general many-body representation of the valence bond states,

$$|\psi\rangle = (\overbrace{\hat{c}_{i_1\uparrow}^{\dagger} \hat{c}_{i_1\downarrow}^{\dagger} \hat{c}_{i_2\uparrow}^{\dagger} \hat{c}_{i_2\downarrow}^{\dagger}}^{\text{doublons}})(\overbrace{\hat{c}_{j_1\sigma_1}^{\dagger} \hat{c}_{j_2\sigma_2}^{\dagger}}^{\text{spinons}})(\overbrace{\hat{\chi}_{k_1 P k_1}^{l_1\dagger} \hat{\chi}_{k_2 P k_2}^{l_2\dagger} \cdots \hat{\chi}_{k_N P k_N}^{l_N\dagger}}^{\text{valence bonds}})|vac\rangle. \tag{3.29}$$

Here the spinons are ordered by their indexes $j_1 < j_2$. This last convention can seem unnecessary at the moment, but it ensures that the pictographical representation of a valence bond state, which we are about to introduce, is wholly unambiguous.

Note that the actual ordering of doublons and valence bond states can be completely arbitrary, because both states are bosonic, and they can readily be interchanged without altering the represented valence bond state.

3.5 Valence Bond States Pictionary

In the original game of Pictionary® you compete to guess an unknown word from a drawing. However, the title does not alleviate to mere guesswork, but is instead a reference to the portmanteau components *picture* and *dictionary*... although, you may think of this as a simple game of "Find the ground state". As we shall see, the valence bond states have a direct interpretation in terms of bond diagrams. Because the Hamiltonian can be split into local operators acting on nearest neighbor pairs or three connected sites, one can easily chart the workings of the t-J Hamiltonian on a set of example states.

This picture dictionary of the Hamiltonian, can then quite easily be applied to molecular systems of choice. If this descriptions seems puzzling, everything will hopefully be much clearer when we have ended this short section.

The underlying lattice is composed of sites and bonds. A site i is depicted as a gray circle, while a bond t_{ij} is shown as a gray bars connecting sites i and j. To create a pictionary we must start with our equivalent of letters: valence bond states. A *holon* is depicted as an empty circle, a *spinon* is a filled circle, and a *doublon* is two filled circles. A singlet state is drawn as a black line connecting the sites, while a triplet state is represented by a directed arrow.

name	operator representation	pictionary representation
spinon	$\hat{c}^{\dagger}_{i\downarrow}|vac\rangle$	
doublon	$\hat{c}^{\dagger}_{i\uparrow}\hat{c}^{\dagger}_{i\downarrow}|vac\rangle$	
singlet valence bond	$\hat{\chi}^{0\dagger}_{ij}|vac\rangle$	
triplet valence bond[b]	$\hat{\chi}^{1\dagger}_{ij}|vac\rangle$	

Having developed our alphabet, we can put them together and form extended valence bond states. The next step in our linguistic endeavor is to consider the *action* - the verbs - the operators. Taking the Hamiltonian operators of the *t-J* model term by term, our vocabulary increases quickly.

Note that we will mostly be considering singlet or doublet ground state molecules, and as a result the entries related to triplet valence bonds are only sporadically included in the pictionary.

3.5.1   The Hopping $\mathcal{T}$

The local hopping operator can be written as a sum of local terms, $\mathcal{P}\mathcal{T}\mathcal{P} = \sum_{i \neq j} \mathcal{P}\mathcal{T}_{ij}\mathcal{P}$, where

$$\mathcal{T}_{ij} = -t_{ij} \sum_{\sigma} \hat{c}^{\dagger}_{i\sigma}\hat{c}_{j\sigma}. \tag{3.30}$$

The wrapping projection operator $\mathcal{P}$ ensures that the Hamiltonian only applies to states in the projected space. Hence only operations which conserve the number of singly occupied sites should be considered.

As an example consider the case, when site i is occupied by a doublon and site j by a spinon. Then

$$\mathcal{T}_{ji}\hat{c}^{\dagger}_{i\uparrow}\hat{c}^{\dagger}_{i\downarrow}\hat{c}^{\dagger}_{j\uparrow}|vac\rangle = -t_{ji}\hat{c}^{\dagger}_{j\downarrow}\hat{c}_{i\downarrow}\hat{c}^{\dagger}_{i\uparrow}\hat{c}^{\dagger}_{i\downarrow}\hat{c}^{\dagger}_{j\uparrow}|vac\rangle = t_{ji}\hat{c}^{\dagger}_{i\uparrow}\hat{c}^{\dagger}_{j\uparrow}\hat{c}^{\dagger}_{j\downarrow}|vac\rangle. \tag{3.31}$$

Interpreted as a pictionary entry the result can be written

$$\mathcal{T}_{ji}\left|\,\begin{matrix} \end{matrix}\,\right\rangle = t_{ji}\left|\,\begin{matrix} \end{matrix}\,\right\rangle. \tag{3.32a}$$

Similarly when considering a holon and a spinon,

$$\mathcal{T}_{ij}\left|\,\begin{matrix} \end{matrix}\,\right\rangle = -t_{ij}\left|\,\begin{matrix} \end{matrix}\,\right\rangle, \tag{3.32b}$$

and by direct analogy the pictorial valence bond case looks like

$$\mathcal{T}_{ji}\left|\,\begin{matrix} \end{matrix}\,\right\rangle = t_{ji}\left|\,\begin{matrix} \end{matrix}\,\right\rangle, \tag{3.32c}$$

$$\mathcal{T}_{ij}\left|\,\begin{matrix} \end{matrix}\,\right\rangle = -t_{ij}\left|\,\begin{matrix} \end{matrix}\,\right\rangle. \tag{3.32d}$$

Acting on any other categories of pairs yield zero in the projected space.

3.5.2 The Quantum Heisenberg Hamiltonian $\mathcal{K}$

The quantum Heisenberg Hamiltonian can also be decomposed into local operators $\mathcal{PKP} = \frac{1}{2}\sum_{i,j}\mathcal{K}_{ij} = \sum_{\langle i,j\rangle}\mathcal{K}_{ij}$, where

$$\mathcal{K}_{ij} = J_{ij}\left(\hat{\mathbf{S}}_i \cdot \hat{\mathbf{S}}_j - \frac{\hat{n}_i\hat{n}_j}{4}\right) \quad \left[= \mathcal{K}_{ji}\right]. \tag{3.33}$$

Since this operator commutes with local number operator, $\hat{n}_i$, the projection $\mathcal{P}$ is implicit. When applied to connected sites with either holons or doublons the result vanishes, and only states containing combinations of valence bonds and spinons contribute.

Two valence bonded sites constitute an eigenstate of the Heisenberg Hamiltonian, and one can easily verify that,

$$\mathcal{K}_{ij}\left|\underset{i\qquad j}{\rule{0pt}{0pt}\text{⬤——⬤}}\right\rangle = -J\left|\underset{i\qquad j}{\rule{0pt}{0pt}\text{⬤——⬤}}\right\rangle \tag{3.34a}$$

$$\mathcal{K}_{ij}\left|\underset{i\qquad j}{\rule{0pt}{0pt}\text{⬤➙⬤}}\right\rangle = 0. \tag{3.34b}$$

Applying $\mathcal{K}_{ij}$ to a nearest neighbor pair results in the following entries in our pictionary,

$$\mathcal{K}_{ij}\left|\text{<image>}\right\rangle = \tfrac{1}{2}J\left|\text{<image>}\right\rangle, \tag{3.34c}$$

and finally when considering two valence bond states,

$$\mathcal{K}_{jk}\left|\text{<image>}\right\rangle = \tfrac{1}{2}J\left|\text{<image>}\right\rangle. \tag{3.34d}$$

Since the Heisenberg Hamiltonian yields zero when applied to empty of doubly occupied sites, these are all the dictionary entries we need.

3.5.3 The Mixed Term $\mathcal{J}$

The only remaining term of the t-J Hamiltonian is $\mathcal{J}$, which can be written as a sum of local terms $\mathcal{PJP} = \sum_{ijk}^{i\neq k}\mathcal{PJ}_{ijk}\mathcal{P}$. Note that $\mathcal{J}_{ijk}$ acts on three consecutively connected sites i,j and k, and

$$\mathcal{J}_{ijk} = \frac{1}{2}\frac{4t_{ij}t_{jk}}{U}\left(\hat{\mathbf{S}}_{ik}\cdot\hat{\mathbf{S}}_j - \frac{\sum_s \hat{c}^\dagger_{is}\hat{c}_{ks}\hat{n}_j}{4}\right) = \frac{1}{2}\tilde{J}_{ijk}\left(\hat{\mathbf{S}}_{ik}\cdot\hat{\mathbf{S}}_j - \frac{\sum_s \hat{c}^\dagger_{is}\hat{c}_{ks}\hat{n}_j}{4}\right), \tag{3.35}$$

where $\tilde{J}_{ijk} = 4t_{ij}t_{jk}/U$.

This local operator only conserves the number of singly occupied sites when acting on a combination of two singly connected sites and one doubly occupied (or empty) site. The dictionary contains three distinct cases. Initially, we consider that states, where the triply connected sites ijk are occupied by a holon and a valence bond, and

$$\mathcal{J}_{ijk}\left|\text{<image>}\right\rangle = -\tilde{J}_{ijk}\left|\text{<image>}\right\rangle, \tag{3.36a}$$

$$\mathcal{J}_{ijk}\left|\text{<image>}\right\rangle = 0. \tag{3.36b}$$

Secondly, when the three sites are occupied by a valence bond and a spinon, we have

$$\mathcal{J}_{ijk} \left| \underset{i \quad j \quad k}{\text{⬡}} \right\rangle = \tfrac{1}{2}\tilde{J}_{ijk} \left| \text{⬡} \right\rangle, \tag{3.36c}$$

$$\mathcal{J}_{ijk} \left| \underset{i \quad j \quad k}{\text{⬡}} \right\rangle = \tfrac{1}{2}\tilde{J}_{ijk} \left| \text{⬡} \right\rangle. \tag{3.36d}$$

Finally, this can easily be generalized to the last case, where the two sites are valence bonded with two other sites.

$$\mathcal{J}_{ijk} \left| \underset{i \quad j \quad k}{\text{⬡}} \right\rangle = \tfrac{1}{2}\tilde{J}_{ijk} \left| \text{⬡} \right\rangle. \tag{3.36e}$$

For doublons the entries are very similar. All you need to do is to replace the holon with a doublon and reverse the order of i, j and k.

3.6 Valence Bond States Non-Orthogonality

The pictionary now details the valence bond graphical language for dealing with many-body calculations in the t-J model. However, it turns out that our words may not be wholly unambiguous...

Consider e.g., two valence bond states $|A\rangle = \hat{\chi}_{12}^{0\dagger}\hat{\chi}_{34}^{0\dagger}|vac\rangle$ and $|B\rangle = \hat{\chi}_{23}^{0\dagger}\hat{\chi}_{14}^{0\dagger}|vac\rangle$ in a four site model. Writing out the states in terms of creation operators it is relatively straight-forward to show that their mutual overlap is given by, $\langle A|B\rangle = \tfrac{1}{2}$, and in fact the valence bond states are in general non-orthogonal.

3.6.1 Overlaps

Following Beach and Sandvik[8] we consider as an example, a general pure singlet valence bond state,

$$|\psi_i\rangle = \hat{\chi}_{i_1 i_2}^{0\dagger}\hat{\chi}_{i_3 i_4}^{0\dagger}\cdots\hat{\chi}_{i_{N-1} i_N}^{0\dagger}|vac\rangle. \tag{3.37}$$

The mutual overlap between two such states is written like

$$\left\langle\psi_j|\psi_i\right\rangle = \langle vac|\hat{\chi}_{j_{N+1} j_N}^{0}\cdots\hat{\chi}_{j_3 j_4}^{0}\hat{\chi}_{j_1 j_2}^{0}\hat{\chi}_{i_1 i_2}^{0\dagger}\hat{\chi}_{i_3 i_4}^{0\dagger}\cdots\hat{\chi}_{i_{N-1} i_N}^{0\dagger}|vac\rangle. \tag{3.38}$$

Graphically the two states are superposed on the lattice, and the valence bonds will either overlap directly or form loops. Any overlapping bonds correspond to identical valence bonds and they can all safely be ignored. The loops can be contracted by repeated use of the commutation relation, $[\hat{\chi}_{ij}^{0}, \hat{\chi}_{ik}^{0\dagger}\hat{\chi}_{jl}^{0\dagger}]|vac\rangle = -\tfrac{1}{2}\hat{\chi}_{kl}^{0\dagger}|vac\rangle$, which removes two sites from the loop at the cost of $-\tfrac{1}{2}$ until only two sites are left. This means that each n-site loop contributes with a factor of $(-2)^{2-n/2}$. An example is shown in Figure 3.1(a).

Letting N_o be the total number of sites in loops, and $N_\circlearrowleft$ counting the number of loops, the overlap can be calculated using the formula

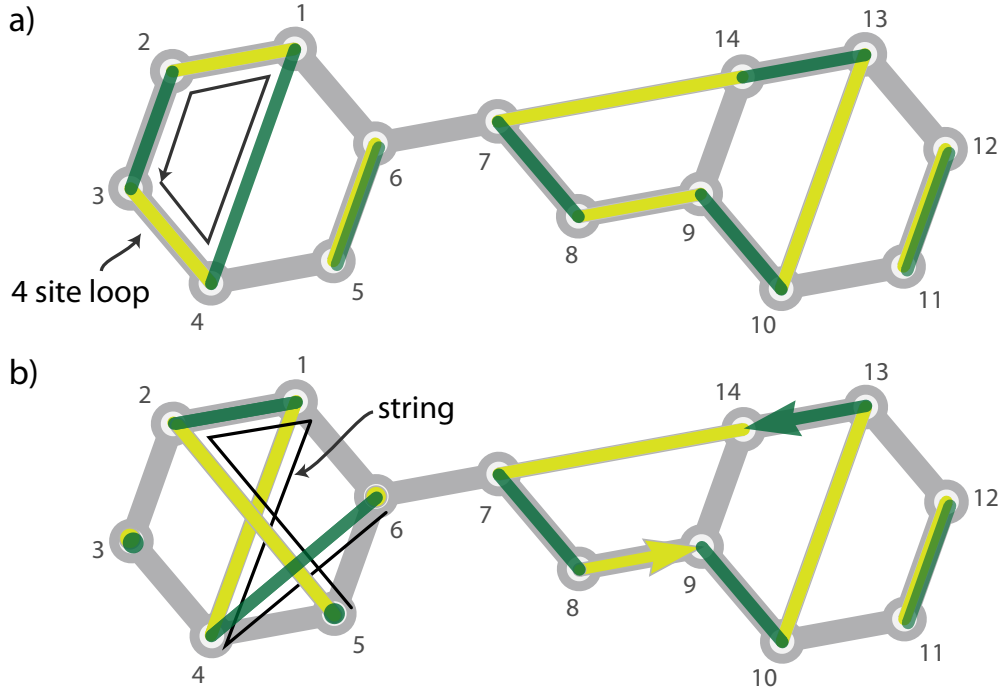$$\langle i|o\rangle = (-2)^{N_\circlearrowleft - N_o/2}. \tag{3.39}$$

Figure 3.1: Two examples of stilbene valence bond states (green and yellow) superposed on each other. In this visualization it is rather easy to see the loop and string structure determining the mutual overlap of the two states.

Valence bond states containing holons (doublons) are simple to deal with, since the overlap vanishes when there is any mismatch between the holons (doublons) of the two states. When considering spinons, we need the commutation relation,

$$\left[\hat{c}_{i\sigma}, \hat{\chi}_{ij}^{0\dagger}\right] = \frac{1}{\sqrt{2}}\hat{c}_{j\bar{\sigma}}^{\dagger}. \tag{3.40}$$

Graphically a spinon in each state will mark the end of a string of valence bond states. The string can be contracted one site at time at the cost of $i/\sqrt{2}$ per contraction, and a string of length n contributes to the overlap with a factor $(-2)^{n/2}$. Hence the presence of spinons does not alter equation (3.39).

The triplet states can in principle be dealt with by using equation (3.28), but we will not cover all the cases here. Graphically any loop must contain an even number of triplet bonds and the sign of the contribution will depend on the mutual direction of the involved triplets. An example is shown in Figure 3.1(b).

3.6.2 Overcompleteness

The valence bond states are not only non-orthogonal, but as a basis they are also over-complete. For the simple four site model at half-filling, we can write down three different valence bond states. However, consulting Table 3.1 only two singlet states exist in this case. In fact the three states are related, so

$$\hat{\chi}_{12}^{0\dagger}\hat{\chi}_{34}^{0\dagger} + \hat{\chi}_{13}^{0\dagger}\hat{\chi}_{23}^{0\dagger} + \hat{\chi}_{23}^{0\dagger}\hat{\chi}_{14}^{0\dagger} = 0. \tag{3.41}$$

For a given set of valence bond states $|v_1\rangle, |v_2\rangle, \ldots, |v_N\rangle$, we can construct the overlap matrix $\mathbf{S}$ with the matrix elements $S_{ij} = \langle i|j\rangle$ (not to be confused with the spin operator). If the set forms an overcomplete basis the dimension of $\mathbf{S}$ is larger than the rank, i.e.,

$$\dim(\mathbf{S}) > \mathrm{rank}(\mathbf{S}). \tag{3.42}$$

The overcomplete basis can be reduced to a complete basis by Gaussian elimination of the overlap matrix S. From the reduced row echelon form, the complete basis $|v_i\rangle$ subset can then be extracted.

Another approach is due to Rumer,[90] where a full basis can be constructed by placing the lattice sites in a circle, and only include states with *non-crossing* valence bonds. These Rumer diagrams can also be constructed by repeated application of the pictionary on the Kekulé state on a chain (all valence bonds along the chain bonds, cf. equation (3.54)).

Any valence bond state can be re-expressed in the complete basis $|v_i\rangle$,

$$|\psi\rangle = \sum_i \alpha_i |v_i\rangle \tag{3.43}$$

The overlap with a particular basis state $|v_j\rangle$ is then,

$$\langle v_j|\psi\rangle = \sum_i \alpha_i \langle v_j|v_i\rangle = \sum_i \alpha_i S_{ji}, \tag{3.44}$$

and the the expansion coefficients α_i can then be found by solving this set of linear equations,

$$\mathbf{S} \begin{pmatrix} \alpha_1 \\ \vdots \\ \alpha_n \end{pmatrix} = \begin{pmatrix} \langle v_1|\psi\rangle \\ \vdots \\ \langle v_n|\psi\rangle \end{pmatrix}. \tag{3.45}$$

3.6.3   Operators in a Non-Orthogonal Basis

While valence bond states and valence bond operators can be written in a bra-ket fashion, it is desirable to work with state vectors and operator matrices. While the translation between the two representations is trivial fin a orthogonal basis, we must be careful, when working in anon-orthogonal basis.

A valence bond state can be written on ket or vector form,

$$|\phi\rangle = \sum_i c_i |v_i\rangle \quad \sim \quad \phi = \begin{pmatrix} c_1 \\ c_2 \\ \vdots \\ c_n \end{pmatrix}. \tag{3.46}$$

Consider then an operator $\hat{A}$ written in both representations,

$$\hat{A} = \sum_{ij} |v_i\rangle \alpha_{ij} \langle v_j| \quad \sim \quad \mathbf{A} = \begin{pmatrix} a_{11} & \ldots & a_{1n} \\ \vdots & & \vdots \\ a_{n1} & \ldots & a_{nn} \end{pmatrix}. \tag{3.47}$$

In an orthogonal basis, the coefficients are identical $a_{ij} = \alpha_{ij}$, however, in a non-orthogonal basis this is no longer the case. Here we will design the matrix representation, such that $\hat{A}|\phi\rangle$ and $\mathbf{A}\phi$ produces the same results.

Sandwiching the operator $\hat{A}$ between two basis states $|v_k\rangle$ and $|v_l\rangle$, the matrix representation produces,

$$\langle v_k|\hat{A}|v_l\rangle \sim \langle v_k|\mathbf{A}\mathbf{v}_l\rangle = \sum_j a_{jl}\langle v_k|v_j\rangle = \sum_j S_{kj}a_{jl}, \tag{3.48}$$

while the operator representation gives,

$$\langle v_k|\hat{A}|v_l\rangle = \sum_{ij} \alpha_{ij}\langle v_k|v_i\rangle\langle v_j|v_l\rangle = \sum_{ij} S_{ki}\alpha_{ij}S_{jl}. \tag{3.49}$$

Equating those two expressions we end up with a set of linear equations, $\mathbf{S}a = \mathbf{S}\alpha\mathbf{S}$. When the basis is complete the overlap matrix is invertible and the above equation reduces to, $a = \alpha\mathbf{S}$.

In the matrix representation, the identity operator, $\mathbf{I}$, takes the usual diagonal form with matrix elements $a_{ij} = \delta_{ij}$. In a complete valence bond basis it is straightforward to find the corresponding coefficients $\alpha_{ij} = a_{ik}(\mathbf{S}^{-1})_{kj} = (\mathbf{S}^{-1})_{ij}$, giving us the valence bond operator representation $\hat{I} = \sum_{ij}|v_i\rangle\mathbf{S}_{ij}^{-1}\langle v_j|$.

3.7 Schrödinger's Equation

Having dealt with the non-orthogonality of the valence bond basis, the next important goal is to find the many-body ground state and excited states. Hence we wish to solve Schrödinger's equation. The pictionary of equation (3.32)-(3.34) already constitutes a matrix representation of the Hamiltonian. This means that

$$\hat{H}_{t\text{-}J}|v_i\rangle = \sum_j |v_j\rangle h_{ji}. \tag{3.50}$$

Then expand the eigenfunctions in the valence bond basis, such that $|\psi\rangle = \sum_j c_j|v_j\rangle$. We can rewrite Schrödinger's equation in terms of this non-orthogonal basis,

$$\hat{H}|\psi\rangle = \hat{H}\sum_j c_j|v_j\rangle = \sum_{kj} h_{kj}c_j|v_k\rangle = E\sum_k c_k|v_k\rangle. \tag{3.51}$$

This can be rewritten as a matrix equation

$$\mathbf{S}(h - E\mathbf{I})\mathbf{c} = 0. \tag{3.52}$$

When the overlap matrix $\mathbf{S}$ is invertible, we obtain the usual Schrödinger's equation, $h|\psi\rangle = E|\psi\rangle$. Then proper normalization of the ground states requires that $\langle\psi|\psi\rangle = 1$, hence giving that

$$\langle\psi|\psi\rangle = \sum_{ij} c_i^* c_j\langle v_i|v_j\rangle = \sum_{ij} c_i^* S_{ij}c_j = \mathbf{c}^\dagger\mathbf{S}\mathbf{c} = 1. \tag{3.53}$$

3.8 Examples

3.8.1 Benzene

Having developed the valence bond pictionary, our first example is the the aromatic benzene molecule considered by Pauling and Wheland[80], with a π-system consisting of six p_z orbitals connected in a ring. According to the Lieb-Mattis theorem, the ground state is a singlet.
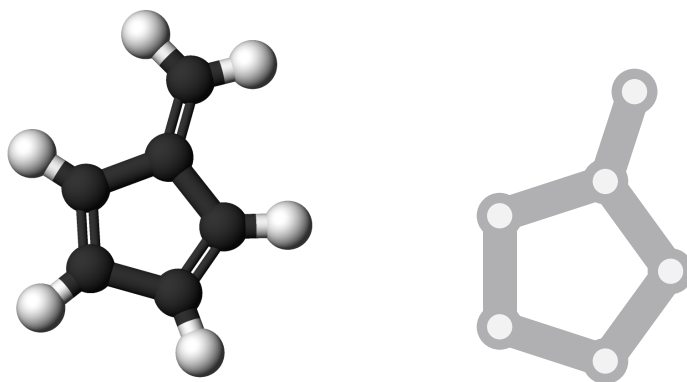
Figure 3.2: **Fulvene**, showing both the molecular structure diagram and the π-system lattice.

The five Rumer diagrams are given by the two Kekulé structures (all valence bonds between nearest neighbors),

$$\text{and}\qquad\qquad. \tag{3.54}$$
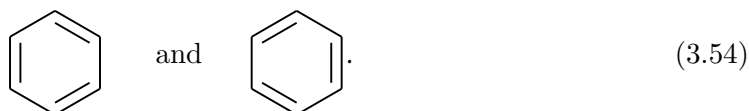
and the three Dewar states,

$$\tag{3.55}$$
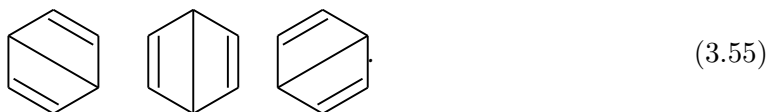
The Hamiltonian can be derived directly from the pictionary. The result is given by,

$$\hat{H}_J = J \begin{pmatrix} -3 & 0 & \frac{1}{2} & \frac{1}{2} & \frac{1}{2} \\ 0 & -3 & \frac{1}{2} & \frac{1}{2} & \frac{1}{2} \\ 1 & 1 & -2 & 0 & 0 \\ 1 & 1 & 0 & -2 & 0 \\ 1 & 1 & 0 & 0 & -2 \end{pmatrix}. \tag{3.56}$$

Here the ground state is right away

$$|GS\rangle = 0.4098 \left(\quad + \quad \right) - 0.1780 \left(\quad + \quad + \quad \right),$$

confirming the original result of Pauling and Wheland[80].

3.8.2   Fulvene

The Fulvene (C_6H_6) molecule is depicted in Figure 3.2, and the π-system contains six p_z orbitals. While we could begin our analysis from the five Rumer diagrams, this is undesirable because the π-system structure forces the pictionary to produce states outside the Rumer basis.

Instead the symmetry of the molecule is exploited in order to construct a complete basis. From the pictionary (section 3.5), we generate the eleven singlet states shown in Figure 3.3. A suitable choice of mirror symmetric or anti-mirror-symmetric superpositions of the valence bond states, creates a proper basis,
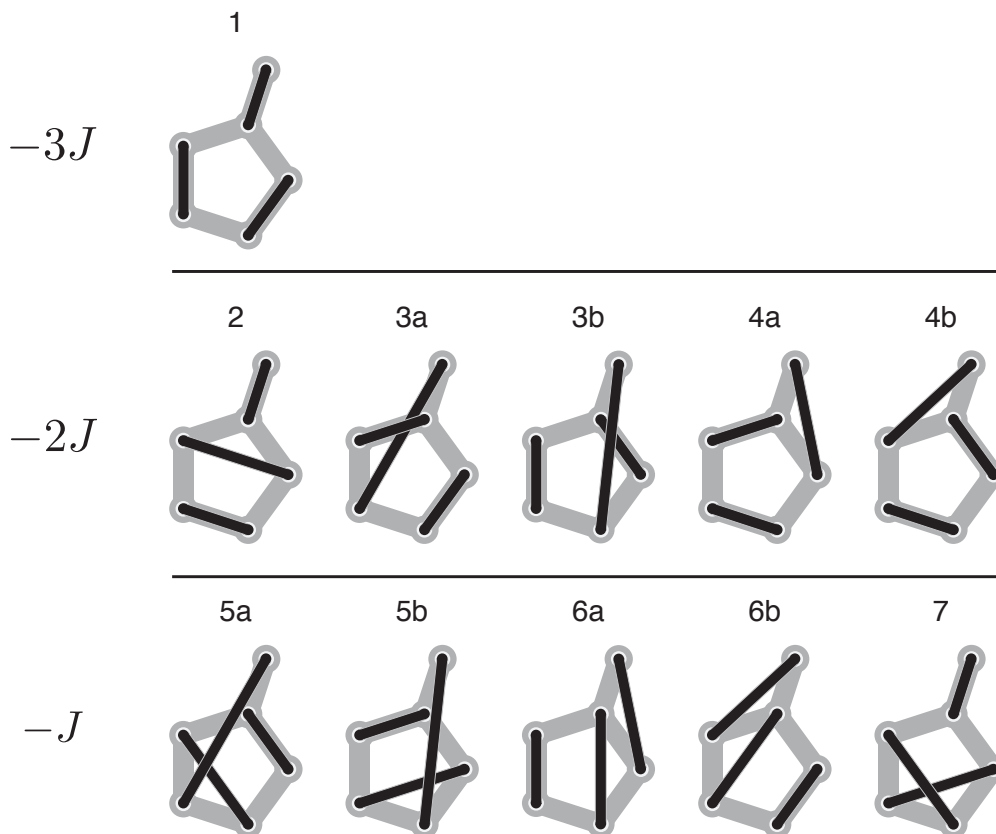
Figure 3.3: **Fulvene**, molecular model states ordered by their diagonal element in the Hamiltonian

$$|\psi_a\rangle = |\psi_1\rangle, \tag{3.57a}$$
$$|\psi_b\rangle = |\psi_{3a}\rangle + |\psi_{3b}\rangle, \tag{3.57b}$$
$$|\psi_c\rangle = |\psi_{4a}\rangle + |\psi_{4b}\rangle, \tag{3.57c}$$
$$|\psi_d\rangle = |\psi_{3a}\rangle - |\psi_{3b}\rangle, \tag{3.57d}$$
$$|\psi_e\rangle = |\psi_{4a}\rangle - |\psi_{4b}\rangle. \tag{3.57e}$$

In this basis the Hamiltonian separates completely into two subspaces composed of either *mirror-symmetric* states or the *mirror-anti-symmetric* states. For simplicity we assume that all Js are identical, giving the result,

$$H = J \begin{pmatrix} -3 & 1/2 & -1/2 & 0 & 0 \\ 2 & -2 1/2 & 0 & 0 & 0 \\ -1 & 0 & -2 1/2 & 0 & 0 \\ 0 & 0 & 0 & -1 1/2 & 1 \\ 0 & 0 & 0 & 1 & -2 1/2 \end{pmatrix}. \tag{3.58}$$

The overlap matrix takes an unusual form because the states are not normalized,

$$
S = \begin{pmatrix}
1 & -1 & 1/2 & 0 & 0 \\
-1 & 2\,1/2 & -1/2 & 0 & 0 \\
1/2 & -1/2 & 1 & 0 & 0 \\
0 & 0 & 0 & 1\,1/2 & -1\,1/2 \\
0 & 0 & 0 & -1\,1/2 & 3
\end{pmatrix}.
\tag{3.59}
$$

The actual ground state of the system belongs to the *parity symmetric* subspace, and has a total energy of $E_{GS} = -4J$,

$$
|\psi_{GS}\rangle \propto |\psi_a\rangle - \tfrac{1}{3}|\psi_b\rangle + \tfrac{1}{3}|\psi_c\rangle.
\tag{3.60}
$$

In principle the state should be properly normalized. Because our basis is non-orthogonal the coefficients of the valence bond states in the ground state representation should be interpreted very carefully. It is not correct to just take the ratios of the coefficients and conclude that the Kekulé state $|\psi_a\rangle$ constitutes 60% of ground state.

To emphasize this point consider a slightly different basis, where $|\psi_b\rangle$ and $|\psi_c\rangle$ are replaced with

$$
|\psi_{b'}\rangle = |\psi_{5a}\rangle + |\psi_{5b}\rangle,
\tag{3.61}
$$
$$
|\psi_{c'}\rangle = |\psi_{6a}\rangle + |\psi_{6b}\rangle.
\tag{3.62}
$$

In this basis the symmetric ground state is,

$$
|\psi_{GS}\rangle \propto |\psi_a\rangle - \tfrac{1}{7}|\psi_{b'}\rangle + \tfrac{2}{7}|\psi_{c'}\rangle.
\tag{3.63}
$$

with a somewhat larger total weight on the Kekulé state $|\psi_a\rangle$.

Instead one should consider the normalized overlap between the ground-state and the Kekulé state,

$$
\frac{\langle\psi_a|\psi_{GS}\rangle}{\sqrt{\langle\psi_{GS}|\psi_{GS}\rangle}\sqrt{\langle\psi_a|\psi_a\rangle}} \approx 0.95
\tag{3.64}
$$

This shows that in this case the Kekulé state is a surprisingly good substitute for the total ground state. The remaining 1/20 of the ground state is captured by the two other basis states. However, one should not mistakenly think that the overlap with the two remaining states is just 1/20.

Repeating the calculation of equation (3.64) for the different basis states allow us to produce the overlap table,

	$|\psi_a\rangle$	$|\psi_b\rangle$	$|\psi_c\rangle$	$|\psi_{b'}\rangle$	$|\psi_{c'}\rangle$
$\langle\psi_{GS}|$	0.95	0.80	0.63	0.40	0.40

While the Kekulé state has the largest overlap with the ground state, it turns out that the $|\psi_b\rangle$ state with one 'long' valence bond also has a large overlap with the ground state.

The fact that two valence bond states with valence bonds of different lengths both have a large overlap with the ground state, emphasizes that the length of valence bonds should not be directly interpreted as the spin correlation length.

When replacing a resonating valence bond state with a large overlap state one should ensure that the complete symmetry of the original state is retained in the replacement state. Also the actual ground state energy is sometimes much smaller than the energy of the overlap state, $\langle\psi|\hat{H}|\psi\rangle$.

3.9   Benchmarks

We can easily benchmark the calculations done by our neoclassical valence bond theory against exact numerical calculations of the parent Hubbard model described in the previous chapter.

To get a sense of how well the valence bond theory works for systems of varying size, we will choose to do the comparison for non-dimerized chains of varying lengths. We choose to compare the overlap between the valence bond ground state $|\psi_{vb}\rangle$ and the renormalized projection of the Hubbard model ground state to the S subspace $\mathcal{P}|\psi_H\rangle/\langle\psi_H|\mathcal{P}|\psi_H\rangle$. The result is presented in Figure 3.4, along with the norm of the S projected norm $\langle\psi_H|\mathcal{P}|\psi_H\rangle$. This (almost perfect) agreement with valence bond theory independent of the value of U is
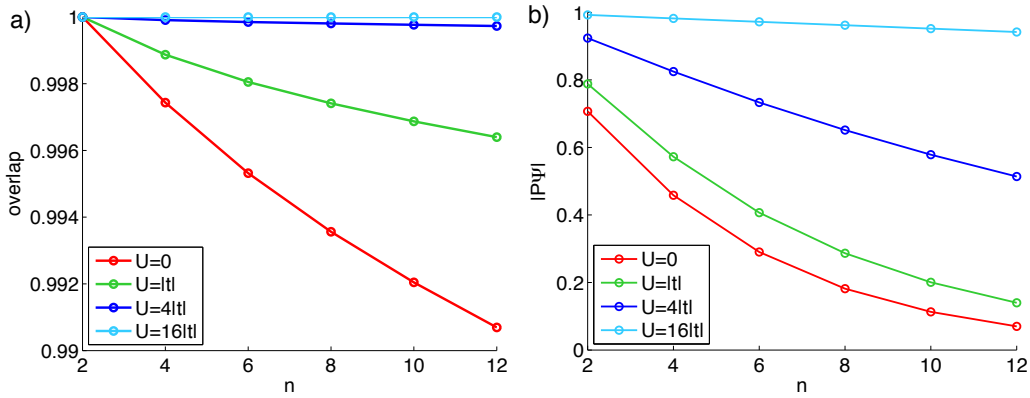
Figure 3.4: Comparing $\mathcal{P}$ projected ground states calculated by exact diagonalization and VB theory. a) Shows the direct overlaps as a function of chain length n. b) The norm of the ground state in the projected subspace S calculated from the parent Hubbard model.

somewhat surprising. If you remember that we performed an expansion in terms $t/(E-U)$ when deriving the effective Hamiltonian, then the obvious conclusion may be that the expansion was solid and well-defined. However, the truth is a little more complicated than this.

In order to understand this we expand our Hamiltonian to fourth order in the hopping using equation (3.8),

$$H^{(2)} = \mathcal{P}\mathcal{T}\mathcal{Q}\left(\frac{1}{E-\mathcal{Q}U\mathcal{Q}}\mathcal{Q}\mathcal{T}\mathcal{Q}\right)^2\frac{1}{E-\mathcal{Q}U\mathcal{Q}}\mathcal{Q}\mathcal{T}\mathcal{P}. \tag{3.65}$$

Half of the relevant t^4 order processes involving only two connections sharing a single site t_{ij} and t_{jk} (assuming $t_{ik} = 0$), are given by

$$
\begin{aligned}
\uparrow\uparrow\uparrow \quad &\rightarrow \quad\quad 0. \\
\downarrow\uparrow\uparrow \quad &\rightarrow \quad -0\,2\uparrow \quad \rightarrow \quad 0\uparrow 2 \quad \rightarrow \quad -0\,2\uparrow \quad \rightarrow \quad \downarrow\uparrow\uparrow \text{ or } -\uparrow\downarrow\uparrow. \\
& \rightarrow \quad\quad\ \uparrow 0\,2 \quad \rightarrow \quad \uparrow\uparrow\downarrow \text{ or } -\uparrow\downarrow\uparrow. \\
&\rightarrow \quad -2\,0\uparrow \quad \rightarrow \quad -2\uparrow 0 \quad \rightarrow \quad -2\,0\uparrow \quad \rightarrow \quad \downarrow\uparrow\uparrow \text{ or } -\uparrow\downarrow\uparrow. \\
& \rightarrow \quad\quad\ \uparrow 2\,0 \quad \rightarrow \quad \uparrow\uparrow\downarrow \text{ or } -\uparrow\downarrow\uparrow. \\
\uparrow\downarrow\uparrow \quad &\rightarrow \quad\ 0\,2\uparrow \quad \rightarrow \quad -0\uparrow 2 \quad \rightarrow \quad\ 0\,2\uparrow \quad \rightarrow \quad \uparrow\downarrow\uparrow \text{ or } -\downarrow\uparrow\uparrow. \\
& \rightarrow \quad -\uparrow 0\,2 \quad \rightarrow \quad \uparrow\downarrow\uparrow \text{ or } -\uparrow\uparrow\downarrow. \\
&\rightarrow \quad\ 2\,0\uparrow \quad \rightarrow \quad 2\uparrow 0 \quad \rightarrow \quad\ 2\,0\uparrow \quad \rightarrow \quad \uparrow\downarrow\uparrow \text{ or } -\downarrow\uparrow\uparrow. \\
& \rightarrow \quad -\uparrow 2\,0 \quad \rightarrow \quad \uparrow\downarrow\uparrow \text{ or } -\uparrow\uparrow\downarrow.
\end{aligned}
\tag{3.66}
$$

The remaining half can be found by flipping *all* the spins and/or reversing the order of sites.

In this case the effective interaction will always come with a prefactor, $J_3 = |t_{ij}|^2 |t_{jk}|^2 / (E - U)^3$, and the effective spin Hamiltonian capturing the above rules takes the form,

$$
H_{ijk}^{(2)} = -8 \left(\mathbf{S}_i \cdot \mathbf{S}_j - \frac{1}{4} \right) - 8 \left(\mathbf{S}_j \cdot \mathbf{S}_k - \frac{1}{4} \right) + 4 \left(\mathbf{S}_i \cdot \mathbf{S}_k - \frac{1}{4} \right).
\tag{3.67}
$$

To keep the algebra simple, we will instead work with the local Heisenberg operator $\mathcal{K}_{ij} = \mathbf{S}_i \cdot \mathbf{S}_j - \frac{\hat{n}_i \hat{n}_j}{4}$. Assuming for brevity that all hopping integrals are equal, $t_{ij} = t$ and that the molecular graph have no 4-loops, we can easily write down the full Hamiltonian summing over all possible connected three sites $\langle ijk \rangle$ in the molecule.

$$
\sum_{\langle ijk \rangle} J_4 H_{ijk}^{(2)} = \frac{|t|^4}{(E - U)^3} \sum_{\langle i,j,k \rangle} (-8\mathcal{K}_{ij} - 8\mathcal{K}_{jk} + 4\mathcal{K}_{ik}).
\tag{3.68}
$$

This means an enhancement of the singlet pairing between neighboring sites and an additional triplet pairing between next nearest neighbors $\langle\langle i,j \rangle\rangle$.

Let us consider the other case, where the two pairs of neighbors *do not* share a site, meaning that we must consider two sets of neighbor vertices (i, j) and (k, l) with $i, j \neq k, l$. The resulting Hamiltonian is simply the direct product of singlet pairings between the two neighbor pairs, and

$$
H_{ijkl}^{(2)} = \frac{16 |t_{ij}|^2 |t_{kl}|^2}{(E - U)^2} \frac{2}{E - 2U} \left\{ \mathcal{K}_{ij}, \mathcal{K}_{kl} \right\}.
\tag{3.69}
$$

The additional factor of 2 comes from counting all the possible sequences of spin flip processes. For brevity we assume (again) equal couplings $t_{ij} = t_{kl} = t$, and

$$
H_{ijkl}^{(2)} = \frac{2}{E - 2U} \frac{16 |t|^4}{(E - U)^2} \left[\left(\sum_{\langle i,j \rangle} \mathcal{K}_{ij} \right)^2 - \sum_{\langle i,j,k \rangle} \left\{ \mathcal{K}_{ij}, \mathcal{K}_{jk} \right\} - \sum_{\langle i,j \rangle} \mathcal{K}_{ij}^2 \right].
\tag{3.70}
$$

So starting from the product $\mathcal{K}^2$ we must remove the additional contributions from all sets of neighbor pairs sharing a single vertex, $\langle i, j \rangle$ and $\langle j, k \rangle$ with $i \neq k$.

If one remembers that the anti-commutator involving the spatial components (x, y, z) of the Pauli spin operators behave like, $\{S_i^a, S_i^b\} = \frac{1}{2} \delta_{a,b}$, it is straightforward to show that

$$\left\{ \mathcal{K}_{ij}, \mathcal{K}_{jk} \right\} = -\frac{1}{2} \left(\mathcal{K}_{ij} + \mathcal{K}_{jk} - \mathcal{K}_{ik} \right). \tag{3.71}$$

We can rewrite all this as

$$H^{(2)} = \frac{8|t|^4}{(E-U)^2} \frac{2}{E-2U} \left(2\mathcal{K}^2 + \sum_{\langle i,j,k \rangle} (\mathcal{K}_{ij} + \mathcal{K}_{jk} - \mathcal{K}_{ik}) + 2\mathcal{K} \right). \tag{3.72}$$

Expressing H in units of hopping $|t|$ allow to write the Hamiltonian in terms of the dimensionless parameter $\alpha = |t|/(E-U)$.

$$H' = 4\alpha\mathcal{K} + 32\alpha^3(\mathcal{K} + \mathcal{K}^2) + 4\alpha^3 \sum_{\langle i,j,k \rangle} \left(2\mathcal{K}_{ij} + 2\mathcal{K}_{jk} - 3\mathcal{K}_{ik} \right). \tag{3.73}$$

When $|U| \gg |E|$ instead (note that α changes with $E - U$),

$$H' \approx 4\alpha\mathcal{K} + 16\alpha^3(\mathcal{K} + \mathcal{K}^2) - 4\alpha^3 \sum_{\langle\langle i,k \rangle\rangle} \mathcal{K}_{ik}. \tag{3.74}$$

Ignoring the terms with three connected sites, both Hamiltonians are of the form

$$H' = a(E', U')\mathcal{K} + b(E', U')\mathcal{K}^2. \tag{3.75}$$

Solving Schrödinger's equation $H'|\psi\rangle = E'|\psi\rangle$, shows us that while the relevant energies E' can depend on the coefficient functions a and b, the actual *eigenfunctions* are *still* the same. Hence the eigenfunctions to first order in J, are *very* close to the eigenfunctions even up to J^2 order.

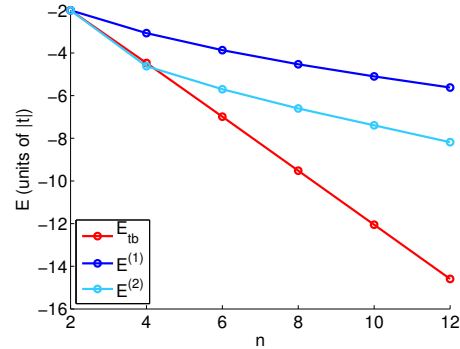| n	$E_{TB}/|t|$	$E_{vb}^{(1)}/|t|$	$E_{vb}^{(2)}/|t|$
2	-2	-2	–
4	-4.472	-3.07	-4.62
6	-6.988	-3.87	-5.70
8	-9.518	-4.53	-6.60
10	-12.053	-5.10	-7.39
12	-14.593	-5.62	-8.18

Figure 3.5: Comparison of the valence bond energies $E_{vb}^{(1)}$, $E_{vb}^{(2)}$, and the exact tight-binding ground state energy for chains of length n at $U = 0$.

To benchmark how well the ground state energy is determined, we calculate the energy using the usual t-J model E_J with $J = 4t^2/U$, or the usual $E^{(1)}$ with $J = 4t^2/(U - E)$. Lastly we calculate the energy $E^{(1)}$ from the full self-consistent equation including corrections $H^{(2)}$ (but ignoring the term concerned with three connected sites).

n	E_H /$|t|$	E_J /$|t|$	$E_{vb}^{(1)}$ /$|t|$	$E_{vb}^{(2)}$ /$|t|$
2	-0.828	-1	-0.83	–
4	-1.952	-2.37	-1.65	-2.18
6	-3.093	-3.74	-2.36	-3.11
8	-4.236	-5.12	-2.95	-3.93
10	-5.381	-6.51	-3.48	-4.66
12	-6.526	-7.89	-3.96	-5.32

Figure 3.6: Comparison of the valence bond energies E_J, $E_{vb}^{(1)}$, $E_{vb}^{(2)}$, and the Hubbard ground state energy for chains of length n at $U = 4|t|$.

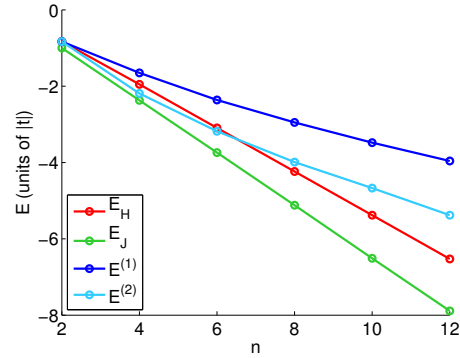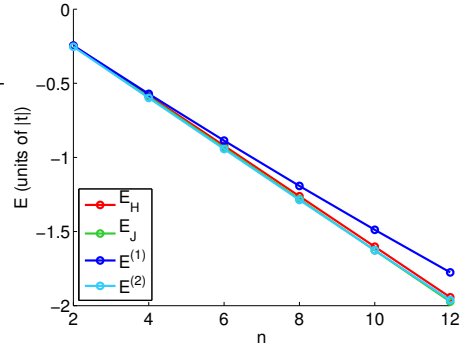| n	E_H /$|t|$	E_J /$|t|$	$E_{vb}^{(1)}$ /$|t|$	$E_{vb}^{(2)}$ /$|t|$
2	-0.2462	-0.2500	-0.2462	–
4	-0.5826	-0.5915	-0.5711	-0.5986
6	-0.9219	-0.9359	-0.8867	-0.9438
8	-1.2621	-1.2812	-1.1924	-1.2868
10	-1.6028	-1.6270	-1.4885	-1.6265
12	-1.9437	-1.9730	-1.7759	-1.9624

Figure 3.7: Comparison of the valence bond energies E_J, $E_{vb}^{(1)}$, $E_{vb}^{(2)}$, and the Hubbard ground state energy for chains of length n at $U = 16|t|$.

For chains of different lengths, and using various values of U the resulting energies are shown in Figures 3.5, 3.6 and 3.7 along with the exact results. Obviously the second highest order of perturbation theory yields the best result, but perhaps surprisingly valence bond theory seems equally adequate at describing both non-interacting and strongly interacting systems.

3.10   Conclusions

In this chapter we have derived the fundamentals of the *neoclassical* valence bond theory, and shown how the valence bond method offers a controlled way of calculating many-body properties perturbatively in the exchange coupling $J/U = 4|t|^2/U^2$. The solution of the molecular many-body problem converges quickly and the treatment can in principle be calculated to higher orders.

We have shown how to calculate the molecular ground state, and how to consistently deal with the non-orthogonal Rumer basis. We have further shown that even though valence bond theory is restricted to a subspace of the Hamiltonian the results of the valence bond energy calculation still offer precise results.

Chapter 4

Quantum Transport

The advent of nanotechnology have made it possible to build devices and perform experiments on the molecular scale. One field, which this technological development have furthered, owes its existence to a human urge as old as Mary Shelley, the author of "Dr. Fankenstein". The field of *quantum transport* mercilessly probes miniscule quantum systems by passing an electrical current through them. And who knows, one day the molecules finally produce an experimental physicist will experience the Eureka moment of bringing one of those systems to life...

Quantum transport is mostly concerned with probing low dimensional systems in the form of various semi-conductor hetereostructures[38] or synthesized organic molecules. Molecule experiments can be done in several ways. One approach is to deposit the molecule as a thin film on a conducting surface and probe the electric properties of the molecule using a scanning tunneling microscope (STM).[47] Another approach involves creating a break junction, where a small gold constriction is broken lightly by mechanical means, creating a nano gap where the molecules can be deposited.[65,66] There exist various other techniques, e.g. electromigration[40,120] or nano-sized junctions with graphene electrodes formed from electroburning.[85]
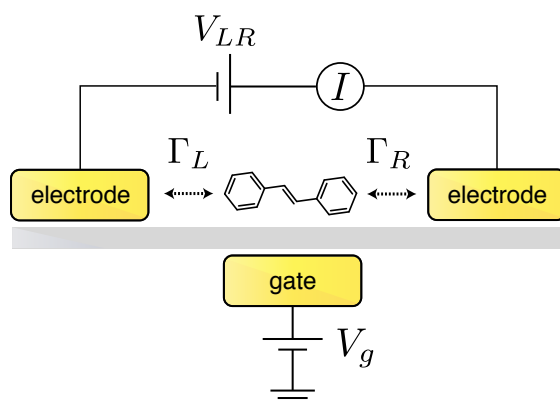
Figure 4.1: Schematic of a quantum junction. A quantum system (in this case a molecule) is coupled to two macroscopic electrodes – also called *leads*. By controlling the local electrostatic environment by a backgate V_g, and applying a voltage V_{LR} across the junction the current response I is measured. The size of the coupling between the molecule and the electrodes are captured by the tunneling rates Γ_L, Γ_R.

In general we shall model the typical quantum transport setup as a quantum system (molecule) attached to two electrodes between which there is a bias voltage V_{LR}. A backgate V_g controls the local electrostatic environment. A schematic is presented in Figure 4.1.

In this chapter we will first describe a general quantum dot using the constant interaction model, and use this model to obtain a phenomenological understanding the transport features of a Coulomb blockaded quantum junction. Then we turn to a perturbative analytical derivation of the quantum transport, focusing on the off-resonant coherent transport. The treatment is finished with a quick discussion about the differences and similarities of single-orbital transport and multiple orbital transport (a molecule).

4.1   The Constant Interaction Model

The constant interaction model[53] is a simplified representation of the quantum system energy levels. The model assumes that the quantum system (independent of the number of electrons occupying it) can be described using single particle states with an energy spectrum E_i. The Coulomb interaction between the electrons in the quantum system can be modeled by a uniform (constant) electron-electron repulsion, U. The backgate V_g simply changes the local electrostatic potential on the quantum system.

The many-body ground state energy $\mathcal{E}_N$ then depends directly on the number of the dot electrons N, and we have the energies $\mathcal{E}_N = \frac{1}{2}UN(N-1) + \sum_{i=1}^{N} E_{\lfloor i/2 \rfloor} + eNV_g$. Then the energy differences are

$$\Delta\mathcal{E}_N = \begin{cases} \Delta E_{(N+1)/2} + U(N-1) - eV_g & \text{for } N \text{ odd,} \\ U(N-1) - eV_g & \text{for } N \text{ even,} \end{cases} \tag{4.1}$$

where we have introduced $\Delta E_i = E_i - E_{i-1}$.
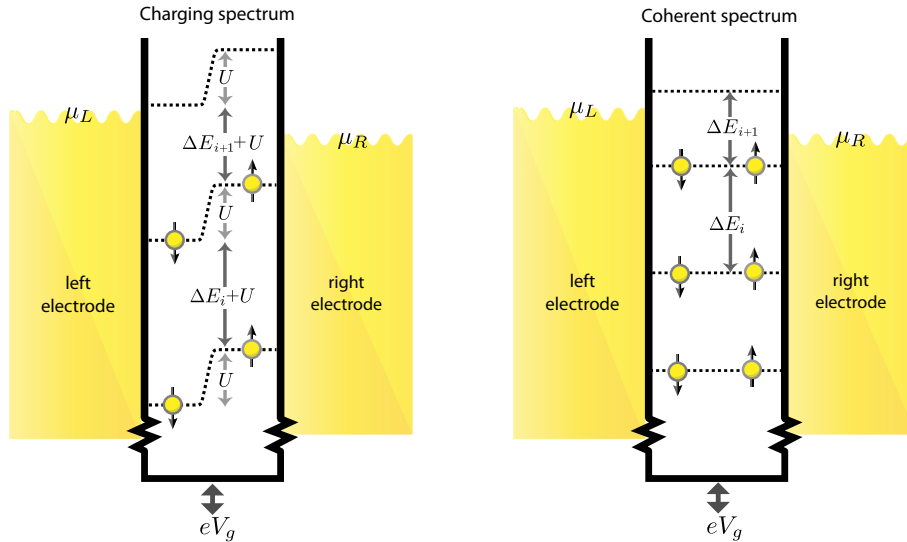
Figure 4.2: **The constant interaction model** models a quantum dot as an artificial atom which can be charged by tuning the gate voltage. *The charge spectrum* describes the energies related to the charging of the quantum system. Whenever a sublevel is present within the bias window there is resonant transport. *The coherent spectrum* with the interaction removed is relevant for the coherent transport, which does not charge the system.

In the constant interaction model two different charge ground states are degenerate $\Delta \mathcal{E}_N = 0$, when the gate is tuned at

$$eV_g = \begin{cases} \Delta E_{N/2} + UN & \text{for } N \text{ odd,} \\ UN & \text{for } N \text{ even,} \end{cases} \qquad (4.2)$$

where we have removed a superfluous offset, U. The gate difference between consecutive charge degeneracy points is also called the charging energy or the addition energy,

$$E_{add}^N = \begin{cases} \Delta E_{N/2} + U & \text{for } N \text{ odd,} \\ U & \text{for } N \text{ even.} \end{cases} \qquad (4.3)$$

A graphical depiction of the charge degeneracy points of the constant interaction model is shown in Figure 4.2.

4.1.1 Coulomb Blockade

Assume that the lead electrons are kept at a temperature $k_B T > \hbar\Gamma$. When the coupling rates between the molecule and the electrodes are much smaller than the electronic charging energy, $\hbar\Gamma_L, \hbar\Gamma_R \ll E_{add}$, the quantum system is weakly coupled to the electrodes. According to perturbation theory the coherent transport processes are then suppressed by a factor $\hbar^2 \Gamma_L \Gamma_R / (E - E_{add})^2$. However, when the electron energy E resonates with the addition energy $E_{add} = E = -\alpha e V_g + \varepsilon$ electrons can tunnel trough the junction effortlessly. This is the resonant transport regime, and by consulting the charging spectrum in Figure 4.2, it can be shown that resonant tunneling is only possible when an energy level lies within the bias window, i.e., $\Delta \mathcal{E}_i \in [\mu_R, \mu_L]$.
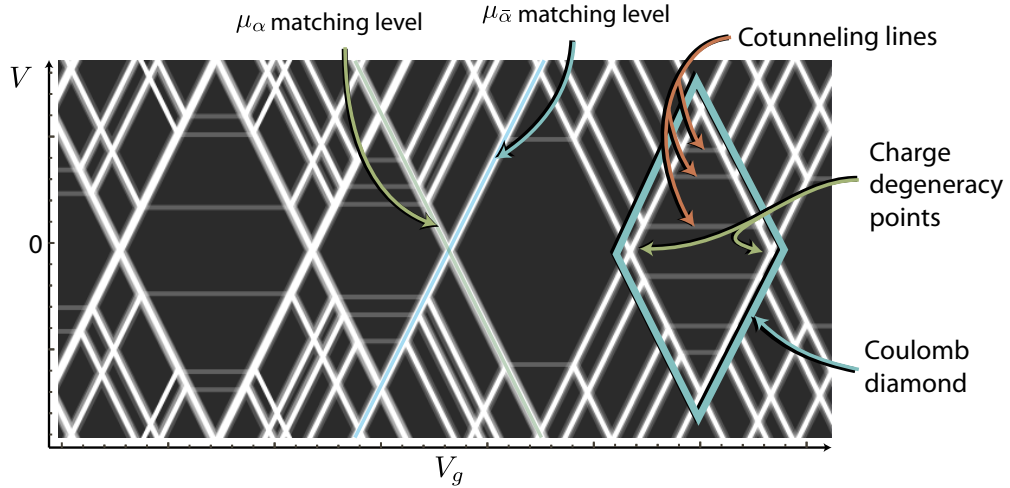

Figure 4.3: **Charge stability diagram**. The differential conductance dI/dV_{LR} plotted as a function of gate V_g and bias V_{LR}. Note the pattern of alternating diamond size in consistency with the constant interaction model. Here we have chosen a symmetric bias $\mu_L = eV/2$ and $\mu_R = -eV/2$. However, for asymmetric couplings, the edges of the diamond structure are controlled by chemical potential, as indicated in the figure. Asymmetric couplings will in general produce skewed diamonds.

Usually only the bias voltage $eV_{LR} = \mu_R - \mu_L$ can be controlled experimentally. It can be argued that when the molecule couples more strongly to one electrode, the chemical

potential of that electrode will be pinned to the quantum energy levels, and the bias will only control the chemical potential of the other electrode. When the electrodes couple symmetrically to the molecule, the bias controls the chemical potentials symmetrically: $\mu_L = V/2$ and $\mu_R = -V/2$.

Figure 4.3 shows a typical charge stability diagram plotting the differential conductance dI/dV_{LR} as a function of bias voltage V_{LR} and backgate V_g. The resonant transport is clearly visible as lines of enhanced conductance forming a *Coulomb* diamond structure. Note the alternation of diamond size, which is consistent with the constant interaction model.

In the off-resonant regime within the Coulomb diamonds, the resonant tunneling is exponentially suppressed by the distance to the diamond edge as well as the inverse temperature. At low temperatures electron transport is dominated by coherent processes known as *co-tunneling*. The quantum system does not change charge state during these processes and hence the (aptly named) coherent spectrum of Figure 4.2 applies. By increasing the bias voltage co-tunneling can also happen via excited states of the quantum system. This sudden increase in the number of transport channels is the explanation for the co-tunneling lines, which show up in the charge stability diagrams (cf. Figure 4.3).

It is well known that many semiconductor quantum junctions can be Coulomb blockaded, and experiments have also found molecular junctions exhibiting such blockade effects.[74]

4.2 Current

Applying a bias voltage V across the molecular junction causes a current, I to flow through the device. We calculate this current perturbatively to second order in the coupling between the molecule and the leads. Assuming that the molecular junction is in the Coulomb blockade regime with the couplings being small compared to the addition energy, this perturbative expansion is well-behaved in the off-resonant transport regime.

Both the left and the right electrode are modeled as a non-interacting electron gas at thermal equilibrium, with an electrode chemical potential μ_α and a density of states $\rho_\alpha(\varepsilon)$, and are described by simple quadratic Hamiltonian,

$$\hat{H}_\alpha = \sum_{\nu\sigma} \xi_{\alpha\nu}\hat{c}^\dagger_{\alpha\nu\sigma}\hat{c}_{\alpha\nu\sigma} = \int_{-\infty}^{\infty} d\varepsilon\, \rho_\alpha(\varepsilon)\hat{c}^\dagger_{\alpha\sigma}(\varepsilon)\hat{c}_{\alpha\sigma}(\varepsilon) \qquad \text{with } \alpha \in \{Left, Right\} \qquad (4.4a)$$

Here $\xi_{\alpha\nu} = \varepsilon_{\alpha\nu} - \mu_\alpha$, where $\varepsilon_{\alpha\nu}$ is the dispersion of electrodes and ν are the quantum numbers of the electrode continuum states.

The molecular electronic system is described by a Hamiltonian $\hat{H}_m$. With N electrons occupying the molecule, it is solved by the electronic eigenfunctions $|\psi_i^N\rangle$ with eigenenergies E_i^N. Let us introduce the excitation energies $\varepsilon_i^0 = E_i^N - E_0^N$. The energy costs of adding an electron to the N electron molecular eigenstate $|\psi_m^N\rangle$, are given by $\varepsilon_{nm}^p = E_n^{N+1} - E_m^N$, and the energies needed to remove an electron from that same eigenstate, are given by $\varepsilon_{nm}^h = E_m^N - E_n^{N-1}$.

The presence of a backgate V_g allow us to tune the electrostatic energy of the molecule,

$$\hat{H}_g = -\kappa e V_g \hat{N}, \qquad (4.4b)$$

where we have introduced the dimensionless electrostatic coupling parameter κ. By adding this term to the molecular Hamiltonian the energies of the N-electron molecular eigenstates $|\psi_i^N\rangle$ are shifted to $\tilde{E}_i^N = E_i^N - \kappa e V_g N$.

The starting point for our perturbative analysis is the completely uncoupled system, described by the Hamiltonian,

$$\hat{H}_0 = \sum_{\alpha=L,R} \hat{H}_\alpha + \hat{H}_m + \hat{H}_g. \tag{4.4c}$$

Introduce a hybridization $\hat{H}_T$, which couples the molecule and the electrodes. For brevity we assume that only one molecular orbital i_α couples to either lead $\alpha = L, R$. In that case the hybridization can be written

$$\hat{H}_T = \sum_{\alpha,\nu,\sigma} (t_{\alpha,i_\alpha} \hat{c}^\dagger_{i_\alpha\sigma} \hat{c}_{\alpha\nu\sigma} + h.c.). \tag{4.4d}$$

Applying a bias voltage $V_{LR} = \mu_L - \mu_R$ across the molecular junction by tuning the chemical potentials of the two electrodes, the system can sustain a current through the molecule by the tunneling of either electrons or holes from one electrode to the other.

4.2.1 The Fermi Golden Rule

The transition of a quantum system from an initial state $|i\rangle$ to the final state $|f\rangle$ happens at at rate Γ_{fi}, given by Fermi's golden rule [14, p. 86-88],

$$\Gamma_{fi} = \frac{2\pi}{\hbar} \left| \langle f | \hat{T} | i \rangle \right|^2 \delta(E_f - E_i). \tag{4.5}$$

Here the $\hat{T}$-matrix is given as,

$$\hat{T}(E) = \hat{H}_T + \hat{H}_T \frac{1}{E_i - \hat{H}_0 + i\eta} \hat{T}. \tag{4.6}$$

4.2.2 Sequential Tunneling

There are no coherent transport processes when expanding to second order in the hybridization $\hat{H}_T$. However, sequential transport with electrons incoherently tunneling on and off the molecule are permitted.

The rate at which electrons tunnel onto the molecule and excite it from the eigenstate n to the state m is given by

$$\Gamma^{p\alpha}_{nm} = \Gamma_\alpha n_\alpha(\varepsilon^{pN}_{nm} - \kappa e V_g) \left| \langle \Psi^{N+1}_n | \hat{c}^\dagger_{i_\alpha\sigma} | \Psi^N_m \rangle \right|^2. \tag{4.7}$$

Here we have defined the rate $\Gamma_\alpha = 2\pi |t_{\alpha i_\alpha}|^2 \rho_\alpha / \hbar$ if assuming a constant density of states, $\rho_\alpha(\varepsilon) = \rho_\alpha$. The $n_\alpha(\varepsilon) = 1/(\exp((\varepsilon - \mu_\alpha)k_b T) + 1)$ is the Fermi-Dirac distribution function.

Similarly one can define rates for the holes tunneling off the molecule

$$\Gamma^{h\alpha}_{nm} = \Gamma_\alpha \left(1 - n_\alpha(\kappa e V_g - \varepsilon^{hN}_{nm}) \right) \left| \langle \Psi^N_m | \hat{c}_{i_\alpha\sigma} | \Psi^{N+1}_n \rangle \right|^2. \tag{4.8}$$

At vanishing temperature $T \to 0$, the Fermi-Dirac distribution approaches a Heaviside step function, and within the off-resonant transport regime, either $\Gamma^{p\alpha}_{nm}$ or $\Gamma^{h\alpha}_{nm}$ vanishes. Hence in the zero-temperature limit sequential tunneling only belongs to the resonant transport regime, and turning up the temperature allows for an exponentially suppressed sequential tunneling tail in the off-resonant regime.

At an infinitesimal bias $\mu_L \to \mu_R$, the calculation becomes particularly simple and the sequential tunneling rates vanish anywhere but outside the parameter regime where $|\varepsilon^{pN}_{00}| < |eV_{LR}|$. Hence sequential tunneling marks the edge of the Coulomb diamonds, and the conductance due to sequential tunneling at the charge degeneracy point is usually proportional to the quantum of conductance $G_0 = 2e^2/h$, with a proportionality constant $\Gamma_L \Gamma_R / (\Gamma_L + \Gamma_R)$.

4.2.3 Co-Tunneling

To fourth order in the hybridization, $\hat{H}_T$, we find the first contribution to coherent electron transport across the molecular junction. Initially the molecule is in the ground state of the uncoupled system, $|i\rangle = |\Psi_0\rangle = |\Psi_0^R\rangle|\Psi_0^L\rangle|\Psi_0^N\rangle$. We then consider the transition to a final state $|\Psi_\alpha\rangle = \hat{c}_{\beta\sigma}^\dagger(\varepsilon_\beta)\hat{c}_{\alpha\gamma}(\varepsilon_\alpha)|\Psi_n^N\rangle|\Psi_0^R\rangle|\Psi_0^L\rangle$ with one electron transferred between electrodes α and β, and the molecule possibly transitioned to some eigenstate $|\Psi_n^N\rangle$. The Fermi golden rule (4.5) gives the rate,

$$\Gamma_{\alpha\beta}^{\gamma\sigma}(\varepsilon_\alpha, \varepsilon_\beta) = \frac{2\pi}{\hbar}\left|\langle\Psi_n^N|\langle\Psi_0^R|\langle\Psi_0^L|\hat{c}_{\alpha\gamma}(\varepsilon_\alpha)\hat{c}_{\beta\sigma}(\varepsilon_\beta)\hat{H}_T\frac{1}{E_0 - \hat{H}_0}\hat{H}_T|\Psi_0\rangle\right|^2 \delta(\varepsilon_\alpha + \varepsilon_n^0 - \varepsilon_\beta). \quad (4.9)$$

The next step is to insert the expression for $\hat{H}_T$, keeping only terms in the calculation which effectively transports an electron between the electrodes. Next, utilizing that the initial state is an eigenstate of $\hat{H}_0|\Psi_0\rangle = (E_{0L} + E_{0R} + E_0^N)|\Psi_0\rangle$ and that $\hat{H}_\alpha\hat{c}_\alpha(\varepsilon)|\Psi_{\alpha 0}\rangle = (E_{0\alpha} - \varepsilon)\hat{c}_\alpha(\varepsilon)|\Psi_{\alpha 0}\rangle$ and $\hat{H}_0\hat{c}_\alpha^\dagger(\varepsilon)|\Psi_{\alpha 0}\rangle = (E_{0\alpha} - \varepsilon)\hat{c}_\alpha^\dagger\varepsilon)|\Psi_{\alpha 0}\rangle$ equation (4.9) reduces to

$$\Gamma_{\alpha\beta}^{\gamma\sigma}(\varepsilon_\alpha, \varepsilon_\beta) = \frac{2\pi}{\hbar}|t_{Li_L}|^2|t_{Ri_R}|^2\langle 1 - \hat{n}_{\beta\sigma}(\varepsilon_\beta)\rangle\langle\hat{n}_{\alpha\gamma}(\varepsilon_\alpha)\rangle\sum_n\left|p_{n,0}^{\gamma\sigma}(\varepsilon_\alpha) + h_{n,0}^{\gamma\sigma}(\varepsilon_\alpha)\right|^2 \delta(\varepsilon_\alpha + \varepsilon_n - \varepsilon_\beta).$$

Here the two amplitudes p and h are given by,

$$p_{m,n}^{\gamma\sigma}(V_g, \omega) = \langle\Psi_m|\hat{c}_{i_\alpha\gamma}\frac{1}{\kappa eV_g + \omega + E_0^N - \hat{H}_m + i0^+}\hat{c}_{i_\beta\sigma}^\dagger|\Psi_n\rangle, \quad (4.10)$$

$$h_{m,n}^{\gamma\sigma}(V_g, \omega) = \langle\Psi_m|\hat{c}_{i_\beta\sigma}^\dagger\frac{1}{\kappa eV_g + \omega - E_0^N + \hat{H}_m - i0^+}\hat{c}_{i_\alpha\gamma}|\Psi_n\rangle. \quad (4.11)$$

We assume now for simplicity that the molecule always relaxes to its ground state after each tunneling event. This can be achieved in the limit of asymmetric couplings, e.g. $|t_{Li_L}| >> |t_{Ri_R}|$, where the molecule is in near perfect equilibrium with one electrode.

When applying a bias voltage $eV_{LR} = \mu_L - \mu_R > 0$ across the molecule, the total current is proportional to the sum of the rates of all the current carrying processes taking place. When considering electrodes with a constant density of states, ρ_α, the total current is simply

$$I = I_{RL} - I_{LR} = e\rho_L\rho_R\int_{-\infty}^{\infty}d\varepsilon_L\int_{-\infty}^{\infty}d\varepsilon_R\sum_{\sigma\gamma}\{\Gamma_{RL}(\varepsilon_R, \varepsilon_L) - \Gamma_{LR}(\varepsilon_L, \varepsilon_R)\}. \quad (4.12)$$

When the temperature is the smallest energy scale of the system, we can approximate the Fermi-Dirac distribution with a Heaviside step function. Assuming $V > 0$, the total current can then be simplified to,

$$I(V_g, V_{LR}) = \frac{e\hbar}{2\pi}\Gamma_L\Gamma_R\sum_{m,\sigma}\int_{-eV_{LR}/2+\varepsilon_m^0}^{eV_{LR}/2}\theta(|eV_{LR}| - \varepsilon_m^0)d\omega\left|h_{m,0}^{\gamma\sigma}(V_g, \omega - \varepsilon_m^0) + p_{m,0}^{\gamma\sigma}(V_g, \omega)\right|^2.$$

$$(4.13)$$

And inserting a complete set of states the two amplitudes can be written,

$$p_{m,n}^{\gamma\sigma}(V_g, \omega) = \sum_l \frac{\langle \Psi_m^N | \hat{c}_{i_\alpha\gamma} | \Psi_l^{N+1} \rangle \langle \Psi_l^{N+1} | \hat{c}_{i_\beta\sigma}^\dagger | \Psi_n^N \rangle}{\kappa e V_g + \omega - \varepsilon_{ln}^p + i0^+}, \tag{4.14}$$

$$h_{m,n}^{\gamma\sigma}(V_g, \omega) = \sum_l \frac{\langle \Psi_m^N | \hat{c}_{i_\beta\sigma}^\dagger | \Psi_l^{N-1} \rangle \langle \Psi_l^{N-1} | \hat{c}_{i_\alpha\gamma} | \Psi_n^N \rangle}{\kappa e V_g + \omega - \varepsilon_{ln}^h - i0^+}. \tag{4.15}$$

While the poles of the p and h amplitudes all lie outside the off-resonant regime, we can ignore their imaginary component, i.e., $|p+h|^2 = (\mathrm{Re}(p) + \mathrm{Re}(h))^2$. In a Hubbard/PPP model the ground state can be calculated by exact diagonalization as shown in section 2.3. Then the particle and hole amplitudes can be calculated using the Lanczos method as described in section 2.3.2.

4.3 The Feynman-Dyson Orbitals

Let us define the *Feynman-Dyson orbitals* for a given charge state, N,

$$\langle i\sigma | \phi_n^p \rangle = \langle \Psi_n^{N+1} | \hat{c}_{i\sigma}^\dagger | \Psi_n^N \rangle, \tag{4.16a}$$

$$\langle i\sigma | \phi_n^h \rangle = \langle \Psi_n^{N-1} | \hat{c}_{i\sigma} | \Psi_0^N \rangle. \tag{4.16b}$$

Here we have written the Feynman-Dyson orbitals as state kets, hinting that they constitute a basis in some single particle Hilbert space. In single-particle models like the Hartree self-consistent-field or the non-interacting Hückel models, the Feynman-Dyson orbitals are identical to the molecular orbitals.
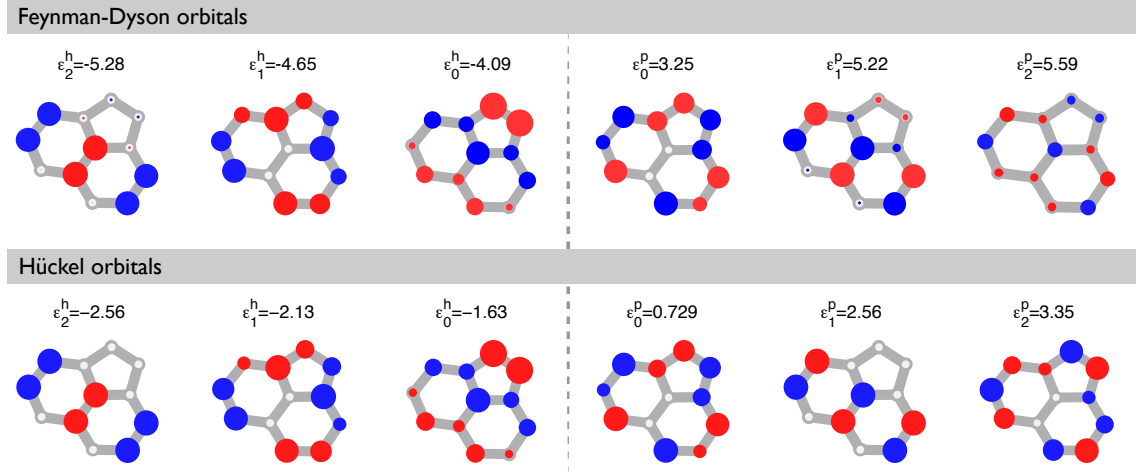

Figure 4.4: Feynman-Dyson orbitals (only the six closest) for the neutral acenaphthylene π-system, and the Hückel molecular orbitals (only six closest). The largest discrepancy happens for the ε_1^p case, where some Hückel nodes have vanished in the PPP model Feynman-Dyson orbital, or at the ε_2^p case, where the orbitals differ substantially.

The Feynman-Dyson orbitals and the excitation spectra constitutes the only requisite ingredients for the sequential tunneling calculation (cf. equation (4.7)) and the co-tunneling calculation (cf. equation (4.15)). The molecular structure determines the Feynman-Dyson

orbitals, and in the next chapter we will discuss some relations between molecular structure and the Feynman-Dyson orbitals, and will investigate the consequences for the off-resonant transport.

For the small set of molecular systems we have considered, the closest Feynman-Dyson orbitals of the PPP model are quite similar to the Hückel molecular orbitals. As a "typical" example consider the neutral acenaphthylene π-system presented in Figure 4.4.

When the lowest Feynman-Dyson orbitals $\phi_0^{p/h}$ vanish on certain sites, sequential tunneling current can be suppressed because the molecule becomes trapped in a single quantum state.[14] This is the common explanation for negative differential resistance[57] present in e.g., charged benzene.[10]

4.4 Conclusions

This chapter presented a short review of some analytical methods for understanding and dealing with electron transport through quantum systems. The main result is the expression of the co-tunneling current (cf. equation (4.13)) expressed in terms of particle and hole amplitudes, which we will return to in the coming chapters.

Chapter 5

Quantum Interference

In the early 1800s Thomas Young demonstrated the wave nature of light using a double slit experimental setup. Coherent light passing through the two slits interfered destructively or constructively depending on the path length difference between them, forming the well-known interference pattern shown in Figure 5.1.

It is even more surprising that Young's double slit experiment works with single particles, where the particle simultaneously "follows both paths" through the double slit and interferes constructively (destructively) with itself. This is indeed impossible in classical physics, and it makes interference an inherent quantum mechanical phenomenon. Young's double slit experiment have also been carried out with single electrons,[28] or even large molecules,[48] hence proving the wave nature of their propagation.
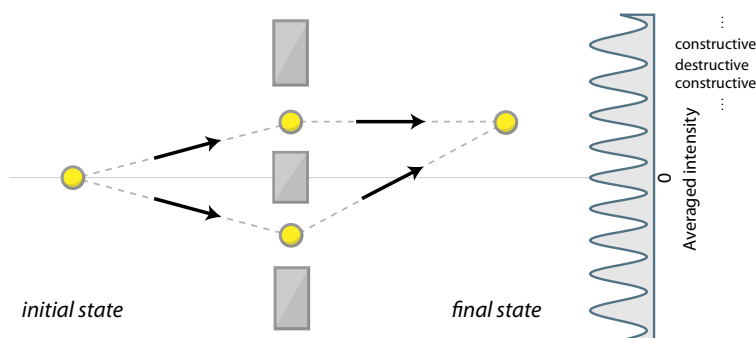

Figure 5.1: Young's double slit experiment demonstrating single particle interference.

It is easy to translate the concept of single particle quantum interference to molecular quantum transport. Naively, electrons tunnel through the molecule and depending on the molecular structure, the propagation of the electronic wavefunction is either enhanced or destroyed due to constructive or destructive interference. Even though this naive picture is oversimplified, quantum interference effects are present in molecular junctions.

The ability to control such quantum interference effects have potential applications in various fields such as molecular quantum information processing,[108] or for the design of effective molecular thermoelectric devices.[49,107,114]

In this chapter we shall examine quantum interference in the off-resonant transport through molecular junctions in the Coulomb blockade regime. Several quantum chemical numerical calculations have already investigated this phenomena in strongly coupled systems.[6,50,62,103,104,119] Some analytical results have been obtained for non-interacting

model systems.[64] Quantum interference in molecules have also been found experimentally in several experiments for quinone molecules.[37,87]

We describe the molecule π-system using the full Pariser-Parr-Pople model from equations (2.15)-(2.18),

$$\hat{H}_{\mathrm{PPP}} = \hat{T} + \hat{H}_\mu + \hat{H}_U + \hat{H}_V \tag{5.1}$$

$$\hat{T} = \sum_{\langle i,j \rangle} \sum_{\sigma=\uparrow,\downarrow} \left(t_{ij}\hat{c}^\dagger_{i,\sigma}\hat{c}_{j,\sigma} + t_{ji}\hat{c}^\dagger_{j,\sigma}\hat{c}_{i,\sigma} \right), \tag{5.2}$$

$$\hat{H}_\mu = \sum_i \mu_i \hat{n}_i, \tag{5.3}$$

$$\hat{H}_U + \hat{H}_V = \sum_i U_i(\hat{n}_{i\uparrow} - \tfrac{1}{2})(\hat{n}_{i\downarrow} - \tfrac{1}{2}) + \frac{1}{2}\sum_{i \neq j} V_{ij}(\hat{n}_i - z_i)(\hat{n}_j - z_j). \tag{5.4}$$

Here $\langle i,j \rangle$ represents all nearest neighbor pairs.

In the following we will divide our analysis of the transport through the π-system according to the electronic ground state degeneracy. Most of our attention will be focused on the investigation of transport through a molecular system, which has a non-degenerate electronic ground state. Later, we also analyze transport through spin-degenerate doublet ground states.

5.1   Non-Degenerate (Spin-Singlet) Ground State

Let us start simple, by assuming that the molecular ground state under consideration is non-degenerate. Later in this chapter we will also investigate spin degenerate ground states, but for now we will try to make a clear case of quantum interference in the off-resonant transport through a non-degenerate (hence spin-singlet) N-electron molecule ground state. Remember that this means that we consider a charge state with an even number of electrons N. The current through the junction at zero temperature $T = 0$ is given by equation (4.13),

$$I(V_g, V_{LR}) = \frac{e\hbar}{2\pi}\Gamma_L\Gamma_L \sum_{m,\sigma} \int_{-eV_{LR}/2+\varepsilon^0_m}^{eV_{LR}/2} \theta(|eV_{LR}| - \varepsilon^0_m)\mathrm{d}\omega \left| h^{\gamma\sigma}_{m,0}(V_g, \omega - \varepsilon^0_m) + p^{\gamma\sigma}_{m,0}(V_g, \omega) \right|^2. \tag{5.5}$$

At zero-bias we can drop the condition that one electrode couples more strongly to the molecule (cf. section 4.2.3), and the off-resonant conductance is simply,

$$G = \frac{e^2\hbar}{2\pi}\Gamma_L\Gamma_R \sum_{\sigma=\uparrow,\downarrow} \left| h^{\sigma\sigma}_{0,0}(V_g, 0) + p^{\sigma\sigma}_{0,0}(V_g, 0) \right|^2, \tag{5.6}$$

with the particle (p) and hole (h) amplitudes,

$$p^{\gamma\sigma}_{0,0}(V_g, \omega) = \sum_l \frac{\langle \Psi^N_0 | \hat{c}_{i_\alpha\gamma} | \Psi^{N+1}_l \rangle \langle \Psi^{N+1}_l | \hat{c}^\dagger_{i_\beta\sigma} | \Psi^N_0 \rangle}{\kappa eV_g + \omega - \varepsilon^p_{l0} + i0^+}, \tag{5.7}$$

$$h^{\gamma\sigma}_{0,0}(V_g, \omega) = \sum_l \frac{\langle \Psi^N_0 | \hat{c}^\dagger_{i_\beta\sigma} | \Psi^{N-1}_l \rangle \langle \Psi^{N-1}_l | \hat{c}_{i_\alpha\gamma} | \Psi^N_0 \rangle}{\kappa eV_g + \omega - \varepsilon^h_{l0} - i0^+}. \tag{5.8}$$

Note that equation (5.6) only holds when the N-electron charge state is also the total ground state, which is true for gate voltages $\kappa eV_g \in [\varepsilon^h_{00}, \varepsilon^p_{00}]$. Note also that we have

ignored the contribution from sequential tunneling, and we should *only* trust this expression anywhere near the charge degeneracy points at $\varepsilon_{00}^{h/p}$.

This zero-bias conductance formula and the transport amplitudes of equation (5.8) houses several clues about molecule quantum interference, and in the following we will in some detail derive those constraints.

The hole and particle amplitudes in equation (5.8), is a sum of simple poles located at gate voltages $\kappa e V_g = \varepsilon_{n0}^{h/p}$. As shown in Figure 5.2, the relative sign of the poles at $\varepsilon_{00}^{h/p}$ puts a *topological constraint* on the quantum interference features:

1. When the two divergences share the same sign, one of the amplitudes, p or h, goes to infinity, and the other goes to minus infinity, when approaching the pole from point within $[\varepsilon_{00}^{h}; \varepsilon_{00}^{p}]$. Hence the total amplitude $h + p$ *must* cross zero an *odd* number of times.

2. On the other hand when the divergences have opposite signs h and p will both go to positive or negative infinity from within $[\varepsilon_{00}^{h}; \varepsilon_{00}^{p}]$. This means that the total amplitude $h + p$ must cross zero an even number of times, meaning an *even* number of zeros in the conductance G.

While this fact have been sporadically mentioned for non-interacting systems,[62,110–112] we will show that many more interesting consequences come from this simple observation.

To formalize our arguments we introduce a classification of the quantum interference pattern, and a transport process with an odd (even) number of nodes belongs in the odd (even) quantum interference class. Based on this reasoning. we conjure up an entity capturing the quantum interference class, by taking the ratio of the numerators of the two dominating poles of the total amplitude $p + h$ located at $\varepsilon_{00}^{h/p}$,

$$\mathcal{Q}i \equiv \frac{\sum_n \langle \Psi_0^N | \hat{c}_{i_L\sigma}^\dagger | \Psi_{0n}^{N-1} \rangle \langle \Psi_{0n}^{N-1} | \hat{c}_{i_R\sigma} | \Psi_0^N \rangle}{\sum_m \langle \Psi_0^N | \hat{c}_{i_R\sigma} | \Psi_{0m}^{N+1} \rangle \langle \Psi_{0m}^{N+1} | \hat{c}_{i_L\sigma}^\dagger | \Psi_0^N \rangle}, \tag{5.9}$$

where we have added a sum over the degeneracy of the $N \pm 1$ ground states, $|\Psi_{0m}^{N\pm1}\rangle$. Here $\mathcal{Q}i > 0$ means that the two divergences share the same sign resulting in an odd number of nodes in the off-resonant coherent transport, while $\mathcal{Q}i < 0$ means that the divergences have opposite signs, and the result is an even number of nodes. This interference classification lends itself to the graphical representation shown in Figure 5.2.

Applying equation (5.6) and the definition of the $\mathcal{Q}i$ parameter, it is possible to interpret the destructive interference mechanism of each node. In the odd interference class the particle amplitude, p, and the hole amplitude, h, will always have opposite signs and cancel each other near the middle of the off-resonant regime. We will therefore refer to this node as "particle-hole interference".

On the other hand, the two-node case (even interference class) is an example of destructive single-particle interference within the particle (or hole) transport process. If the nodes are located near the edge of the off-resonant regime, the destructive interference is dominated by either particle of hole amplitudes, because the other process is suppressed with a factor inversely proportional to the addition energy, $|\varepsilon_{00}^{p} - \varepsilon_{00}^{h}|$ (the width of the off-resonant regime). However, when the interference pattern is very asymmetric, with either $\mathcal{Q}i \approx 0$ or $\mathcal{Q}i \ll -1$, this interpretation becomes problematic, and any destructive interference in the even interference class is a more complicated mixture of single-particle and particle-hole interference.
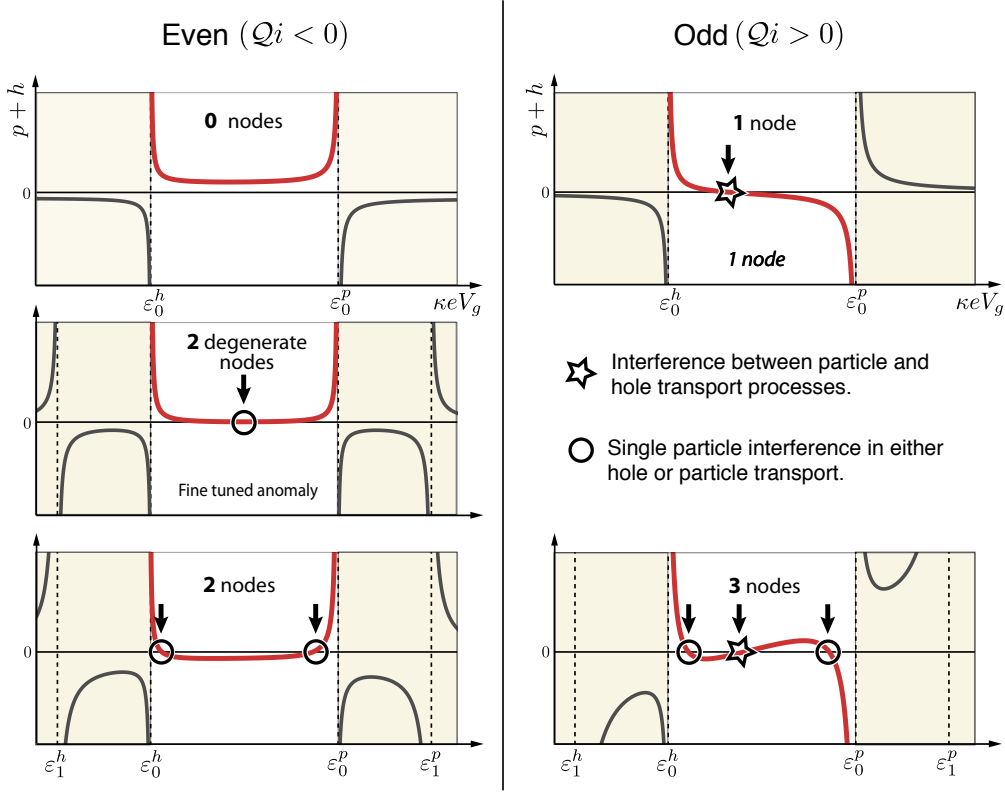
Figure 5.2: Quantum interference classification. Here the even and odd interference classes are determined by the relative sign of the poles at $\kappa e V_g = \varepsilon_{00}^{h/p}$. The highlighted red shows the $p + h$ amplitude within the charge state under consideration. Note that the interference mechanism can be determined confidently in these cases with $|\mathcal{Q}i|$ close to unity.

5.2   The Pairing Theorem for Alternant Hydrocarbons

We now turn our attention to hydrocarbon π-systems, and their corresponding PPP model with $\mu_i = 0$ and $z_i = 1$ for all sites i. Let us further restrict our considerations to bipartite (also referred to as 'alternant') π-systems where the lattice sites can be divided into separate sublattices A and B, where members of A are only connected to members of B and vice versa.

It turns out that the eigenstates of such systems are paired,[24] and to investigate this *Rushbrooke-Coulson pairing theorem* we introduce the anti-unitary particle-hole transformation working on complex numbers z and creation operators in the following way,

$$\mathcal{A} z \hat{c}_{i\sigma}^{\dagger} \mathcal{A}^{\dagger} = z^*(-1)^i \hat{c}_{i\sigma} \tag{5.10}$$

Here the prefactor $(-1)^i$ takes different values when i belong to different sublattices.

$$(-1)^i = \begin{cases} 1 & \text{for } i \in A \\ -1 & \text{for } i \in B \end{cases}. \tag{5.11}$$

The number operator then transforms like

$$\mathcal{A}(\hat{n}_{i\sigma} - \tfrac{1}{2})\mathcal{A}^{\dagger} = -(\hat{n}_{i\sigma} - \tfrac{1}{2}), \tag{5.12}$$

and by extension $\mathcal{A}(\hat{n}_i - 1)\mathcal{A}^\dagger = -(\hat{n}_{i\sigma} - 1)$. From this it is easy to prove that

$$\mathcal{A}\hat{T}\mathcal{A}^\dagger = \hat{T}, \ \ \mathcal{A}\hat{H}_U\mathcal{A}^\dagger = \hat{H}_U, \ \text{and} \ \mathcal{A}\hat{H}_V\mathcal{A}^\dagger = \hat{H}_V. \tag{5.13}$$

However, transforming the local chemical potential gives, $\mathcal{A}\hat{H}_\mu\mathcal{A}^\dagger = -\hat{H}_\mu$. This explains the restriction to hydrocarbon π-systems, where we can take all $\mu_i = 0$. Hence for the considered systems, the total Hamiltonian is *invariant* under the transformation $\mathcal{A}\hat{H}\mathcal{A}^\dagger = \hat{H}$.

Applying the anti-unitary transformation to the completely empty state $|0\rangle$ produces the completely filled state $|2N_a\rangle$,

$$\mathcal{A}|0\rangle = |2N_a\rangle. \tag{5.14}$$

Applying the particle-hole transformation to a state $|\psi_n^N\rangle$ yields $|\phi_n^N\rangle = \mathcal{A}|\psi_n^N\rangle$. The $|\phi_n^N\rangle$ states belongs to the $N_a - N$ charge state, and transforming Schrödinger's equation, it is easy to demonstrate that the transformed states are also eigenstates,

$$\mathcal{A}\hat{H}\mathcal{A}^\dagger\mathcal{A}|\psi_n^N\rangle = E_n\mathcal{A}|\psi_n^N\rangle \ \ \Rightarrow \ \ \hat{H}\mathcal{A}|\psi_n^N\rangle = E_n\mathcal{A}|\psi_n^N\rangle \ \ \Rightarrow \ \ \hat{H}|\phi_n^N\rangle = E_n|\phi_n^N\rangle, \tag{5.15}$$

In fact the $|\psi_n^N\rangle$ even share the same eigenenergy spectrum, E_n. Assuming that $|\psi_n^N\rangle$ is *non-degenerate*, the transformed state $|\phi_n^N\rangle$ is also non-degenerate and up to a phase factor $\gamma \in \{0, \pi\}$ we have,

$$|\phi_n^N\rangle = e^{i\gamma}|\psi_n^{2N_a - N}\rangle. \tag{5.16}$$

In general we will say that the N-electron eigenstates $|\psi_n^N\rangle$ are paired with the $(2N_a - N)$-electron eigenstates $|\psi_n^{2N_a - N}\rangle$. In the special case of half-filling, $2N = N_a$, the transformed state is given by

$$\mathcal{A}|\psi_n^N\rangle = e^{i\gamma}|\psi_n^N\rangle. \tag{5.17}$$

5.2.1 Spin-Degenerate States

As mentioned, the above derivation only holds true for non-degenerate states $|\psi_n^N\rangle$. For degenerate states, the analysis becomes a little bit more involved, so in the following we will only consider the (very common) spin degeneracy. As mentioned in section 2.2.2 the total spin operator $\mathbf{S}^2$ and the spin projection S^z commutes with the PPP Hamiltonian, and hence each eigenstate $|\psi_n^N\rangle$ will be characterized by some total spin S and a spin projection quantum number $m \in -S, -S + 1, \ldots, S$. Eigenstates belonging to the same spin S multiplet will be degenerate, and in general a state $|\psi_n^N(S, m)\rangle$ must transform as

$$\mathcal{A}|\psi_n^N(S, m)\rangle = e^{i\gamma}|\psi_n^{2N_a - N}(S, -m)\rangle. \tag{5.18}$$

Again $\gamma \in 0, \pi$. The $|\psi_n^N(S, m)\rangle$-states are related by a "spin rotation", which reverses the spin projection quantum number, $m \to -m$. To express this relationship mathematically we introduce the general spin lowering operator $\hat{S}^- = \hat{S}^x - i\hat{S}^y$ and the spin raising operator $\hat{S}^+ = \hat{S}^x + i\hat{S}^y$. Acting with either on a spin state produces,[30]

$$\hat{S}^-|\psi_n^N(S, m)\rangle = \sqrt{(S + m)(S - m + 1)}|\psi_n^N(S, m - 1)\rangle, \tag{5.19}$$

$$\hat{S}^+|\psi_n^N(S, m)\rangle = \sqrt{(S - m)(S + m + 1)}|\psi_n^N(S, m + 1)\rangle. \tag{5.20}$$

Repeated application of these spin operators by a number of $2m$ times, produces the "spin rotated state",

$$(\hat{S}^-)^{2m}|\psi_n^N(S,m)\rangle = \prod_{n=m}^{-m+1}\sqrt{(S+n)(S-n+1)}|\psi_n^N(S,-m)\rangle = M_{Sm}|\psi_n^N(S,-m)\rangle, \qquad (5.21)$$

$$(\hat{S}^+)^{2m}|\psi_n^N(S,-m)\rangle = \prod_{n=-m}^{m-1}\sqrt{(S+n)(S-n+1)}|\psi_n^N(S,m)\rangle = M_{Sm}|\psi_n^N(S,m)\rangle. \qquad (5.22)$$

Here we introduced the (positive) pre-factor $M_{Sm} = \prod_{n=-m}^{m-1}\sqrt{(S+n)(S-n+1)}$. The spin lowering and raising operators transform under the anti-unitary transformation like

$$\mathcal{A}\hat{S}^-\mathcal{A}^\dagger = -\hat{S}^+, \qquad \mathcal{A}\hat{S}^+\mathcal{A}^\dagger = -\hat{S}^-. \qquad (5.23)$$

Finally, transforming equation (5.21), gives us that

$$(-1)^{2m}e^{i\gamma}\prod_{n=-m}^{m-1}M_{Sm}|\psi_n^{2N_a-N}(S,+m)\rangle = e^{i\gamma'}M_{Sm}|\psi_n^{2N_a-N}(S,+m)\rangle. \qquad (5.24)$$

Note that for half-integer spin, $2m$ is odd, and the phases between the two transformed states must fulfill that $e^{i(\gamma-\gamma')} = -1$, while for integer spin, $2m$ is even, and $e^{i(\gamma-\gamma')} = 1$.

5.2.2   Interference Classification of Non-Degenerate Alternant Hydrocarbons

For the alternant hydrocarbons at half-filling, $N_a = N$, with a singlet ground state $|\Psi_0^{N_a}\rangle$, the $\mathcal{Q}i$ classification can now be readily evaluated.

First, we note that the orbital overlaps can be transformed,

$$\begin{aligned}
\langle\Psi_n^{N_a-1}|\hat{c}_{i_R\sigma}|\Psi_0^{N_a}\rangle &= \langle\Psi_n^{N_a-1}|\mathcal{A}^\dagger\mathcal{A}\hat{c}_{i\sigma}\mathcal{A}^\dagger\mathcal{A}|\Psi_0^{N_a}\rangle \\
&= (-1)^i\langle\Phi_n^{N_a-1}|(-1)^i\hat{c}_{i\sigma}^\dagger|\Phi_0^{N_a}\rangle \\
&= (-1)^i e^{i(\gamma_0-\gamma_n)}\langle\Psi_n^{N_a+1}|(-1)^i\hat{c}_{i\sigma}^\dagger|\Psi_0^{N_a}\rangle.
\end{aligned} \qquad (5.25)$$

And hence the classification becomes

$$\begin{aligned}
\mathcal{Q}i &= \frac{\langle\Psi_0^N|\hat{c}_{i_L\sigma}^\dagger|\Psi_0^{N-1}\rangle\langle\Psi_0^{N-1}|\hat{c}_{i_R\sigma}|\Psi_0^N\rangle}{\langle\Psi_0^N|\hat{c}_{i_R\sigma}|\Psi_0^{N+1}\rangle\langle\Psi_0^{N+1}|\hat{c}_{i_L\sigma}^\dagger|\Psi_0^N\rangle} \\
&= (-1)^{i_L+i_R}e^{i(\gamma_0-\gamma_n)}e^{i(\gamma_n-\gamma_0)}\frac{\langle\Psi_0^N|\hat{c}_{i_R\sigma}|\Psi_0^{N+1}\rangle\langle\Psi_0^{N+1}|\hat{c}_{i_L\sigma}^\dagger|\Psi_0^N\rangle}{\langle\Psi_0^N|\hat{c}_{i_R\sigma}|\Psi_0^{N+1}\rangle\langle\Psi_0^{N+1}|\hat{c}_{i_L\sigma}^\dagger|\Psi_0^N\rangle} \\
&= (-1)^{i_L+i_R}.
\end{aligned} \qquad (5.26)$$

Quite clearly we conclude that

$$\mathcal{Q}i = \begin{cases} 1 & \text{when } i_L \text{ and } i_R \text{ belong to the same sublattice,} \\ -1 & \text{when } i_L \text{ and } i_R \text{ belong to the different sublattices.} \end{cases} \qquad (5.27)$$

Define the equivalence relation between lattice sites, where $i \equiv j$, if both i and j belong to the same sublattice. Then the quantum interference belongs to the *odd* class if $i_L \equiv i_R$, and the quantum interference pattern belongs to the *even* class when $i_L \not\equiv i_R$. We shall refer to this result as the *coloring rule*, because a simple coloring of the lattice in alternating black and white, makes it easy to calculate the interference class (cf. Figure 5.3).
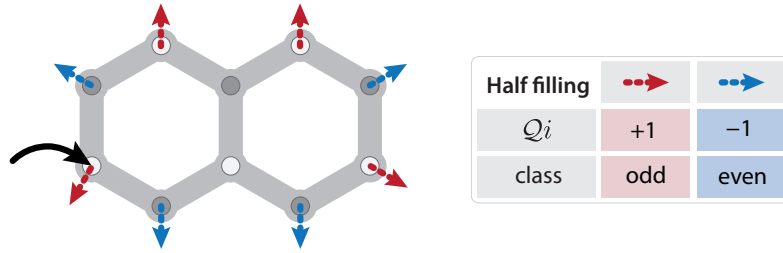
Figure 5.3: **Coloring rule for naphthalene:** Here the solid arrow marks the orbital which couples to one electrode, while the dashed arrows marks orbitals potentially coupling to the remaining electrode. Note how the simple coloring predicts the interference class, with same colored orbitals in the odd class, and differently colored orbitals in the even class.

5.3 Examples (Spin-Singlet)

Having established the pairing theorem and the simple coloring rules for predicting their quantum interference class in equation (5.27), we will look at some simple examples of bipartite lattices presented in Figure 5.4. It is left as (an easy) exercise for the reader, to verify that the coloring rule indeed predicts the correct interference class.
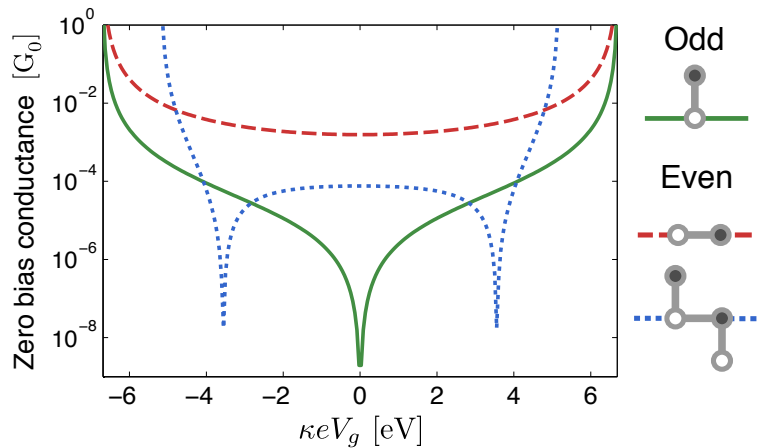
Figure 5.4: Simple bipartite Hubbard model systems, and their zero-bias conductance at half-filling. Note that the interference patterns obey the coloring theorem of equation (5.27).

For all example molecular junctions we calculate the transport by Lanczos diagonalization of the full PPP model and subsequent numerical calculation of the relevant resolvents in equation (5.8). In general we will take $\Gamma_L \Gamma_R = 0.01 e^2 V^2/G_0$. The examples have been chosen for pedagogical reasons. However the Lanczos numerical diagonalization sets an upper limit to the size of the π-system which (currently) can have no more than 16 orbitals.

5.3.1 Benzene

Our first chemically relevant example is the benzene molecule, where it is well-known[50] from both theoretical and experimental work that the meta-substituted neutral molecule

exhibits destructive quantum interference, as shown in Figure 5.5. It is obvious that meta-substituted benzene connects two sites belonging to the same sublattice, and hence we classify the interference as belonging to the *odd* interference class.
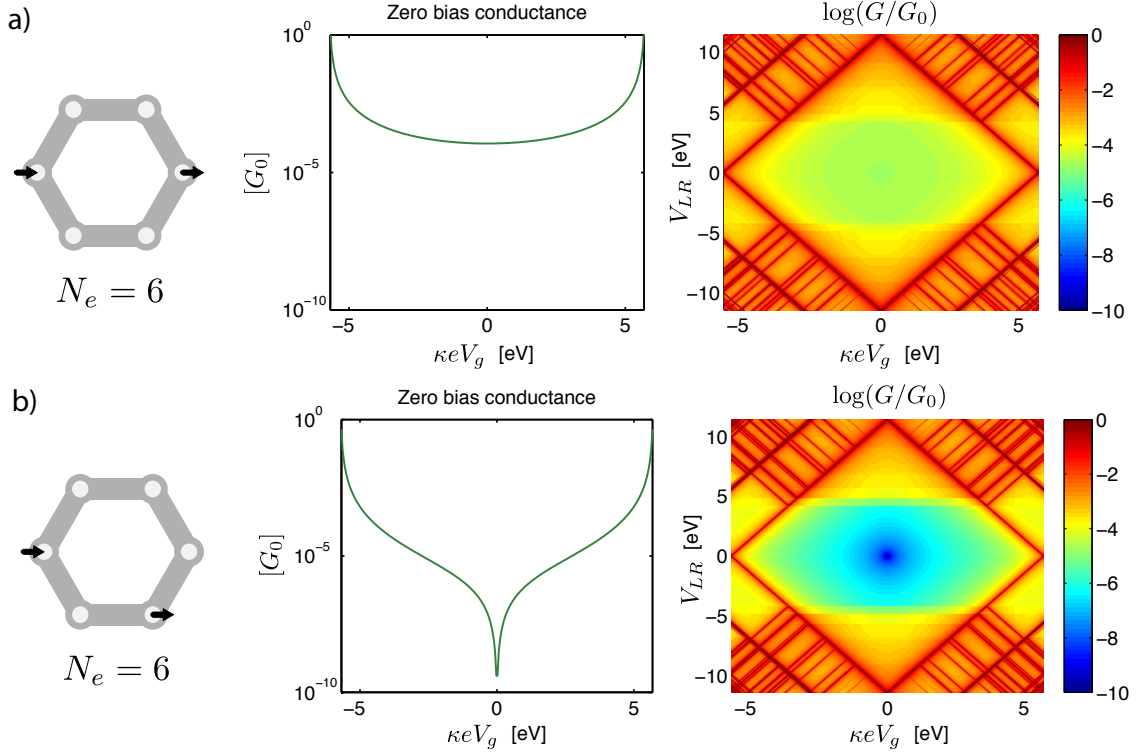

Figure 5.5: Conductance and interference of neutral benzene in the two cases of (a) para-substituted benzene and (b) meta-substituted benzene. Note that the interference in meta-substituted benzene happens between particle and hole transport processes, and hence it is *not* an example of single particle interference.

While some speculated that the interference in benzene, is due to single-particle interference between the two paths around the circular molecule,[91] we can from Figure 5.2 directly conclude that the destructive interference in the off-resonant transport through meta-substituted benzene is due to *interference between hole and particle transport processes*.

5.3.2   Quinone

In our next example we attach two carbon-atoms to the benzene molecule, and end up with a quinone-like chemical structure. Our calculation of the off-resonant transport through the neutral para-substituted molecule is presented in Figure 5.6. In this case the connecting orbitals belong to different sublattices and the off-resonant transport belongs to the *even* interference class. Because $Qi = 1$ we safely conclude that the destructive interference happens completely within the particle transport process, p (and conversely completely within the hole transport process, h). We will return to the "single-particle" interference in the next section, where we will investigate it using neoclassical valence bond theory for the slightly simpler four-orbital model.
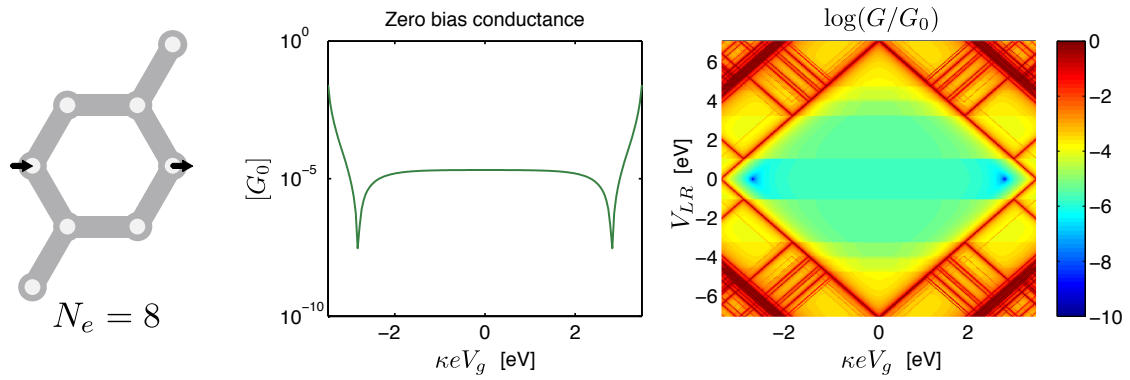
Figure 5.6: Quinone-like structure and the result of our transport calculation. The para-configuration places the interference in the even class, and we do indeed find two destructive interference nodes.

As a fun example we may also show an extreme case with a ridiculous amount of four quantum transport nodes, by considering the [**4**]-dendralene *cross-conjugated* system presented in Figure 5.7. As an emperical rule the number of interference nodes
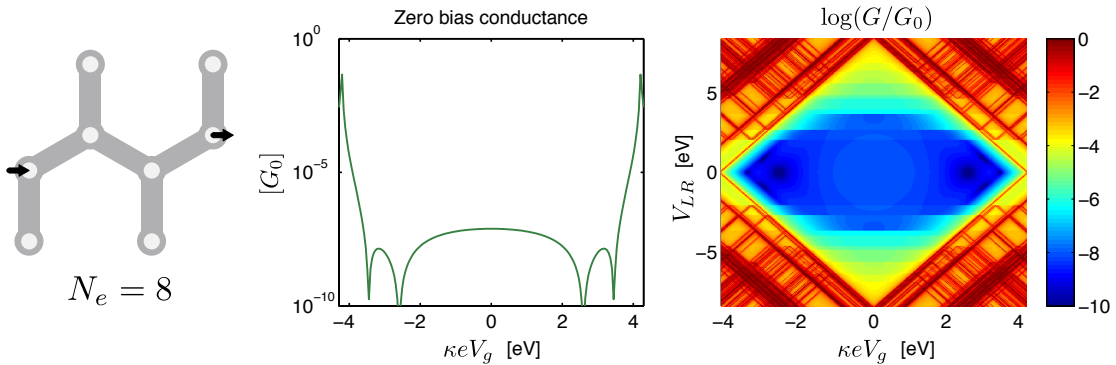

Figure 5.7: Quantum interference belonging to the even class with an impressive four nodes in [**4**]-dendralene. Note the interference pattern near each charge-degeneracy point with two nodes zero bias, and two nodes at finite bias.

However, the coloring rule only applies at half-filling. The quinone-like molecule also exhibits destructive interference in the quarter-filled case as shown in Figure 5.8. It turns out that in this case $\mathcal{Q}i > 0$, and the resulting interference belongs to the *odd* class. While $|\mathcal{Q}i|$ is not of order unity, the destructive interference still happens between particle and hole process.

5.4 Robustness

In this section we shortly discuss the robustness of some of the quantum interference results we have obtained so far.
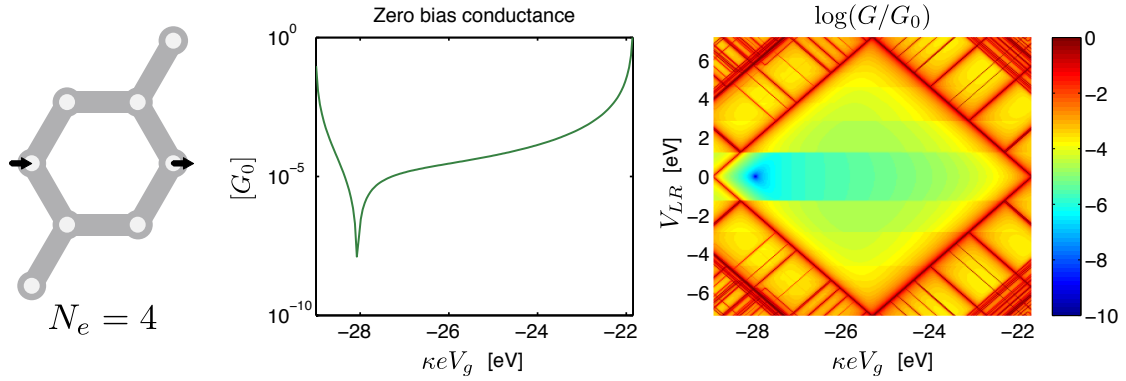
Figure 5.8: Quinone-like structure and the result of a transport calculation in the *quarter-filled case*. Note the conductance asymmetry as a function of gate. In this case the interference also happens between particle and hole transport processes.

5.4.1   Next-Nearest Neighbor Hopping

We have established the coloring rule (5.27) for alternant hydrocarbons ignoring the small but non-zero hopping between next nearest neighbor orbitals. By adding such next-nearest neighbor (NNN) hopping, all molecules become non-alternant. Hence NNN hopping could potentially invalidate our coloring rule for alternant hydrocarbons. However, the NNN hopping is usually about an order of magnitude smaller than the nearest neighbor hopping, and it turns out that our quantum interference classification is quite robust under the introduction of next-nearest neighbor hopping. The quinone-like molecule serves as a prototypical example, and in Figure 5.9 we plot the interference number $\mathcal{Q}i$ as a function of the NNN hopping amplitude.
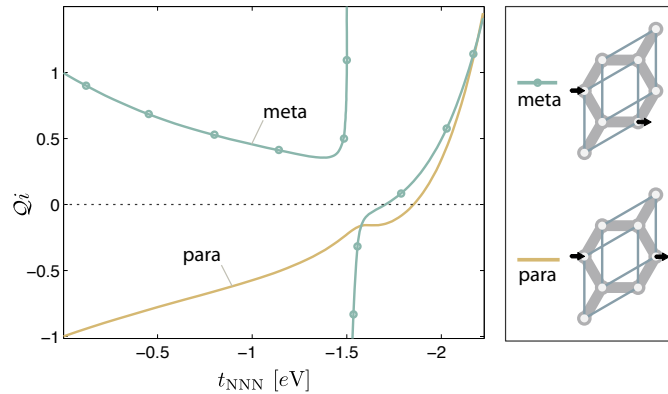

Figure 5.9: Quantum interference classification $\mathcal{Q}i$ as a function of the next-nearest-neighbor hopping t_{NNN}, for the quinone-like hydrocarbon attached to leads in two different ways. The quantum intererence classification survives for even large values of the next-nearest neighbor hopping, and only at $t_{\mathrm{NNN}} \approx -1.5$ eV (which is comparable to the nearest neighbor hopping amplitude), does the class change.

5.4.2   Hetero-Atoms

The 1,4-benzo-quinone molecule is basically a benzene molecule with oxygen atoms substituted at the para orbitals. For hetero-atomic molecules the pairing theorem is broken by the presence of non-zero values of the local chemical potential, $\mu_O \neq 0$. However, the $\mathcal{Q}i$-classification is expected to hold within a certain parameter regime. Calculating the value of $\mathcal{Q}i$ for different values of μ_O and U_O produces the plot in Figure 5.10. The sudden shift of $\mathcal{Q}i$ is due to a change of the ground state in either the 7 or 9 electron charge state.

While the pairing theorem seems to hold for the 1,4-benzo-quinone, this conclusion depends heavily on the effect which μ and U have on the excitation spectrum. In general, larger molecules means smaller excitation energies, and hence larger effects of μ and U.
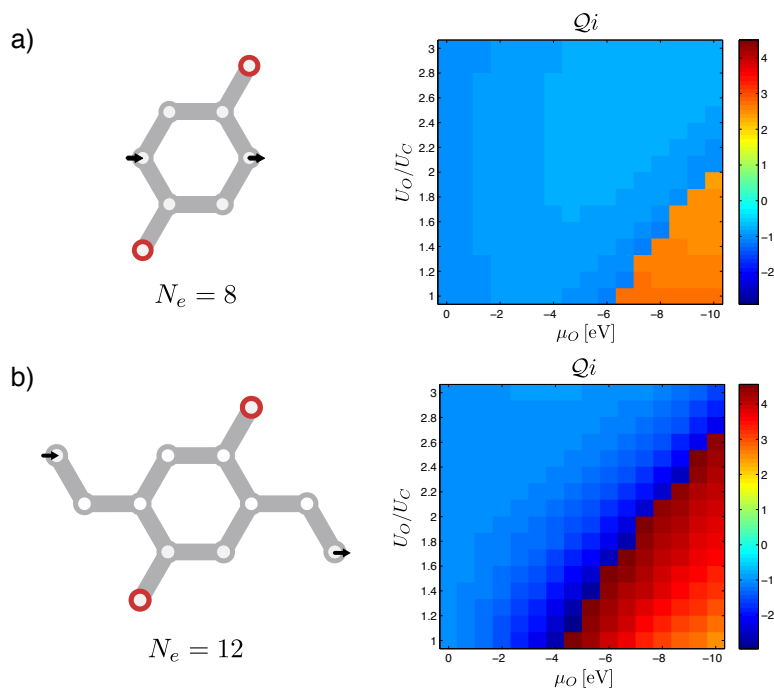

Figure 5.10: 1,4-Benzo-quinone with oxygen at the red sites. The value of $\mathcal{Q}i$ has been calculated for various values of μ_O and U_O. Different semi-empirical parameters for have been found, but they are probably close to $\mu_O \approx -3$ eV and $U_O \approx 1.5U_C$, which does not change the interference class. Note how the attached sidearms changes the red region of positive $\mathcal{Q}i$, hence confirming our intuition that the ground state of larger molecules may more easily change interference class when substituting carbon with hetero-atoms.

5.4.3   Transport Through the σ-System

Note that the quantum interference effects are all shown on a logarithmic scale, which can make it hard to interpret the robustness of our calculation. Additional transport channels through e.g. the σ-system can destroy the interference effect.[50] As an example we consider the transport through para-substituted benzene with various added constant offsets presented in Figure 5.11.

One should note that transport through the σ-system is expected to be suppressed by a factor proportional to the energy difference between σ-system and π-system.
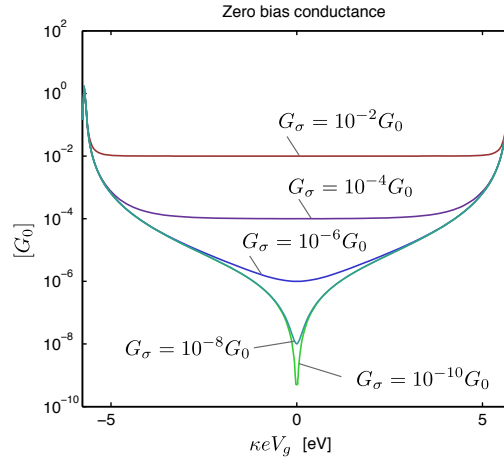
Figure 5.11: Zero-bias conductance of the π-system of meta-substituted benzene with an additional conductance channel through the σ-system. For small values of G_σ the interference is still visible, while large values of G_σ quench it completely.

5.5   Quantum Interference in Hückel Models

Let us shortly turn our attention to the simpler non-interacting Hückel models, which is equivalent to our full PPP model, when setting the Coulomb interaction $U = 0$. Hence, the pairing theorem also applies to these models, and we do not expect large discrepancies between the interference features of the full PPP models and the Hückel models.

For non-interacting models the zero-bias transport is calculated in terms of the transmission $T(E)$ using the Landauer formula,[56] $G(E) = G_0 T(E)$. The transmission through the molecule can then be given explicitly by the particle and hole transport amplitudes,[19,64]

$$T(E) = \pi^2 \eta^2 \langle vac|\hat{c}_{i_R} \left(\frac{1}{E - \mathcal{T} + i\sum_\alpha \hbar\Gamma_\alpha \hat{c}_{i_\alpha}^\dagger \hat{c}_{i_\alpha}} \right) \hat{c}_{i_L}^\dagger |vac\rangle \tag{5.28}$$

with $\eta = \hbar\Gamma_L + \hbar\Gamma_R$. This can be then be written in terms of particle and hole amplitudes

$$T(E) = \pi^2 \eta^2 |\sum_\sigma (p_{00}^{\sigma\sigma} + h_{00}^{\sigma\sigma})|^2, \tag{5.29}$$

where the infinitesimal 0^+ in the definition of the particle and hole amplitudes have been replaced by the finite η. In the limit of small electrode couplings $\Gamma_L, \Gamma_R \ll t$, this reduces to the off-resonant conductance expression of equation (5.6). Hence, the interference classification can be directly carried over to non-interacting Hückel model transport calculations.

For small hydrocarbon π-systems, we have already showed that the Hückel model ground state can have a rather large overlap with the full PPP ground state (cf. Figure 2.4). The most prominent dissonance between the interference features of the two models, happens for the alternant hydrocarbons in the even class with two interference nodes. In a Hückel model the nodes become degenerate and produces the fine-tuned anomaly of Figure 5.2. An example is shown for the quinone-like molecule in Figure 5.12.

The coloring rules are especially valuable here, because they straight-away reveal the degeneracy of the nodes in the even interference class. The PPP Coulomb interaction tends to lift this node degeneracy. A similar effect can be achieved in the Hückel model by
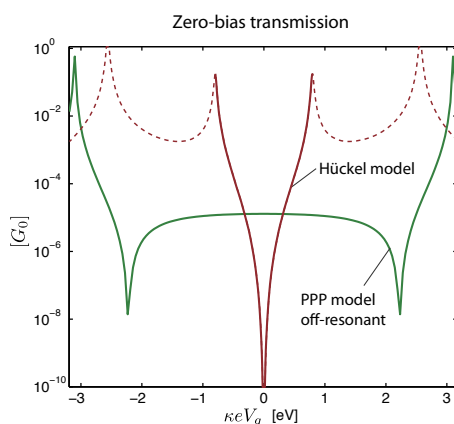
Figure 5.12: Comparison of the calculated transport for the Hückel model and the PPP model of the quinone-like hydrocarbon. The Hückel model produces a single degenerate node, which is split in the full PPP treatment.

opening the charge state gap through the (artificial) introduction of a constant interaction, U. It is not imperative that Hückel+U and PPP models should always share interference node structure, and it would be interesting to find π-systems where the models produce a different number of interference nodes.

5.6 Quantum Interference in Valence Bond Models

In this section we will examine interference in off-resonant transport using the neoclassical valence bond theory presented in chapter 3. In fact it was the valence bond theory which originally brought the quantum interference classification of alternant hydrocarbons to our attention.

Generally speaking, transport through a $\mathcal{P}|\Psi\rangle$ state, is composed of three parts: Initially an electron (or a hole) is created in the orbital connected to one electrode, propagated through the molecule and then removed at the orbital connected to the other electrode. However, the t-J Hamiltonian have equivalent rules regarding holes and electrons, except for the relative minus in their hopping entries of equation (3.32a)-(3.32b).

$$\mathcal{T}_{ji} \left| \underset{i}{\bullet}\!\!-\!\!\underset{j}{\bullet} \right\rangle = t_{ji} \left| \bullet\!\!-\!\!\bullet \right\rangle. \tag{5.30}$$

$$\mathcal{T}_{ij} \left| \underset{i}{\circ}\!\!-\!\!\underset{j}{\bullet} \right\rangle = -t_{ij} \left| \bullet\!\!-\!\!\circ \right\rangle, \tag{5.31}$$

The powers of the Hamiltonian governs the propagation of the doublon (holon). In alternant hydrocarbons the relative sign between doublon and hole propagation is then given by $(-1)^m$, where m is the number of hops between the two connecting sides. This notion implies that the transport through the projected ground state $\mathcal{P}|\Psi\rangle$ also follow the quantum interference coloring rules for alternant hydrocarbons stated in equation (5.27).

While the quantum interference classification follows easily from valence bond theory, a natural next step is to analyze the necessary circumstances for quantum interference additional nodes. According to an empirical rule[103] transport through conjugated (alternating

double and single bonds) molecular paths interferes constructively, while transport through cross-conjugated paths interfere destructively.

This semi-empirical rule works partly because cross-conjugated paths often fall into the odd quantum interference class. Here, we will focus on the cross-conjugated molecules in the even interference class, like this one:

Cross-conjugated path   four-orbital model
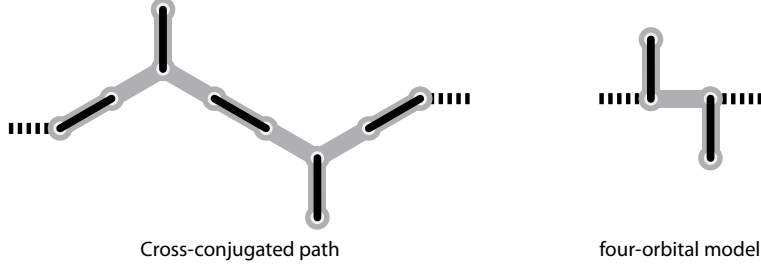
The minimal example is the four-orbital chain attached to electrodes at the two central orbitals. While this transport path is itself conjugated, the following treatment can be generalized to larger cross-cnjugated molecules.

The ground state of the four-orbital chain has the following valence bond representation in the projected subspace,

$$\mathcal{P}|\Psi_0^4\rangle \approx c_1 \left| \text{[figure]} \right\rangle - c_2 \left| \text{[figure]} \right\rangle, \qquad \text{with } c_1 \approx 0.82, \text{ and } c_2 \approx 0.30. \qquad (5.32)$$

Because the interference belongs to the even quantum interference class, a node should be present in the particle amplitude alone (cf. Figure 5.2. The particle amplitude for an electron tunneling through this molecule is given by equation (4.11). For brevity we will only calculate transport amplitudes in the projected space S of single occupied orbitals. This calculation becomes close to exact in the large U limit, where most of the wave-function weight is indeed in this subspace. Formally we approximate,

$$p_{00}^{\sigma\sigma} = \langle \Psi_0^4 | \hat{c}_{3\sigma} \frac{1}{z + E_0^4 - \hat{H}_m} \hat{c}_{2\sigma}^\dagger | \Psi_0^4 \rangle \approx \langle \Psi_0^4 | \mathcal{P} \hat{c}_{3\sigma} \frac{1}{z + E_0 - \hat{H}} \hat{c}_{2\sigma}^\dagger \mathcal{P} | \Psi_0^4 \rangle. \qquad (5.33)$$

Tunneling onto the center orbitals (2 or 3), produces the following combinations of states,

$$\hat{c}_{2\sigma}^\dagger \left| \text{[figure]} \right\rangle = -\frac{1}{\sqrt{2}} \left| \text{[figure]} \right\rangle$$

$$\hat{c}_{2\sigma}^\dagger \left| \text{[figure]} \right\rangle = -\frac{1}{\sqrt{2}} \left| \text{[figure]} \right\rangle = \frac{1}{\sqrt{2}} \left(\left| \text{[figure]} \right\rangle + \left| \text{[figure]} \right\rangle \right)$$

And applied to the ground state,

$$|a\rangle = \hat{c}_{2\sigma}^\dagger \mathcal{P} |\Psi_0^4\rangle = -\alpha \left| \overbrace{\text{[figure]}}^{a_1} \right\rangle - \beta \left| \overbrace{\text{[figure]}}^{a_2} \right\rangle, \qquad (5.34)$$

$$|b\rangle = \hat{c}_{3\sigma}^\dagger \mathcal{P} |\Psi_0^4\rangle = -\alpha \left| \underbrace{\text{[figure]}}_{b_1} \right\rangle - \beta \left| \underbrace{\text{[figure]}}_{b_2} \right\rangle. \qquad (5.35)$$

Here $\alpha = (c_1 + c_2)/\sqrt{2} \approx 0.79$, and $\beta = c_2/\sqrt{2} \approx 0.21$. The particle transport amplitude is then given by,

$$p_{00}^{\sigma\sigma} = \langle\Psi_0^4|\mathcal{P}\,\hat{c}_{3\sigma}\frac{1}{z+E_0-\hat{H}}\hat{c}_{2\sigma}^\dagger\mathcal{P}|\Psi_0^4\rangle = \langle b|\frac{1}{z+E_0-\hat{H}}|a\rangle = \mathbf{b}\mathbf{S}\frac{1}{z+E_0-h}\mathbf{a}. \quad (5.36)$$

Here we have changed to a convenient matrix representation with h given by the pictionary discussed in section 3.5. The overlap matrix between the $|b_1\rangle$ and $|b_2\rangle$ valence bond states, is given by

$$\mathbf{S} = \begin{pmatrix} 1 & -1/2 \\ -1/2 & 1 \end{pmatrix}_b. \quad (5.37)$$

As a first step, we may directly calculate the resolvent by matrix inversion of $(z+E_0-h)$. The resulting amplitude is shown in Figure 5.13. While there is no interference node (as compared to the Hubbard result in Figure 5.4), the amplitude is small even on a logarithmic scale. The absence of nodes is not a failure of valence bond theory, but in fact the correct result in the subspace of single occupied sites as shown in the inset.
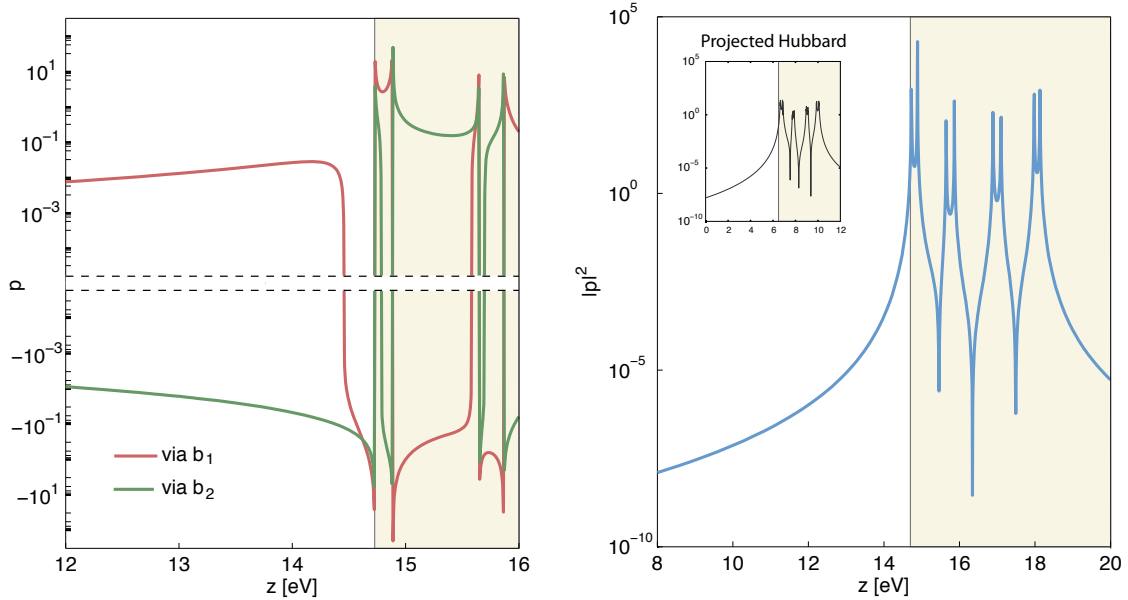

Figure 5.13: Particle transport calculated numerically by matrix inversion for a model with $|U| = 16|t|$. The **right panel** shows the particle amplitude squared, and while it is logarithmically small, there is no interference nodes. The **inset** presents the result of a transport calculation in a Hubbard model using a projected ground state $\mathcal{P}|\Psi\rangle$, hence validating the valence bond result. The **left panel** shows two parts of the amplitudes with the initial state propagated to either $|b_1\rangle$ or $|b_2\rangle$. From this it is clear that these two amplitudes almost cancel each other out completely.

If we wish to capture the interference node, we must extend our calculation to the part of the Hilbert space with double occupied sites, D. In the full Hilbert space the transport amplitude can be expressed in terms of projection operators $\mathcal{P}$ and $\mathcal{Q}$,

$$p_{00}^{\sigma\sigma} \approx \langle\Psi_0^4|(\mathcal{P}+\mathcal{Q})\hat{c}_{3\sigma}\frac{1}{z+E_0-\hat{H}}\hat{c}_{2\sigma}^\dagger\mathcal{P}|\Psi_0^4\rangle + \langle\Psi_0^4|\mathcal{P}\hat{c}_{3\sigma}\frac{1}{z+E_0-\hat{H}}\hat{c}_{2\sigma}^\dagger(\mathcal{P}+\mathcal{Q})|\Psi_0^4\rangle. \quad (5.38)$$

Here we have only left out the contribution from processes which both end and start in the D projected part of the ground state. This is a valid approximation because, $\langle\Psi|\mathcal{Q}|\Psi\rangle \ll \langle\Psi|\mathcal{P}|\Psi\rangle$ for large values of the Coulomb interaction, U.

Because propagation of the projected $\mathcal{Q}|\Psi\rangle$ is suppressed by a factor of $1/U$, we will also approximate $(z + E_0 - \hat{H})^{-1} \approx \mathcal{P}(z + E_0 - \hat{H})^{-1}\mathcal{P}$. This gives us the final expression $p_{00}^{\sigma\sigma} \approx p_{PP}^{\sigma\sigma} + p_{PQ}^{\sigma\sigma} + p_{QP}^{\sigma\sigma}$, with ($A$ and B being stand-ins for projection operators),

$$p_{AB}^{\sigma\sigma} = \langle\Psi_0^4|\mathcal{A}\hat{c}_{3\sigma}\mathcal{P}\frac{1}{z + E_0 - \hat{H}}\mathcal{P}\hat{c}_{2\sigma}^{\dagger}\mathcal{B}|\Psi_0^4\rangle. \tag{5.39}$$

Next step is to construct the state, $\mathcal{P}\hat{c}_{2\sigma}^{\dagger}\mathcal{Q}|\Psi_0^4\rangle$ by using equation (3.5),

$$\mathcal{Q}|\Psi\rangle = \frac{1}{E - \mathcal{Q}\mathcal{H}\mathcal{Q}}\mathcal{Q}\mathcal{T}\mathcal{P}|\Psi\rangle \approx \frac{1}{E - U}\mathcal{T}\mathcal{P}|\Psi\rangle. \tag{5.40}$$

In our case we have that,

$$\mathcal{P}\hat{c}_{2\sigma}^{\dagger}\mathcal{T}\mathcal{P}|\Psi_0\rangle = \left(-\frac{c_1}{\sqrt{2}} - \sqrt{2}c_2\right)\Big|\ \ \Big\rangle + \left(\sqrt{2}c_1 + \frac{c_2}{\sqrt{2}}\right)\Big|\ \ \Big\rangle$$

$$= \Big|\ \ \Big\rangle + \Big|\ \ \Big\rangle + \gamma\Big|\ \ \Big\rangle \tag{5.41}$$

Here we have used that, $c_1/\sqrt{2} + \sqrt{2}c_2 = 1$, and set $\gamma = \sqrt{2}c_1 + c_2/\sqrt{2}$. The sister state $\mathcal{P}\hat{c}_{3\sigma}^{\dagger}\mathcal{T}\mathcal{P}|\Psi_0\rangle$ is calculated in the same way. Having extended our ground state we must ensure that it is correctly normalized. When diagonalizng $\mathcal{P}|\Psi_0^N\rangle$, but in reality we must introduce normalization factors,

$$1 = \left\langle\Psi_0^N|\Psi_0^N\right\rangle = \langle\Psi_0^N|\mathcal{P}|\Psi_0^N\rangle + \langle\Psi_0^N|\mathcal{Q}|\Psi_0^N\rangle = c_P^2 + c_Q^2 \tag{5.42}$$

Because the $\mathcal{Q}$ projected part of the wavefunction is derived from the $\mathcal{P}$ projected part using equation (5.40), we can write $c_Q \approx 2c_P t/U$, giving

$$c_P = \frac{1}{\sqrt{1 + t^2/U^2}} \overset{U=16|t|}{\approx} 1 \tag{5.43}$$

As a result of including part of the D Hilbert space, the transport amplitude have now obtained the predicted nodes. While our endeavor into valence bond theory transport interference stops here, the current investigation have revealed several important points. First and foremost the transport through the projected ground state $\mathcal{P}|\Psi\rangle$ must be quite weak, and this only happens because we keep valence bond states beyond the main Kekulé component. Additionally, the interference nodes are not expected to show up for transport through the projected ground state alone, but adding a small part of the $\mathcal{Q}|\Psi\rangle$ component reveals the nodes (at least in the large U limit). As shown by the $\mathcal{Q}|\Psi\rangle$ case, valence bond theory also offers a controlled way of extending the calculations to the full D subspace, and hence to lower values of U.

These points could probably be used to create a set of rules for the interference based on molecular structure, but we will not pursue these ideas further here.
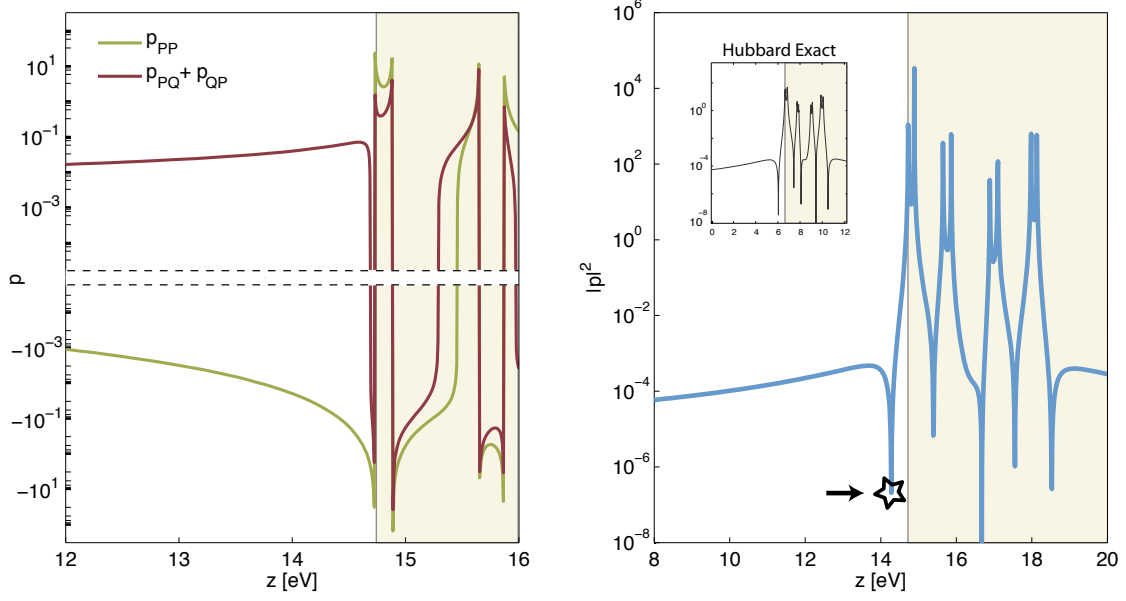
Figure 5.14: Right panel shows the amplitude squared with an interference node present. The inset shows the result of a transport calculation for the full Hubbard model, which agrees almost perfectly with the valence bond result. The left panel shows the components of the amplitude as defined by equation (5.39).

5.7 Spin-Doublet Ground State

When the ground state is a spin doublet $|\Psi_{0\sigma}\rangle$ with $\sigma = \uparrow, \downarrow$, equation (4.13) and equation (5.6) no longer holds. However, because the PPP model is spin rotation symmetric, each of the ground states must be equally occupied. We define the shorthand $A_{l,m}^{\sigma\gamma}(V_g) = h_{l,m}^{\sigma\gamma}(V_g, 0) + p_{l,m}^{\sigma\gamma}(V_g, 0)$. The zero-bias conductance is then composed of three distinct terms,

$$G = \frac{1}{2}\frac{e^2\hbar}{2\pi}\Gamma_L\Gamma_R \sum_\sigma \left(|A_{\sigma,\sigma}^{\sigma\sigma}|^2 + |A_{\sigma,\sigma}^{\bar\sigma\bar\sigma}|^2 + |A_{\bar\sigma,\sigma}^{\bar\sigma\sigma}|^2 \right). \tag{5.44}$$

The first two terms capture the potential scattering of the electrons in the electrodes on the molecule, while the last term captures transport processes which flip the spin of the molecular ground state doublet.

A slight of hand alters the above expression, giving

$$G = \frac{1}{2}\frac{e^2\hbar}{2\pi}\Gamma_L\Gamma_R \sum_\sigma \left(\tfrac{1}{2}|A_{\sigma,\sigma}^{\sigma\sigma} + A_{\sigma,\sigma}^{\bar\sigma\bar\sigma}|^2 + \tfrac{1}{2}|A_{\sigma,\sigma}^{\sigma\sigma} - A_{\sigma,\sigma}^{\bar\sigma\bar\sigma}|^2 + |A_{\bar\sigma,\sigma}^{\bar\sigma\sigma}|^2 \right). \tag{5.45}$$

Our goal for the next page is to put this expression on a simpler form, by employing the overall spin rotation symmetry of the molecule model. The total spin operator is given by

$$\mathbf{S} = \frac{\hbar}{2}\sum_i \sum_{\sigma\gamma} \hat{c}_{i\sigma}^\dagger \boldsymbol{\tau}_{\sigma\gamma} \hat{c}_{i\gamma}. \tag{5.46}$$

Then introduce an overall spin $\pi/2$ rotation about the y-axis described by the operator $\hat{R}^y = e^{i\pi S_y/2\hbar} = \prod_j R_{j\sigma}^y$. In spin space the local rotation of a spin σ at site j is,

$$\hat{R}_{j\sigma}^y = e^{i\pi\tau_j^y/4} = \frac{1}{\sqrt{2}}\left(\mathcal{I}_j + i\tau_j^y\right) = \frac{1}{\sqrt{2}}\begin{pmatrix} 1 & 1 \\ -1 & 1 \end{pmatrix}_{j\sigma}. \tag{5.47}$$

It is then straightforward to show that

$$\hat{R}^y \hat{c}_{i\sigma}^\dagger (\hat{R}^y)^\dagger = \frac{1}{\sqrt{2}}\left(\hat{c}_{i\uparrow}^\dagger - \sigma\hat{c}_{i\downarrow}^\dagger\right). \tag{5.48}$$

For brevity we have introduced the algebraic shorthand $\sigma =\uparrow / \downarrow = 1/-1$. This means reversely that $\hat{R}_i^y(\hat{c}_{i\uparrow}^\dagger + \sigma\hat{c}_{i\downarrow}^\dagger)(\hat{R}_i^y)^\dagger = \sigma\sqrt{2}\hat{c}_{i\sigma}^\dagger$.

The spin rotation of the doublet ground state directly yields,

$$\hat{R}^y|\Psi_{0\sigma}\rangle = e^{i\pi S^y/2\hbar}|\Psi_{0\sigma}\rangle = \frac{1}{\sqrt{2}}\left(|\Psi_{0\uparrow}\rangle - \sigma|\Psi_{0\downarrow}\rangle\right). \tag{5.49}$$

We then begin by calculating,

$$\left(\hat{c}_{i\uparrow}^\dagger + \sigma\hat{c}_{i\downarrow}^\dagger\right)|\Psi_{0\gamma}\rangle = (\hat{R}^y)^\dagger\hat{R}^y\left(\hat{c}_{i\uparrow}^\dagger + \gamma\hat{c}_{i\downarrow}^\dagger\right)(\hat{R}^y)^\dagger\hat{R}^y|\Psi_{0\gamma}\rangle \tag{5.50}$$

$$= (\hat{R}^y)^\dagger(\sigma\hat{c}_{i\sigma}^\dagger)\left(|\Psi_{0\uparrow}\rangle - \gamma|\Psi_{0\downarrow}\rangle\right). \tag{5.51}$$

Next step is to rotate the resolvents,

$$p_{\gamma,\gamma}^{\uparrow\uparrow} + \sigma p_{\gamma,\gamma}^{\downarrow\downarrow} = \langle\Psi_{0\gamma}|\hat{c}_{j\uparrow}\frac{1}{E-\hat{H}}\hat{c}_{i\uparrow}^\dagger|\Psi_{0\gamma}\rangle + \sigma\langle\Psi_{0\gamma}|\hat{c}_{j\downarrow}\frac{1}{E-\hat{H}}\hat{c}_{i\downarrow}^\dagger|\Psi_{0\gamma}\rangle \tag{5.52}$$

$$= \langle\Psi_{0\gamma}|\left(\hat{c}_{j\uparrow} + \hat{c}_{j\downarrow}\right)\frac{1}{E-\hat{H}}\left(\hat{c}_{i\uparrow}^\dagger + \sigma\hat{c}_{i\downarrow}^\dagger\right)|\Psi_{0\gamma}\rangle \tag{5.53}$$

$$= \left(\langle\Psi_{0\uparrow}| - \gamma\langle\Psi_{0\downarrow}|\right)\hat{c}_{j\uparrow}\frac{1}{E-\hat{H}}\sigma\hat{c}_{i\sigma}^\dagger\left(|\Psi_{0\uparrow}\rangle - \gamma|\Psi_{0\downarrow}\rangle\right). \tag{5.54}$$

For $\sigma =\downarrow / -1$ this result is particularly simple, with $p_{\gamma,\gamma}^{\uparrow\uparrow} - p_{\gamma,\gamma}^{\downarrow\downarrow} = \gamma p_{\downarrow,\uparrow}^{\uparrow\downarrow}$, which can be directly generalized to $A_{\gamma,\gamma}^{\uparrow\uparrow} - A_{\gamma,\gamma}^{\downarrow\downarrow} = \gamma A_{\downarrow,\uparrow}^{\uparrow\downarrow}$.

This finishes our calculation with the result

$$G = \frac{e^2\hbar}{2\pi}\Gamma_L\Gamma_R\left(\frac{1}{2}|W|^2 + \frac{3}{2}|J|^2\right), \quad \text{with } W = A_{\sigma,\sigma}^{\sigma\sigma} + A_{\sigma,\sigma}^{\bar{\sigma}\bar{\sigma}} \text{ and } J = A_{\bar{\sigma},\sigma}^{\bar{\sigma}\sigma}. \tag{5.55}$$

This result is identical to the perturbative calculation of the conductance in an effective Kondo model for the $|\Psi_\gamma\rangle$ subspace. Anticipating the treatment of the Kondo effect in the next chapter, J will be referred to as the exchange transport amplitude, while W is the potential scattering amplitude.

5.7.1 Quantum Interference Classification

Let us now turn to the classification of first the potential scattering, W, followed by the classification of the exchange transport processes, J. The potential scattering amplitude

can be written,

$$W = \sum_\sigma A^{\sigma\sigma}_{\gamma,\gamma} = \sum_\sigma \left(h^{\sigma\sigma}_{\gamma,\gamma} + p^{\sigma\sigma}_{\gamma,\gamma} \right) \tag{5.56}$$

$$= \frac{\langle \Psi_{0\gamma}|\left(\sum_\sigma \hat{c}_{i_R\sigma}\right)|\Psi_n^{N+1}\rangle\langle\Psi_n^{N+1}|\left(\sum_\sigma \hat{c}^\dagger_{i_L\sigma}\right)|\Psi_{0\gamma}\rangle}{\omega - \varepsilon^p_{n0}}$$

$$+ \frac{\langle \Psi_{0\gamma}|\left(\sum_\sigma \hat{c}^\dagger_{i_L\sigma}\right)|\Psi_n^{N-1}\rangle\langle\Psi_n^{N-1}|\left(\sum_\sigma \hat{c}_{i_R\sigma}\right)|\Psi_{0\gamma}\rangle}{\omega - \varepsilon^h_{n0}}. \tag{5.57}$$

The Qi-parameter determining the quantum interference class is defined by the ratio,

$$Qi_W = \frac{\sum_m \langle \Psi_{0\gamma}|\left(\hat{c}^\dagger_{i_L\uparrow} + \hat{c}^\dagger_{i_L\downarrow}\right)|\Psi^{N-1}_{0m}\rangle\langle\Psi^{N-1}_{0m}|\left(\hat{c}_{i_R\uparrow} + \hat{c}_{i_R\downarrow}\right)|\Psi_{0\gamma}\rangle}{\sum_n \langle \Psi_{0\gamma}|\left(\hat{c}_{i_R\uparrow} + \hat{c}_{i_R\downarrow}\right)|\Psi^{N+1}_{0n}\rangle\langle\Psi^{N+1}_{0n}|\left(\hat{c}^\dagger_{i_L\uparrow} + \hat{c}^\dagger_{i_L\downarrow}\right)|\Psi_{0\gamma}\rangle}, \tag{5.58}$$

where we explicitly sum over the ground state degeneracy in each of the neighbor charge states. Similarly for the exchange amplitude $J = A^{\uparrow\uparrow}_{\gamma,\gamma} - A^{\downarrow\downarrow}_{\gamma,\gamma}$ one can define the classification

$$Qi_J = \frac{\sum_m \langle \Psi_{0\gamma}|\left(\hat{c}^\dagger_{i_L\uparrow} - \hat{c}^\dagger_{i_L\downarrow}\right)|\Psi^{N-1}_{0m}\rangle\langle\Psi^{N-1}_{0m}|\left(\hat{c}_{i_R\uparrow} + \hat{c}_{i_R\downarrow}\right)|\Psi_{0\gamma}\rangle}{\sum_n \langle \Psi_{0\gamma}|\left(\hat{c}_{i_R\uparrow} + \hat{c}_{i_R\downarrow}\right)|\Psi^{N+1}_{0n}\rangle\langle\Psi^{N+1}_{0n}|\left(\hat{c}^\dagger_{i_L\uparrow} - \hat{c}^\dagger_{i_L\downarrow}\right)|\Psi_{0\gamma}\rangle}. \tag{5.59}$$

When the states $|\Psi_0^{N-1}\rangle$ and $|\Psi_0^{N+1}\rangle$ are both *singlets* (and otherwise non-degenerate), we have that

$$\frac{Qi_W}{Qi_J} = \frac{\langle \Psi_{0\gamma}|\left(\hat{c}^\dagger_{i_L\uparrow} + \hat{c}^\dagger_{i_L\downarrow}\right)|\Psi^{N-1}_0\rangle\langle\Psi^{N+1}_0|\left(\hat{c}^\dagger_{i_L\uparrow} - \hat{c}^\dagger_{i_L\downarrow}\right)|\Psi_{0\gamma}\rangle}{\langle \Psi_{0\gamma}|\left(\hat{c}^\dagger_{i_L\uparrow} - \hat{c}^\dagger_{i_L\downarrow}\right)|\Psi^{N-1}_0\rangle\langle\Psi^{N+1}_0|\left(\hat{c}^\dagger_{i_L\uparrow} + \hat{c}^\dagger_{i_L\downarrow}\right)|\Psi_{0\gamma}\rangle} < 0. \tag{5.60}$$

This is because only one of the $\hat{c}^\dagger_{i_L\downarrow}$ operators contribute for each choice of γ, adding only *one* minus to the overall calculation. Hence with singlet neighbor charge states the W and J amplitudes must always belong to *different interference classes*.

In the case of odd-alternant hydrocarbons (i.e., alternant hydrocarbons with an odd number of carbon atoms), the pairing theorem applies. In the case of half-filling we have from equation (5.24) that

$$\mathcal{A}|\Psi_\sigma^{N_a}\rangle = -|\Psi_{\bar\sigma}^{N_a}\rangle \tag{5.61}$$

Additionally we introduce a π spin rotation $\hat{R}_\pi$, which transforms $\hat{R}_\pi \hat{c}^\dagger_{i\sigma} \hat{R}^\dagger_\pi = -\sigma \hat{c}^\dagger_{i\bar\sigma}$. From this it can be shown that acting on spin eigenstates $|S, m\rangle$,

$$\hat{R}^\dagger_\pi|0,0\rangle = |0,0\rangle, \tag{5.62a}$$

$$\hat{R}^\dagger_\pi|\tfrac{1}{2},\sigma\rangle = -\sigma|\tfrac{1}{2},\bar\sigma\rangle \tag{5.62b}$$

$$\hat{R}^\dagger_\pi|1,0\rangle = -|1,0\rangle, \quad \hat{R}^\dagger_\pi|1,\pm 1\rangle = |1,\mp 1\rangle. \tag{5.62c}$$

In general we write $\hat{R}^\dagger_\pi|S, m\rangle = e^{i\varphi_m}|S, -m\rangle$. This makes it possible to transform (assuming m is only due to singlet or triplet spin degeneracy),

$$\langle \Psi^{N-1}_{0m}|\left(\hat{c}_{i_R\uparrow} \pm \hat{c}_{i_R\downarrow}\right)|\Psi_{0\gamma}\rangle = \langle \Psi^{N-1}_{0m}|\mathcal{A}^\dagger\mathcal{A}\left(\hat{c}_{i_R\uparrow} \pm \hat{c}_{i_R\downarrow}\right)\mathcal{A}^\dagger\mathcal{A}|\Psi_{0\gamma}\rangle$$

$$= (-1)^{i_R} e^{i(\gamma_0 - \gamma_m)}\langle \Psi^{N+1}_{0,-m}|\left(\hat{c}^\dagger_{i_R\uparrow} \pm \hat{c}^\dagger_{i_R\downarrow}\right)|\Psi_{0\bar\gamma}\rangle$$

$$= \pm(-1)^{i_R} e^{i(\gamma_0 - \gamma_m)} e^{-i\varphi_m}\langle \Psi^{N+1}_{0,m}|\left(\hat{c}^\dagger_{i_R\uparrow} \pm \hat{c}^\dagger_{i_R\downarrow}\right)|\Psi_{0\gamma}\rangle, \tag{5.63}$$

where we in the last expression applied the $\hat{R}_\pi$ spin rotation,

$$
\begin{aligned}
\mathcal{Q}i_W &= \frac{\sum_m \langle \Psi_{0\gamma} | \left(\hat{c}_{i_L\uparrow}^\dagger + \hat{c}_{i_L\downarrow}^\dagger \right) | \Psi_{0m}^{N-1} \rangle \langle \Psi_{0m}^{N-1} | \left(\hat{c}_{i_R\uparrow} + \hat{c}_{i_R\downarrow} \right) | \Psi_{0\gamma} \rangle}{\sum_n \langle \Psi_{0\gamma} | \left(\hat{c}_{i_R\uparrow} + \hat{c}_{i_R\downarrow} \right) | \Psi_{0n}^{N+1} \rangle \langle \Psi_{0n}^{N+1} | \left(\hat{c}_{i_L\uparrow}^\dagger + \hat{c}_{i_L\downarrow}^\dagger \right) | \Psi_{0\gamma} \rangle}, \\
&= (-1)^{i_R+i_L} \frac{\sum_m \langle \Psi_{0\gamma} | \left(\hat{c}_{i_L\uparrow}^\dagger + \hat{c}_{i_L\downarrow}^\dagger \right) | \Psi_{0m}^{N+1} \rangle \langle \Psi_{0m}^{N+1} | \left(\hat{c}_{i_R\uparrow} + \hat{c}_{i_R\downarrow} \right) | \Psi_{0\gamma} \rangle}{\sum_n \langle \Psi_{0\gamma} | \left(\hat{c}_{i_R\uparrow} + \hat{c}_{i_R\downarrow} \right) | \Psi_{0n}^{N+1} \rangle \langle \Psi_{0n}^{N+1} | \left(\hat{c}_{i_L\uparrow}^\dagger + \hat{c}_{i_L\downarrow}^\dagger \right) | \Psi_{0\gamma} \rangle}, \\
&= (-1)^{i_L+i_R}.
\end{aligned} \tag{5.64}
$$

Also for the exchange amplitude,

$$
\begin{aligned}
\mathcal{Q}i_J &= \frac{\sum_m \langle \Psi_{0\gamma} | \left(\hat{c}_{i_L\uparrow}^\dagger - \hat{c}_{i_L\downarrow}^\dagger \right) | \Psi_{0m}^{N-1} \rangle \langle \Psi_{0m}^{N-1} | \left(\hat{c}_{i_R\uparrow} + \hat{c}_{i_R\downarrow} \right) | \Psi_{0\gamma} \rangle}{\sum_n \langle \Psi_{0\gamma} | \left(\hat{c}_{i_R\uparrow} + \hat{c}_{i_R\downarrow} \right) | \Psi_{0n}^{N+1} \rangle \langle \Psi_{0n}^{N+1} | \left(\hat{c}_{i_L\uparrow}^\dagger - \hat{c}_{i_L\downarrow}^\dagger \right) | \Psi_{0\gamma} \rangle} \\
&= -(-1)^{i_R+i_L} \frac{\sum_m \langle \Psi_{0\gamma} | \left(\hat{c}_{i_L\uparrow}^\dagger - \hat{c}_{i_L\downarrow}^\dagger \right) | \Psi_{0m}^{N+1} \rangle \langle \Psi_{0m}^{N+1} | \left(\hat{c}_{i_R\uparrow} + \hat{c}_{i_R\downarrow} \right) | \Psi_{0\gamma} \rangle}{\sum_n \langle \Psi_{0\gamma} | \left(\hat{c}_{i_R\uparrow} + \hat{c}_{i_R\downarrow} \right) | \Psi_{0n}^{N+1} \rangle \langle \Psi_{0n}^{N+1} | \left(\hat{c}_{i_L\uparrow}^\dagger - \hat{c}_{i_L\downarrow}^\dagger \right) | \Psi_{0\gamma} \rangle} \\
&= -(-1)^{i_R+i_L} = -\mathcal{Q}i_W
\end{aligned} \tag{5.65}
$$

Hence for odd-alternant hydrocarbons the potential scattering transport and the exchange amplitude transport have opposite interference classes at half-filling.

5.8 Examples (Spin-Doublet)

The simplest example is the odd-alternant three site chain at half-filling. While the Feynman-Dyson orbital weight vanishes at the middle site, $\langle \Psi_{0\gamma} | \hat{c}_{2\sigma}^\dagger | \Psi_{0m}^{N-1} \rangle = 0$, the next orbitals in our expansion still obey the pairing theorem and the coloring rule holds. According to the doublet coloring rules the W amplitude belongs to the even interference class, while the J amplitude belongs to the odd class.
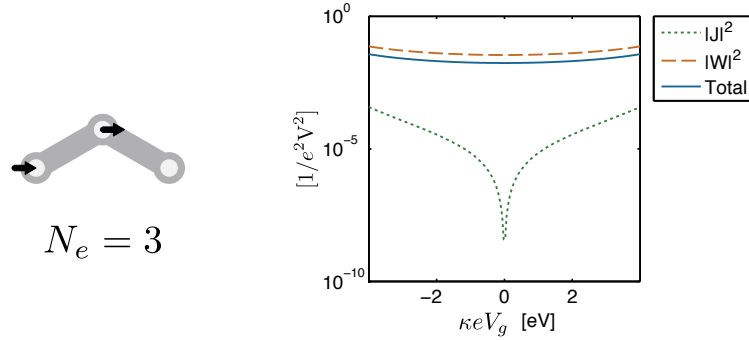

$$N_e = 3$$

Figure 5.15: The potential scattering and the excchange ampltidues for a simple three-site chain. The resulting total amplitude $|W|^2/2 + 3|J|^2/2$, shows no sign of the interference of $|J|^2$ correctly predicted by our coloring rule.

Alternatively we consider a an odd-alternant chain with a two side-coupled orbitals. Again the transport result obeys the coloring rule, but because both transport channels exhibit destructive interference the total conductance also shows some (although weaker)
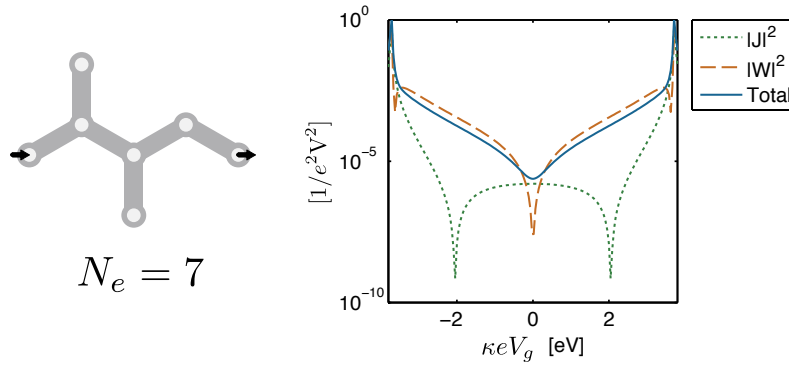
Figure 5.16: The potential scattering and the exchange amplitudes for a a seven-orbital model. While exchange and potential scattering belong to different interference classes, the interference is somewhat visible in the total amplitude $|W|^2/2 + 3|J|^2/2$.

interference feature. The coloring rules does not prohibit all interference features in the total conductance, but the rule still ensures that interference nodes are somewhat obscured.

Away from half-filling the coloring rule can be broken if (and only if) a neighbor charge states has (at least) a spin-triplet ground state. Using Lieb's theorem we engineer a molecule with a spin triplet ground state at half-filling. An example is shown in Figure 5.17 for the neutral−1 charge state of a cross-conjugated system.
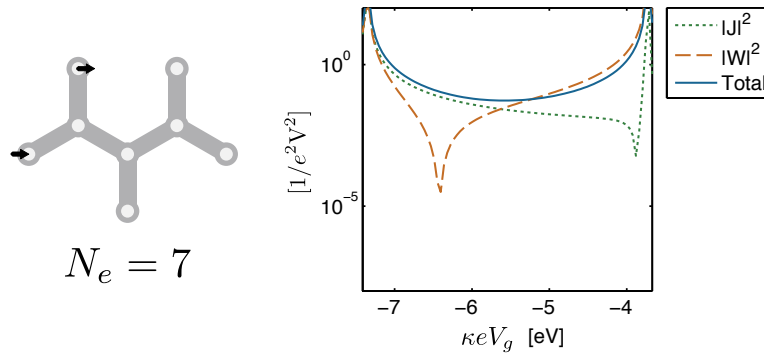

Figure 5.17: Here the 8-electron ground state is a triplet, hence voiding our interference theorem. As is obvious both W and J belong to the odd interference class.

Interference in transport through benzene in the 7 (or 5) electron charge state have previously been investigated. Here the interference effect was due to a vanishing Feynman-Dyson orbital weight, giving rise to a suppression of the sequential tunneling at one diamond edge.[9,10] Since the 6-electron ground state is a singlet, and the 4-electron (8-electron) ground state is a triplet, the theorem of equation (5.60) does no longer hold, and both W and J may belong to the same interference class. This is clearly illustrated in Figure 5.18 showing both $|W|^2$, $|J|^2$ and the total amplitude $\frac{1}{2}|W|^2 + \frac{3}{2}|J|^2$.
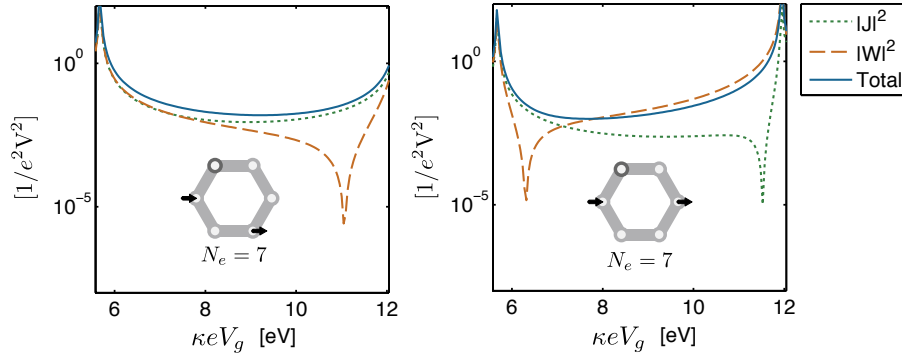
Figure 5.18: Calculation of transport amplitudes through benzene away from half-filling in the 7-electron charge state. In the meta-configuration the Feynman-Dyson overlap with the triplet ground state in the 8-electron charge state vanishes, and our theorem $\mathcal{Q}i_J = -\mathcal{Q}i_W$ holds. In the para-configuration this is not the case, and then $\mathcal{Q}i_J = \mathcal{Q}i_W < 0$. Note that in order to lift an additional orbital symmetry of the 7-electron ground state, we have introduced a small offset $\mu = -0.1$ eV at the colored site.

5.9   Conclusions

In this chapter we have investigated quantum interference in the off-resonant transport through Coulomb blockaded molecule junctions. We have found two quantum interference mechanism: between particle and hole transport, and within either particle (hole) channel.

We introduced the even and odd quantum interference classes determining the number of interference nodes in the off-resonant transport. For neutral alternant hydrocarbons with a singlet ground state we proved that the interference class be calculated using a simple coloring rule.

For doublet ground state molecules we showed that the transport is composed of a potential scattering channel and an exchange channel. When the neighbor charge states both have a singlet ground state, or for neutral odd-alternant hydrocarbons the two channels belong to different interference classes. For neutral hydrocarbons a coloring rule still predicts the interference class.

The work presented in this chapter is currently under preparation for publication in collaboration with M. Leijnse, M. Strange, G. Solomon and J. Paaske.

Chapter 6

Kondo Interference

The Kondo effect is a rich many-body phenomena still part of active research today. The Kondo model describes how a localized magnetic moment interacts with the electrons in a conduction band. At *very low temperatures* the magnetic moment and the free electrons can form a complex many-body anti-ferromagnetic state, where the electrons "try" to screen the local magnetic moment. In a metallic host the Kondo correlated many-body state increases the scattering cross-section of the magnetic impurity, and increases the resistivity of the conductor.[43]
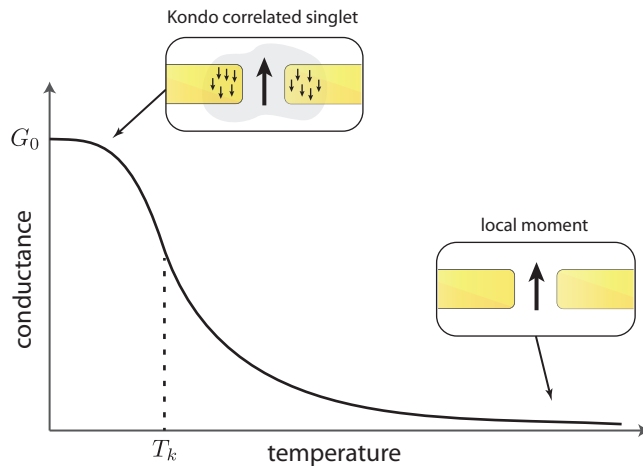

Figure 6.1: Kondo enchanced conductance at low temperatures, where the local magnetic moment form a spin-singlet like many-body state with the conduction electrons.

In quantum transport a quantum dot spin-doublet ground state can similarly be screened by the conduction electrons in both leads, and forms a spin-singlet like state (cf. Figure 6.1). The resulting increase in electron scattering from one lead to the other gives rise to a Kondo enhanced conductance at zero bias voltage. In the constant interaction model every odd-electron charge state is a spin doublet. At low temperatures every second Coulomb diamond then carries a Kondo enhanced zero-bias conductance[25,86] (cf. Figure 6.2).

Kondo effect has been found in quantum dot setups[34,35] as well as molecular junctions.[72,74a,95] However, according to Natelson et al.[68] some irregularities have been found in Kondo effect through molecules. In the previous chapter we investigated quantum interference in the off-resonant transport through organic molecule π-systems. The structure of the molecule and the contact geometry turned out to give and an interesting impact on the
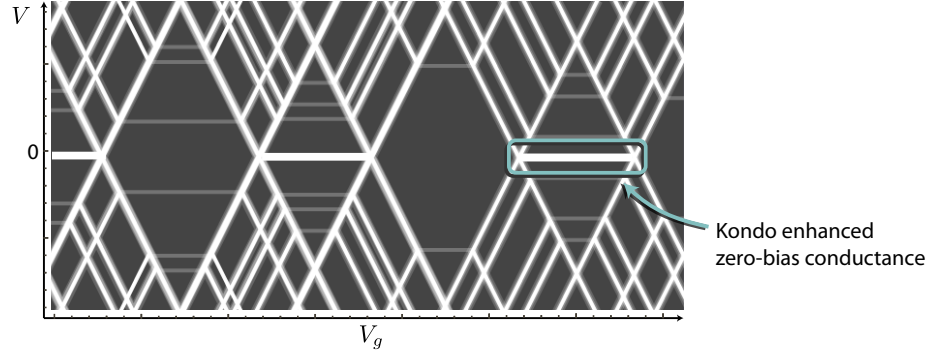
Figure 6.2: Every second charge state have a spin-doublet ground state, and at low temperatures the formation of a Kondo correlated state between the spin-doublet and the lead electrons will give rise to a Kondo enhanced zero-bias conductance anomaly.

interference features. In the following we wish to investigate whether quantum interference can influence the Kondo enhanced current.

6.1   The Schrieffer-Wolff Transformation

Our starting point is the full Hamiltonian describing a transport junction with a molecule (multiple quantum dot) coupled to two electrodes (cf. equation (4.4)),

$$\hat{H} = \hat{H}_0 + \hat{H}_T = \hat{H}_L + \hat{H}_R + \hat{H}_m + \hat{H}_g + \hat{H}_T. \tag{6.1a}$$

Here the operators are still given by,

$$\hat{H}_\alpha = \sum_{\nu\sigma} \xi_\nu \hat{c}^\dagger_{\alpha\nu\sigma} \hat{c}_{\alpha\nu\sigma}, \quad \alpha \in \{L, R\}, \tag{6.1b}$$

$$\hat{H}_g = -\kappa e V_g \sum_i \hat{n}_i, \tag{6.1c}$$

$$\hat{H}_T = \sum_{\nu\sigma} \left(t_L \hat{c}^\dagger_{L\nu\sigma} \hat{c}_{i_L\sigma} + t_R^* \hat{c}^\dagger_{i_R\sigma} \hat{c}_{R\nu\sigma} \right) + h.c. \tag{6.1d}$$

The molecule Hamiltonian $\hat{H}_m$ commutes with the number of electrons on the molecule $\hat{N}$, meaning that $\hat{H}_m$ is block-diagonal within each charge state N, and have eigenfunctions $|\Psi_i^N\rangle$ with corresponding eigenvalues E_i^N. The ground state in the N-particle charge state is assumed to be a spin-doublet $|\Psi_\sigma^N\rangle$ indexed by $\sigma = \uparrow, \downarrow$ with an eigenenergy E_0^N.

The first step is to perform a Schrieffer-Wolff transformation,[14,92] which reduces our model to an effective Kondo Hamiltonian. As a service to the reader, we perform this transformation in some detail. The Schrieffer-Wolff transformation projects out all states on the molecule except the doublet ground state $|\Psi_\sigma\rangle$. It is rather straightforward to calculate the effective Hamiltonian for this reduced molecule up to second order in the electrode hybridization, $\hat{H}_T$,

$$\hat{H}^{(0)}_{\sigma\sigma'} = \hat{H}^0_{\sigma\sigma'} = \langle \Psi_\sigma | \hat{H}_0 | \Psi_{\sigma'} \rangle, \tag{6.2a}$$

$$\hat{H}^{(1)}_{\sigma\sigma'} = \hat{H}^T_{\sigma\sigma'} = \langle \Psi_\sigma | \hat{H}^T_{\sigma\sigma'} | \Psi_{\sigma'} \rangle, \tag{6.2b}$$

$$\hat{H}^{(2)}_{\sigma\sigma'} = \langle \Psi_\sigma | \hat{H}_T \frac{1}{E_0 - \hat{H}_0} \hat{H}_T | \Psi_{\sigma'} \rangle. \tag{6.2c}$$

Here the indices σ and σ' run over the two doublet ground states $\Psi_\uparrow$ and $\Psi_\downarrow$. The first order term vanishes trivially, because the hybridization Hamiltonian $\hat{H}_T$ does not couple the two ground states. The zeroth order effective Hamiltonian is,

$$\hat{H}^{(0)} = \hat{H}_{LR} + E_0 + \hat{H}_g. \tag{6.3}$$

In order to deal with the the second order contribution, we introduce the annihilation and creation operator shorthand $\hat{c}^\eta$ with $\eta \in \{\dagger, \}$. Let $|n\rangle$ and $|n'\rangle$ symbolize two many-body lead states, and then rewrite the matrix elements of the second order contribution,

$$\langle n'|\hat{H}^{(2)}_{\sigma'\sigma}|n\rangle = \langle n'|\langle \Psi_{\sigma'}|\hat{H}_T \frac{1}{E_0 - \hat{H}_{LR} - \hat{H}_m - \hat{H}_g} \hat{H}_T |\Psi_\sigma\rangle|n\rangle$$

$$= \frac{1}{2} \sum_{\substack{\alpha\nu\gamma\eta \\ \alpha'\nu'\gamma'\eta'}} \sum_{|l\rangle} \langle n'|\hat{c}^{\eta'}_{\alpha'\nu'\gamma'}|l\rangle \langle \Psi_{\sigma'}|\hat{c}^{\bar{\eta}'}_{i_{\alpha'}\gamma'} \frac{t^*_{\alpha'} t_\alpha}{E_0 - \kappa e V_g N - \hat{H}_m - \hat{H}_g \pm \varepsilon_l} \hat{c}^{\bar{\eta}}_{i_\alpha\gamma}|\Psi_\sigma\rangle \langle l|\hat{c}^\eta_{\alpha\nu\gamma}|n\rangle. \tag{6.4}$$

Here l index the eigenspectra of either the $N+1$-electron or the $N-1$-electron charge state. The sign of ε_l depends on the actual values of α, α', η and η'. However, as is customary, we will drop ε_l.[14] Inspired by the previous chapters we introduce the particle and hole excitation energies $\varepsilon^h_{nm} = E^N_m - E^{N-1}_n$ and $\varepsilon^p_{nm} = E^{N+1}_n - E^N_m$, as well as the corresponding amplitudes,

$$p^{\alpha\gamma,\alpha'\gamma'}_{\sigma',\sigma}(V_g) = \sum_l \frac{\langle \Psi^N_{\sigma'}|\hat{c}_{i_\alpha\gamma}|\Psi^{N+1}_l\rangle\langle \Psi^{N+1}_l|\hat{c}^\dagger_{i_{\alpha'}\gamma'}|\Psi^N_\sigma\rangle}{\kappa e V_g - \varepsilon^p_{l0}}, \tag{6.5}$$

$$h^{\alpha\gamma,\alpha'\gamma'}_{\sigma',\sigma}(V_g) = \sum_l \frac{\langle \Psi^N_{\sigma'}|\hat{c}^\dagger_{i_{\alpha'}\gamma'}|\Psi^{N-1}_l\rangle\langle \Psi^{N-1}_l|\hat{c}_{i_\alpha\gamma}|\Psi^N_\sigma\rangle}{\kappa e V_g - \varepsilon^h_{l0}}. \tag{6.6}$$

The sum over $|l\rangle$ drops out, and assuming that the hopping amplitudes t_α can be chosen real, the second order contribution can be written on operator form,

$$\hat{H}^{(2)}_{\sigma'\sigma} = \sum_{\substack{\alpha\nu\gamma \\ \alpha'\nu'\gamma'}} t^*_{\alpha'} t_\alpha \left(\left(h^{\alpha\gamma,\alpha'\gamma'}_{\sigma',\sigma} + p^{\alpha\gamma,\alpha'\gamma'}_{\sigma',\sigma} \right) \hat{c}^\dagger_{\alpha\nu\gamma}\hat{c}_{\alpha'\nu'\gamma'} - h^{\alpha\gamma,\alpha'\gamma'}_{\sigma',\sigma} \delta_{\alpha\nu\gamma,\alpha'\nu'\gamma'} \right)$$

$$= \sum_{\substack{\alpha\nu\gamma \\ \alpha'\nu'\gamma'}} t^*_{\alpha'} t_\alpha \left(h^{\alpha\gamma,\alpha'\gamma'}_{\sigma',\sigma} + p^{\alpha\gamma,\alpha'\gamma'}_{\sigma',\sigma} \right) \hat{c}^\dagger_{\alpha\nu\gamma}\hat{c}_{\alpha'\nu'\gamma'} - \sum_{\alpha,\gamma} t^*_{\alpha'} t_\alpha h^{\alpha\gamma,\alpha\gamma}_{\sigma',\sigma}. \tag{6.7}$$

It is readily seen that the constant contribution $h^{\alpha\gamma,\alpha\gamma}_{\sigma',\sigma}$ is diagonal in $\sigma - \sigma'$ space. In fact this contribution is merely a constant which together with the $H^{(0)}$ contribution can be safely ignored in the following, i.e., $h^{\alpha\gamma,\alpha\gamma}_{\uparrow,\uparrow} = h^{\alpha\gamma,\alpha\gamma}_{\downarrow,\downarrow}$. We re-introduce the total amplitude $A^{\alpha\gamma,\alpha'\gamma'}_{\sigma,\sigma'} = h^{\alpha\gamma,\alpha'\gamma'}_{\sigma,\sigma'} + p^{\alpha\gamma,\alpha'\gamma'}_{\sigma,\sigma'}$. It can then be shown that,

$$\hat{H}^{(2)}_{\sigma\sigma} = \sum_{\substack{\alpha\nu\gamma \\ \alpha'\nu'\gamma}} t^*_{\alpha'} t_\alpha A^{\alpha\gamma,\alpha'\gamma}_{\sigma,\sigma} \hat{c}^\dagger_{\alpha\nu\gamma}\hat{c}_{\alpha'\nu'\gamma},$$

$$\hat{H}^{(2)}_{\bar{\sigma}\sigma} = \sum_{\substack{\alpha\nu\gamma \\ \alpha'\nu'\gamma}} t^*_{\alpha'} t_\alpha A^{\alpha\gamma,\alpha'\bar{\sigma}}_{\bar{\sigma},\sigma} \hat{c}^\dagger_{\alpha\nu\sigma}\hat{c}_{\alpha'\nu'\bar{\sigma}}. \tag{6.8}$$

The effective Hamiltonian can be written as a spin model in terms of the usual spin-like operators given by,

$$s^i_{\alpha v;\alpha' v'} = \frac{1}{2} \sum_{\sigma \sigma'} \hat{c}^\dagger_{\alpha v \sigma} \tau^i_{\sigma \sigma'} \hat{c}_{\alpha' v' \sigma''}, \text{ and} \tag{6.9}$$

$$S^i = \frac{1}{2} \sum_{\sigma \sigma'} \hat{c}^\dagger_\sigma \tau^i_{\sigma \sigma'} \hat{c}_{\sigma'}. \tag{6.10}$$

Here $\tau^i \in \{\tau^0, \tau^x, \tau^y, \tau^z\}$ are the usual Pauli matrices with $\tau^0 = \hat{I}$ being the identity operator. The effective *Kondo Hamiltonian* for the doublet ground state, then takes the usual form,

$$\hat{H}_K = \sum_{\alpha v} \sum_{\alpha' v'} J_{\alpha \alpha'} \mathbf{s}_{\alpha v;\alpha' v'} \cdot \mathbf{S} + \sum_{\alpha v \sigma} \sum_{\alpha' v'} W^\sigma_{\alpha \alpha'} \hat{c}^\dagger_{\alpha v \sigma} \hat{c}_{\alpha' v' \sigma}. \tag{6.11}$$

Here the exchange couplings J and the potential scattering W are given by,

$$J_{\alpha \alpha'} = 2 t_{\alpha'} t_\alpha A^{\alpha \sigma, \alpha' \bar{\sigma}}_{\bar{\sigma}, \sigma}, \quad \text{and} \quad W_{\alpha \alpha'} = \frac{1}{2} t_{\alpha'} t_\alpha \sum_\gamma A^{\alpha \gamma, \alpha' \gamma}_{\sigma, \sigma} \tag{6.12}$$

One arrives at this expression by using that $A^{\alpha \gamma, \alpha' \gamma}_{\sigma \sigma} - A^{\alpha \bar{\gamma}, \alpha' \bar{\gamma}}_{\sigma \sigma} = \sigma A^{\alpha \sigma, \alpha' \bar{\sigma}}_{\bar{\sigma}, \sigma}$ as discussed in the previous chapter 5 (remember the algebraic shorthand $\sigma = \downarrow \sim -1$ and $\sigma = \uparrow \sim +1$). For a given molecular system all relevant amplitudes can be evaluated numerically.

For a single-orbital quantum system (the so-called Anderson model) it is well known that the Schrieffer-Wolff transformation produces the *single-channel Kondo model* with all exchange couplings satisfying

$$\det \begin{pmatrix} J_{LL} & J_{LR} \\ J_{RL} & J_{RR} \end{pmatrix} = 0, \tag{6.13}$$

and with the potential scattering amplitudes proportional to the exchange coupling $W_{\alpha \beta}(V_g) = K(V_g) J_{\alpha \beta}(V_g)$. Extended structures consisting of more than one orbital, also reduce to a single-channel Kondo model, when the same orbital, $i_L = i_R$, connects to *both* electrodes.

For molecules with *different* sites connected to electrodes, the couplings are in general not identical, and in this case the effective Hamiltonian is a two-channel Kondo model. The two-channel Kondo model is known to have a non-Fermi liquid fixed point in some part of parameter space.

6.2 Poor Man's Scaling

We will attack the Kondo problem using the Poor man's scaling approach pioneered by Anderson[3] for the equilibrium Kondo problem with electrodes modeled as having constant density of states and bandwidth $2D_0$. The effect of integrating out an infinitesimal part δD of the conduction band can be calculated perturbatively in the coupling $J_{\alpha \beta}$. To second order the exchange J is then renormalized according to the Poor man's scaling equation, given by[81,88,89]

$$d_{\ln D} J_{\alpha \alpha'} = -\sum_\beta J_{\alpha \beta} J_{\beta \alpha'} \rho_\beta. \tag{6.14}$$

In the anti-ferromagnetic Kondo model the exchange couplings diverge at a critical bandwidth $D \sim T_K$, called the *Kondo temperature*. The Kondo temperature marks the breakdown

of the Poor man's perturbative scaling equations. In the already mentioned single-channel Kondo model (all $J_{\alpha\beta}$ equal), more advanced approaches like Wilson's numerical renormalization group[117] show that the couplings converge to a universal Fermi liquid fixed point.[69] At this fixed point the impurity spin and the electrons in both electrodes form a complex many-body antiferromagnetic state, where the electrons screen the impurity spin. In this screened state the junction acts as a single transport channel carrying a unit of conductance G_0.

For unequal couplings we assume equal density of states $\rho_L = \rho_R$, and define $g_{\alpha\beta} = J_{\alpha\beta}\rho_\alpha$ in order to simplify the scaling equation,

$$\mathrm{d}_{\ln D} g_{\alpha\alpha'} = -\sum_\beta g_{\alpha\beta} g_{\beta\alpha'}. \tag{6.15}$$

Here $g_{\alpha\alpha'}$ is a two-by-two tensor in the electrode indices. To simplify the calculations we write the couplings on the form,

$$g_{LR} = n_x + in_y \tag{6.16a}$$
$$g_{RL} = n_x - in_y \tag{6.16b}$$
$$g_{LL} = g_0 + n_z \tag{6.16c}$$
$$g_{RR} = g_0 - n_z. \tag{6.16d}$$

Then the $\mathbf{g}$ tensor can be written, $\mathbf{g} = g_0 \mathbf{I} + \mathbf{n} \cdot \boldsymbol{\tau}$, where τ_{ab}^i is the usual Pauli tensor. This allow us to write the scaling equation on the matrix form

$$\frac{\mathrm{d}\mathbf{g}}{\mathrm{d}\ln D} = -\mathbf{g} \cdot \mathbf{g} = g_0^2 + n^2 + 2g_0 \mathbf{n} \cdot \boldsymbol{\tau} \tag{6.17}$$

It is then easy to show that

$$\frac{\mathrm{d}g_0}{\mathrm{d}\ln D} = \frac{1}{2} \frac{\mathrm{d}(g_{LL} + g_{RR})}{\mathrm{d}\ln D} = -g_{LL}^2 - g_{RR}^2 - 2g_{LR}g_{RL} = (g_0^2 + n^2). \tag{6.18}$$

Similarly it is easy to find the derivative of the $\mathbf{n}$ vector.

$$\frac{\mathrm{d}\mathbf{n}}{\mathrm{d}\ln D} = 2g_0\mathbf{n}. \tag{6.19}$$

In fact the *length of the n vector* conforms to the *same* differential equation (6.19),

$$\frac{\mathrm{d}n}{\mathrm{d}\ln D} = \frac{\mathrm{d}\sqrt{n^2}}{\mathrm{d}\ln D} = \frac{\mathbf{n}}{n} \cdot \frac{\mathrm{d}\mathbf{n}}{\mathrm{d}\ln D} = 2g_0 n. \tag{6.20}$$

Interestingly the direction of $\mathbf{n}$ is preserved during scaling because,

$$\frac{\mathrm{d}\hat{n}}{\mathrm{d}\ln D} = \frac{1}{n}\frac{\mathrm{d}\mathbf{n}}{\mathrm{d}\ln D} - \frac{\mathbf{n}}{n^2}\frac{\mathrm{d}n}{\mathrm{d}\ln D} = 0. \tag{6.21}$$

By adding or subtracting equation (6.18) and equation (6.20), we obtain the two final scaling equations

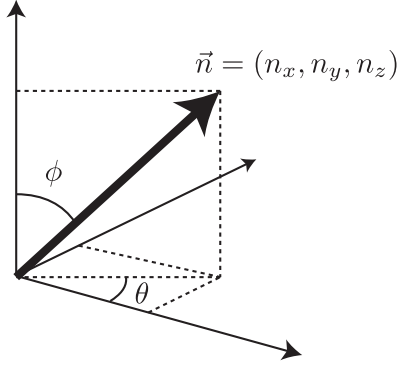$$\frac{\mathrm{d}(g_0 \pm n)}{\mathrm{d}\ln D} = -(g_0 \pm n)^2 \tag{6.22}$$

Figure 6.3: The **n** vector. The direction is preserved during scaling (cf. equation (6.21)).

Like in the original Poor man's scaling problem, these scaling equations have a constant of motion called the *Kondo Temperature* T_k. In this case there are two such constants of motion, given by,

$$T_k = De^{-1/(g_0+n)}, \qquad \text{and} \qquad T^* = De^{-1/(g_0-n)}. \tag{6.23}$$

The Kondo temperatures can be calculated from the initial values of the band width $D = D_0$ and the exchange couplings $J^0_{\alpha\beta}$. It is convenient to introduce the dimensionless Kondo parameters,

$$F_k = \left(\frac{T_k}{D_0}\right)^{-eV/(2|t|^2\rho)}, \qquad \text{and} \qquad F^* = \left(\frac{T^*}{D_0}\right)^{-eV/(2|t|^2\rho)}. \tag{6.24}$$

Here we have introduced the average $t = (t_L + t_R)/2$. Knowing the two constants of motion, the rescaled couplings are given as a function of the scaling parameter D, in the following way,

$$\frac{g_0}{\rho|t|^2/eV} = \frac{1}{\ln(F_k D/D_0)} + \frac{1}{\ln(F^* D/D_0)}, \tag{6.25a}$$

$$\frac{n}{\rho|t|^2/eV} = \frac{1}{\ln(F_k D/D_0)} - \frac{1}{\ln(F^* D/D_0)} \tag{6.25b}$$

Scaling the bandwidth D from some value D_0 towards zero, the running couplings g_0 or n diverge at some point during the scaling if either $F_k < 1$ or $F^* < 1$.

The scaling of the bandwidth is terminated, when the bandwidth approaches the typical energy scale of the junction – normally given by the temperature of the electrodes, T, the bias voltage, V, or an external magnetic field, B.[89] Poor man's scaling captures the behavior of the junction, when the typical energy scale lies above the Kondo temperature, i.e., $k_b T > T_K$. Here the differential conductance is proportional to the rescaled g_{LR}, which for real exchange couplings $g_{LR} = |n|\sin(\phi)$, and

$$\frac{dI}{dV} \propto |g_{LR}|^2 = |n|^2 \sin^2(\phi) = \left|\frac{1}{\ln(T/T_k)} - \frac{1}{\ln(T/T^*)}\right|^2 \frac{|J^0_{LR}|^2}{|J^0_{LR}|^2 + |J^0_{LL} - J^0_{RR}|^2/4}. \tag{6.26}$$

Alternatively, if we wish to calculate the universal conductance below the Kondo temperature, Goldhaber-Gordon have developed a phenomenological expression for the conductance[34,54] based on NRG simulations of the single-channel Kondo model,

$$G(k_b T) = G_0 \left(1 + \left(\frac{k_b T}{T'_k}\right)\right)^{-s}, \quad \text{with} \quad T'_k = \frac{T_k}{\sqrt{2^s - 1}}, \quad \text{and} \quad s = 0.22. \qquad (6.27)$$

Introduce the dimensionless temperature, $F = (k_b T/D_0)^{-eV/(2|t|^2 \rho)}$, which runs from unity to zero during scaling. The Goldhaber-Gordon formula is then,

$$G(F) = G_0 \left(1 + \left(\frac{F}{F'_k}\right)\right)^{-s} \quad \text{with} \quad F'_k = \frac{F_k}{\sqrt{2^s - 1}}, \quad \text{and} \quad s = 0.22. \qquad (6.28)$$

It is generally believed that the potential scattering $W_{\alpha\beta}$ is irrelevant for the scaling of the exchange couplings.[70] However, because we are interested in interference, the potential scattering W can be orders of magnitudes larger than the exchange, J. A more detailed analysis can reveal to what degree we should be concerned about the potential scattering. However, we will expose such an analysis to later works, and continue with the scaling equations (6.15) in the following.

6.3 Interference in the Kondo-Enhanced Conductance

We can only speculate whether interference in the initial value of the J_{LR} coupling constant, discussed in the previous chapter, will survive the scaling.
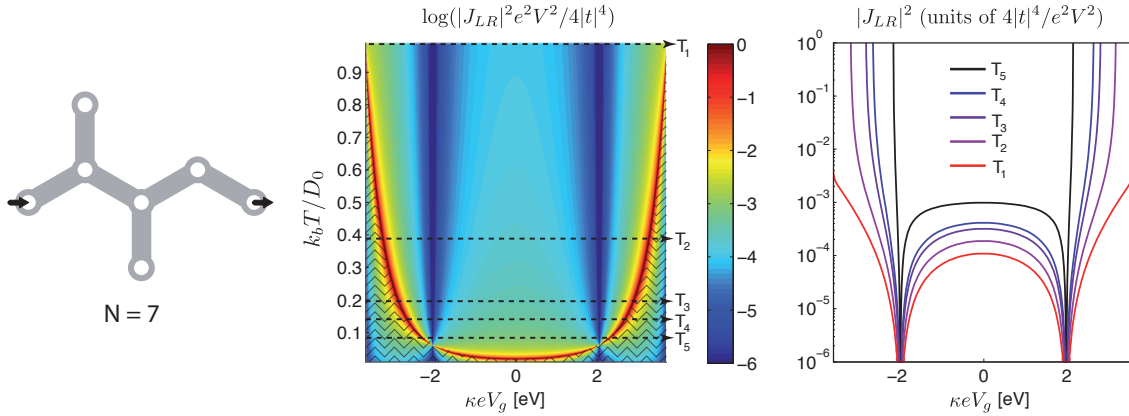

Figure 6.4: Interference in the zero-bias Kondo enhanced conductance. We assume equal coupling to both electrodes with $t = t_L = t_R$. The color plot shows the scaling of $|J_{LR}|^2$ in units of $4|t|^4/e^2 V^2$, where the shaded region marks the complete break down of the perturbative scaling. The line cuts hihglight, how the persistence of the destructive interference feature for temperatures larger than the Kondo temperature.

Above the Kondo temperature the Poor man's scaling analysis provides a useful tool for calculating the rescaled conductance. For a biradical hydrocarbon with two interference nodes in the initial exchange coupling (also considered in the previous chapter), we perform the Poor man's scaling analysis for temperatures above the Kondo temperature (cf. Figure 6.4). The two destructive interference nodes prevail, but the feature becomes

more abrupt at lower temperatures. This is easily seen to be consistent with the scaling
equations (6.15), where $\mathrm{d}_{\ln D} J_{LR} \propto J_{LR}$.

It is still unclear whether such destructive interference features will prevail in the
unitary limit as $T \to 0$, and perturbative scaling methods cannot settle this issue. In
order to determine the relevance of interference below the Kondo temperature, a further
analysis is necessary using more sophisticated numerical methods such as Wilson's numerical
renormalization group.[117]

6.4   Partial Ferromagnetic Kondo Effect

When the exchange coupling J is negative, the scaling equations (6.15) do not diverge as
the bandwidth is reduced. Instead they converge to the (unstable) fixed-point $J = 0$. For
equal couplings this is a direct consequence of the scaling equation, $\mathrm{d}g/\mathrm{d}\ln D = -2g^2$. In
this case the exchange couplings are quenched and only the potential scattering contributes
to the total current.

For general values of the exchange couplings J_{LL}, J_{RR} and J_{LR}, ferromagnetic scaling
depends on at least two of the couplings being negative, or alternatively that only one of
the same-electrode couplings, J_{LL} or J_{RR}, is negative and completely dominates the scaling
behavior. While the destructive interference of J_{LR} coupling constant depend on which two
orbitals couple to the electrodes. For the same electrode couplings J_{LL} and J_{RR}, we can
dissect the amplitudes $A^{\alpha\sigma,\alpha\bar{\sigma}}_{\sigma\bar{\sigma}}$, starting with the hole amplitude. Because the sign of the
amplitude is important, we will not introduce an interference class. Instead we consider
the *numerators*, h_n, of the poles, which constitutes the hole amplitude,

$$h_n = \sum_\sigma \langle \Psi_{0\bar{\sigma}} | \hat{c}^\dagger_{i_\alpha \bar{\gamma}} | \Psi^{N-1}_n \rangle \langle \Psi^{N-1}_n | \hat{c}_{i_\alpha \gamma} | \Psi_{0\sigma} \rangle. \tag{6.29}$$

If the state $|\Psi^{N-1}_n\rangle$ is a spin singlet (ignoring any other symmetries), choosing e.g. $\sigma = \uparrow$,
we have that

$$\begin{aligned} h_n &= \langle \Psi_{0\bar{\gamma}} | \hat{c}^\dagger_{i_\alpha \bar{\gamma}} | \Psi^{N-1}_n \rangle \langle \Psi^{N-1}_n | \hat{c}_{i_\alpha \gamma} | \Psi_{0\gamma} \rangle \\ &= \langle \Psi_{0\gamma} | \hat{c}^\dagger_{i_\alpha \gamma} | \Psi^{N-1}_n \rangle \langle \Psi^{N-1}_n | \hat{c}_{i_\alpha \gamma} | \Psi_{0\gamma} \rangle \geq 0. \end{aligned} \tag{6.30}$$

At the last equality we employed the spin reversion $\hat{R}_\pi$, which in spin $1/2$ space transforms
$\hat{R}^\pi \hat{c}^\dagger_{i\sigma} (\hat{R}^\pi)^\dagger = -\sigma \hat{c}^\dagger_{i\bar{\sigma}}$. The corresponding particle amplitude (with $|\Psi^{N+1}_n\rangle$ assumed to be a
singlet) have the numerators,

$$\begin{aligned} p_n &= \langle \Psi_{0\bar{\gamma}} | \hat{c}_{i_\alpha \gamma} | \Psi^{N+1}_n \rangle \langle \Psi^{N+1}_n | \hat{c}^\dagger_{i_\alpha \bar{\gamma}} | \Psi_{0\gamma} \rangle \\ &= -\langle \Psi_{0\gamma} | \hat{c}_{i_\alpha \bar{\gamma}} | \Psi^{N+1}_n \rangle \langle \Psi^{N+1}_n | \hat{c}^\dagger_{i_\alpha \bar{\gamma}} | \Psi_{0\gamma} \rangle \leq 0. \end{aligned} \tag{6.31}$$

Again we used the spin reversion in the last equality.

Adding the positive numerator hole amplitudes and the negative numerator particle
amplitudes result in *positive* values of $J_{\alpha\alpha}$. Assume instead that $|\Psi^{N\pm 1}_{nm}\rangle$ is part of a
spin triplet indexed by $m = -1, 0, 1$. Then spin reversion applied in the evaluation of the
numerators produces an additional sign, $\hat{R}_\pi |\Psi^{N\pm 1}_{n0}\rangle = -|\Psi^{N\pm 1}_{nm}\rangle$. Hence, the only way to
circumvent the "positiveness" of $J_{\alpha\alpha}$ is to couple (strongly) to one or more spin triplet
eigenstates of the neighbor charge states. In the following we will examine some examples,
where the (strong) coupling to triplet states produce ferromagnetic scaling.

6.5 Examples

Here we will investigate various anomalous Kondo Effect behaviors for some chosen example systems. To keep things simple we will in general assume equal hopping between the electrodes and the molecule, $t_L = t_R = t$.
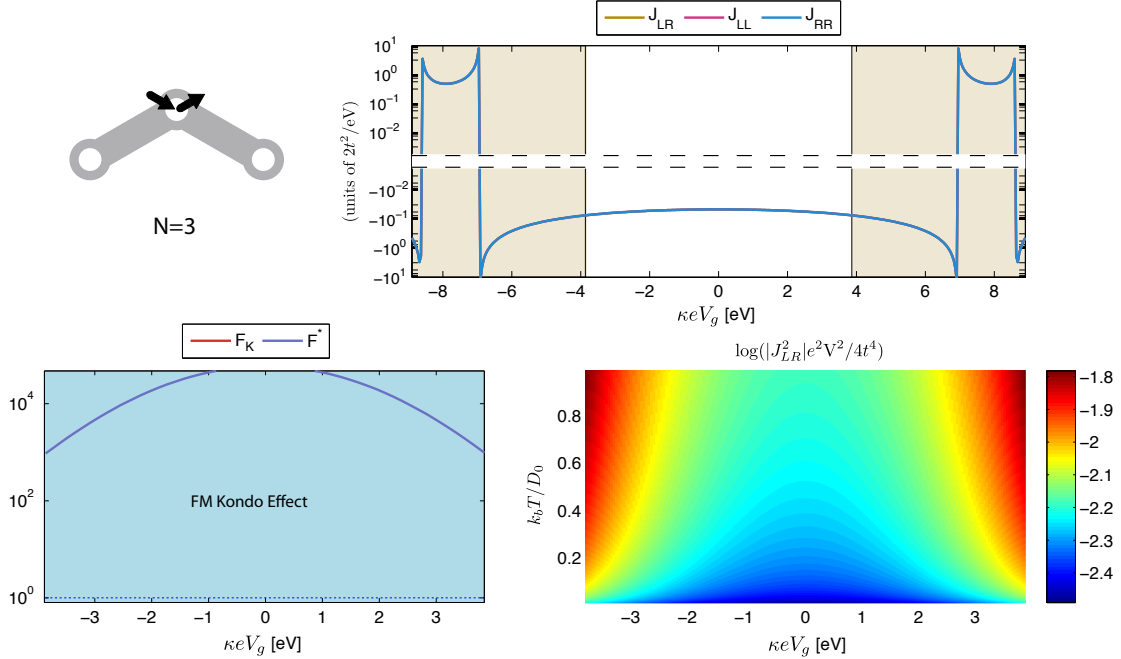

Figure 6.5: Ferromagnetic Kondo effect in a simple three-orbital model. The exchange couplings are shown both within the relevant charge state (unshaded) and extended beyond (shaded). The first Feynman-Dyson orbital vanishes at the center site, and *removes* the pole at the charge-degeneracy point. The coupling to the first excited state does not vanish. This state is a triplet forcing all $J_{LL} = J_{RR} = J_{LR}$ to be negative, and produces FM Kondo effect.

The simplest example is a three-orbital radical model equivalent to a triple quantum dot. Here we couple both electrodes to the center orbital as shown in Figure 6.5. When the three-orbital model is mirror symmetric, the coupling to the neighbor charge states $N \pm 1$ vanishes when coupling through the center orbital. The first excited state is a spin triplet, which forces all the couplings to be negative, and produces a ferromagnetic (FM) Kondo scaling. The ferromagnetic scaling is readily seen from the computed Kondo scaling parameters, which are both *larger* than unity $F_k > 1$ and $F^* > 0$.

Similar systems have also been considered by both Numata et al.[71] and Baruselli et al.[7], using a numerical renormalization group (NRG) approach, and their results confirm our findings.

Benzene have triplet states in the $N = 4$ and $N = 8$ electron charge states. All the N odd charge states of benzene have an additional orbital degeneracy, which can be lifted by a chemical potential offset on a single site. We investigate Kondo effect in the $N = 7$ electron charge state, and the result is presented in Figure 6.6. Towards the 6-electron charge state, we have usual AFM Kondo, while towards the 8-electron side, we have FM
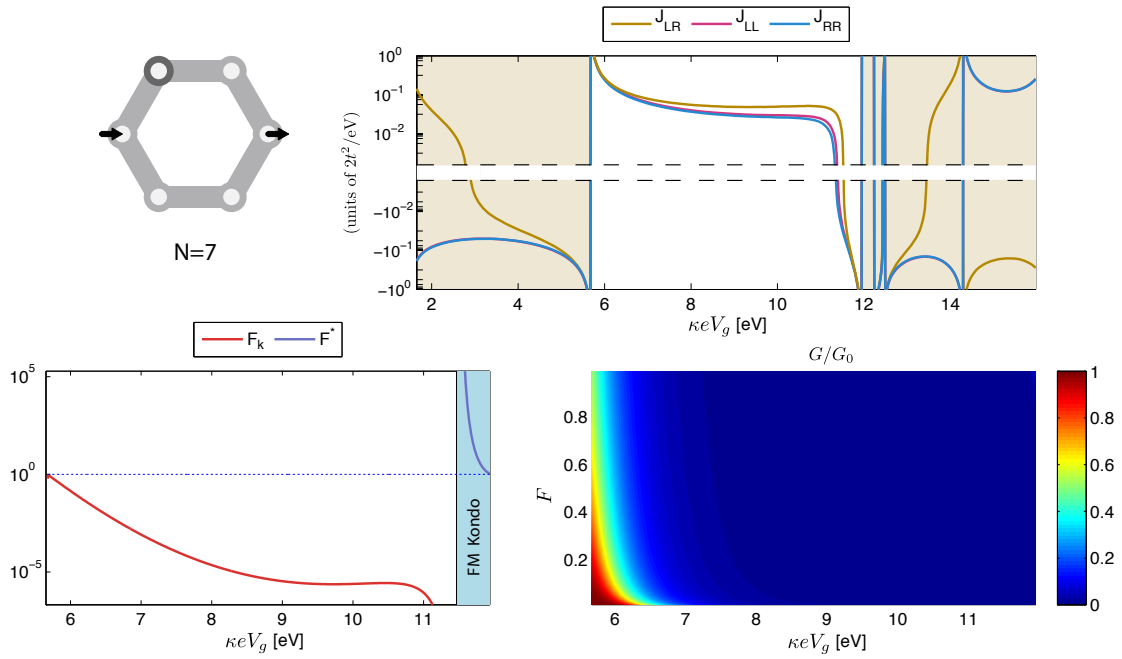
Figure 6.6: Kondo interference in a benzene ring. Note that only a small region of gate exhibits ferromagnetic Kondo effect. Effectively the Kondo interference have been cut out at one site. Note that we have broken the orbital degeneracy with a small offset $\mu = -0.1$ eV at the colored orbital, and that we here plot the conductance as given by equation (6.28).
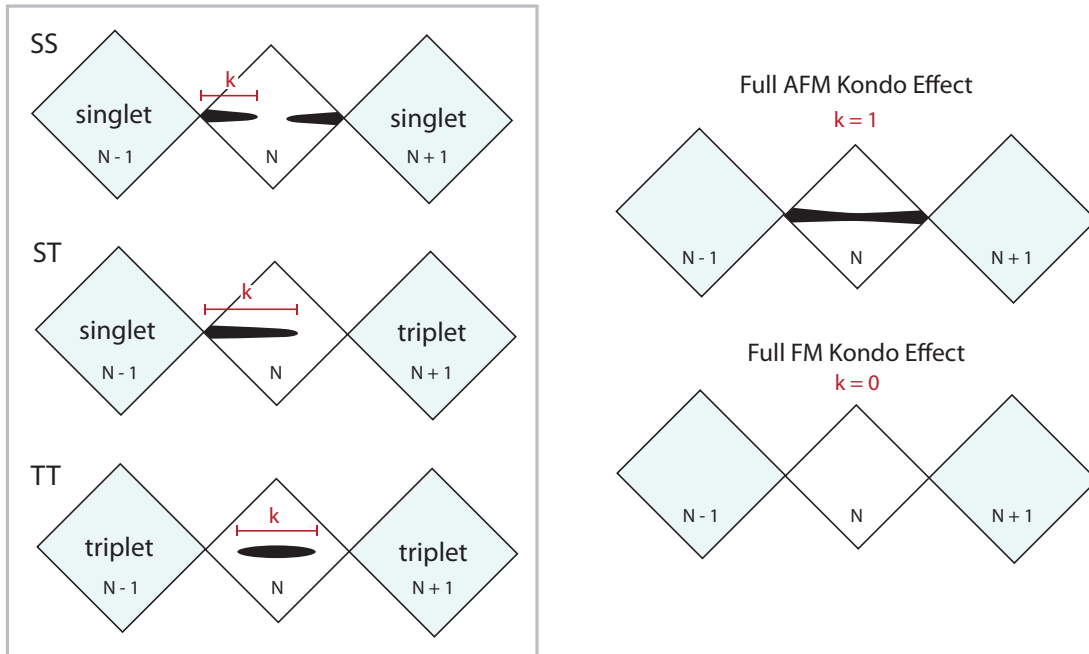

Figure 6.7: Classification of Kondo interference patterns depending on the spin of the ground state of the neighboring charge states. As indicated the full anti-ferromagnetic Kondo effect and the full ferromagnetic Kondo effect are special cases of all the possible patterns.
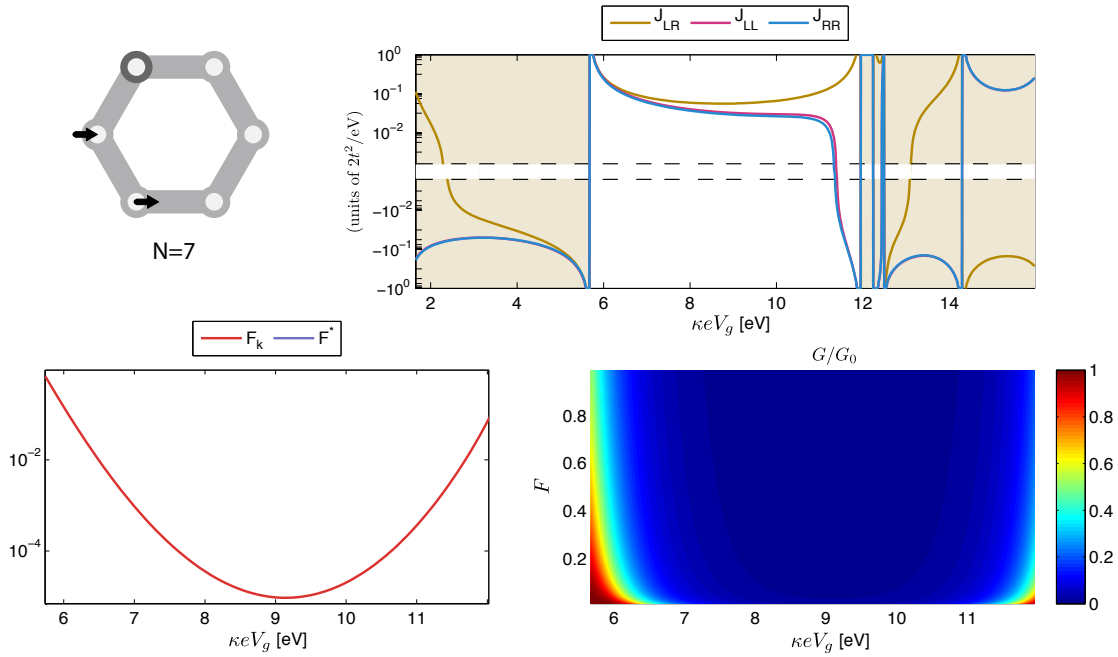
Figure 6.8: Ortho-coupled benzene. when the same site coupling constants become negative close to the triplet charge degeneracy point J_{LR} dominates the scaling. See also the scaling flow in Figure 6.9.
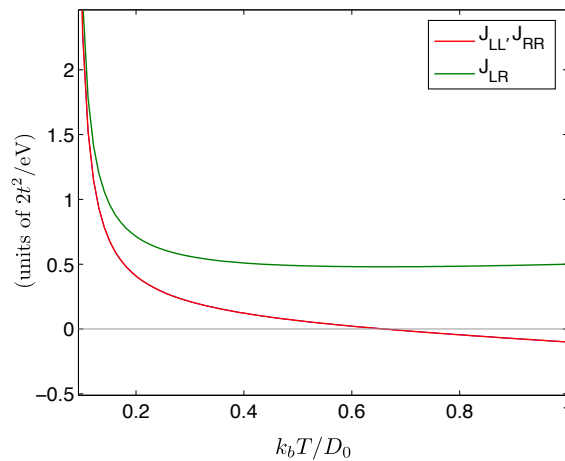
Figure 6.9: Scaling of coupling constants with initial conditions $J_{LL} = J_{RR} = -0.1 \cdot 2|t|^2/e\mathrm{V}$ and $J_{LR} = 0.5 \cdot 2|t|^2/e\mathrm{V}$. Note how J_{LR} dominates the scaling up until the Kondo temperature, where all the couplings flow together.

Kondo. The cross-over between the two types of Kondo effect is directly visible in the dimensionless Kondo scaling parameters. At one side, they are both

The benzene example is prototypical for doublet ground states with singlet and triplet ground states in the two charge state neighbors, of which we show a few more in an appendix. In fact not many possibilities exist for the possible patterns of AFM and FM Kondo effect. We show a simple schematic of the different possibilities in Figure 6.7.

Let us apply this table to the two examples we have considered so far. The three-orbital model is special: It is of the singlet-singlet type, but has $k = 0$ and ends up in the full FM Kondo case. The benzene example is a clearly singlet-triplet case with an intermediate value of k.

Another interesting example is benzene connected to the leads in the ortho configuration. The result of our calculation is shown in Figure 6.8. The main difference compared to the previous example is that the off-diagonal coupling J_{LR} is now positive. In this case J_{LR} alone determines the scaling when the $J_{\alpha\alpha}$ are negative, and the whole charge state has AFM Kondo. It is unusual but interesting to have J_{LR} win over the same-lead couplings, and a plot of the running couplings are shown in Figure 6.9.

6.6 Conclusions

In this chapter we have investigated the interference in the Kondo enhanced zero-bias conductance using a Poor man's scaling approach. We have shown that the interference nodes in the exchange coupling J (and hence the conductance) persists under scaling when considering transport above the Kondo temperature.

We have also shown how the interference structure in the exchange coupling may lead to a ferromagnetic Kondo effect, which repress the zero-bias conductance. If one of the ground states in the two neighbor charge states is a spin-triplet, one may even have both Kondo enhanced and Kondo suppressed zero-bias conductance within the same charge state. This means that it is possible to reach both regimes by tuning the backgate voltage.

The work presented in this chapter, is also being composed into a publication.

Chapter 7

Molecular Electron Pumps

This story begins with the suggestion of a design for an all-electrical molecular motor by Seldenthuis et al.[96]. This molecular motor shown in Figure 7.1 is constructed from an organic molecule with two sidearms comprising different species of hetero-atoms (nitrogen and oxygen). The hetero-atoms create a permanent electric dipole moment in the molecule, and the dipole moment can then be manipulated by the electrostatic backgate. A periodically changing electrostatic potential rotates the sidearms, and this rotation can be detected as a change in the junction conductance.
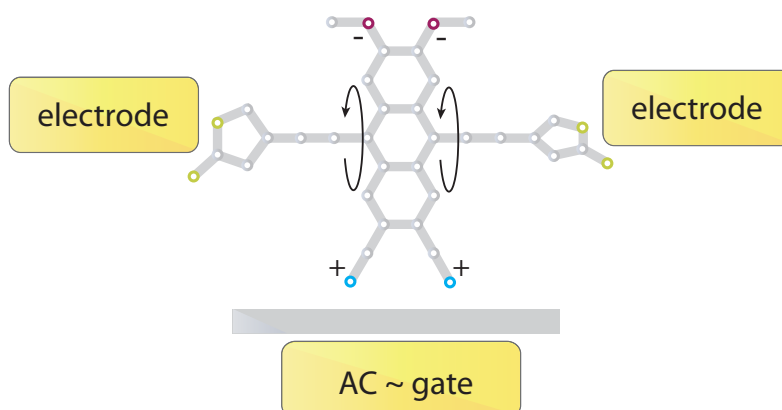
Figure 7.1: The all electrical molecular pump proposed by Seldenthuis et al.[96]. The alternating potential on the backgate repels and attracts the hetero-atoms on the sidearms of the molecule, causing the arms to rotate. The instantaneous conductance through the π-system changes periodically as a function of the rotation angle of the p_z-orbitals on turning carbon backbone.

The rotating molecule can also pump electrons from one electrode to the other, much like a quantum mechanical analog of the Archimedes screw shown in Figure 7.2. It is unknown if the pumping of electrons through the molecule necessitates a full quantum mechanical calculation of the transport, or the pumping can be described semi-classically as a simple charging effect. The aim of this chapter is cast some light upon this conundrum, and the important question we will try to answer is: Whether a coherent quantum pump is significantly different from a semi-classical pump?

It turns out that quantum pumping in mesoscopic systems have already been investigated heavily in the scientific literature, starting with the seminal paper by Thouless[113]. Since
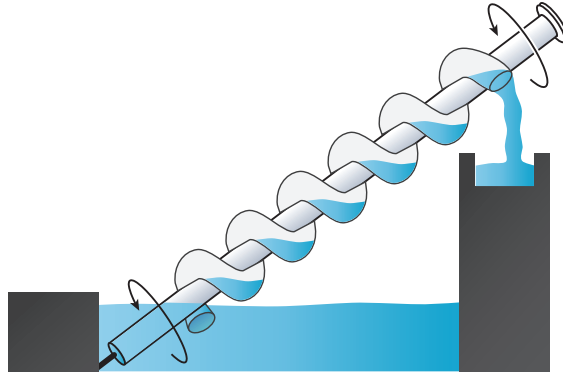
Figure 7.2: **The archimedes screw** is a simple mechanical pump, where the turning of the screw transports water (or other stuff).

then, several works have been dedicated to *adiabatic charge pumping*,[13,18,21,22] where both the size of the pumping perturbation V and the driving period T is small, so $VT \ll 1$.

Most experiments, which investigates electron pumping, have focused on quantum dot turnstile geometries, where a ratchet, which moves back and forth between the electrodes, carry an integer number of electrons from one electrode to the other.[33,84] This kind of pumping is due to a simple charging effect of the ratchett, which makes quantum coherency completely irrelevant. However, coherent quantum pumping have been investigated experimentally in quantum dots by Switkes et al.[109] and (more importantly) Vavilov, Dicarlo, and Marcus[115], who tried to distinguish quantum pumping from classical pumping by examining the symmetry of the pumped current under an applied magnetic field.

In order to investigate quantum coherent transport we develop a fairly intelligible Floquet scattering method. The Floquet method utilizes that the periodic driving scatters an incoming electron into transmitted and reflected components in the many *driving-induced* sidebands. This scattering mechanism was first investigated in the adiabatic regime by Büttiker and Landauer.[16,17] We will apply the Floquet scattering method on the Hückel level of theory ignoring electron-electron interactions completely. The approach is quite close to the work done by Agarwal and Sen[1], and comparable to the non-equilibrium Green's function calculations performed by Arrachea[4].

7.1   Naive Floquet Scattering Theory

Consider a general Hückel model for (spin-less) electrons, described by the Hamiltonian

$$\hat{H} = \hat{T} + \hat{H}_\varepsilon = \sum_{\langle i,j \rangle} \left(t_{ij} \hat{c}_i^\dagger \hat{c}_j + t_{ji} \hat{c}_j^\dagger \hat{c}_i \right) + \sum_i \varepsilon_i \hat{n}_i. \tag{7.1}$$

Assume that some parameters t_{ij}, ε changes periodically on time τ, such that after a period T, $H(\tau) = H(\tau + T)$. The radian frequency of the oscillation is given by $\Omega = 2\pi/T$, and the Hamiltonian for this periodically driven system can be decomposed into Fourier components indexed by ν,

$$H(\tau) = \sum_\nu H^\nu e^{i\nu\Omega\tau}. \tag{7.2}$$

If $H(\tau)$ depends harmonically[a] on time, only $H^{\pm 1}, H^0 \neq 0$. The wavefunction $\psi(\tau)$ can also be written as a sum of Fourier components,

$$\psi_n(\tau) = \sum_{\omega} \psi^{\omega} e^{-i\omega\tau}. \tag{7.3}$$

Writing down Schrödinger's equation in Fourier space, we have,

$$i\hbar\partial_t \psi(\tau) = H(\tau)\psi(\tau), \tag{7.4a}$$

$$\sum_{\omega} \hbar\Omega \psi^{\omega} e^{-i\omega\tau} = \sum_{\nu} H^{\nu} \sum_{\omega'} \psi^{\omega'} e^{i(-\omega'+\nu\Omega)\tau}, \tag{7.4b}$$

$$\hbar\Omega \psi^{\omega} = \sum_{\nu} H^{\nu} \psi^{\omega+\nu\Omega}. \tag{7.4c}$$

Rewriting $\omega = \omega_{\mu} = \omega_0 + \mu\Omega$, we get that

$$\hbar\omega_{\mu}\psi^{\mu} = \sum_{\nu} H^{\nu}\psi^{\mu+\nu}. \tag{7.5}$$

We have up till now considered the Hamiltonian quite generally. In basis of tight-binding orbitals $|n\rangle$ the tight-binding Hamiltonian, takes the form,

$$H_n^{\nu} = |n\rangle\langle n|H^{\nu} = -\sum_{m\neq n} t_{nm}^{\nu}|n\rangle\langle m| + \varepsilon_n^{\nu}|n\rangle\langle n|. \tag{7.6}$$

Note that we have introduced the Fourier components t_{nm}^{ν} of ε_n^{ν} of the tight-binding model parameters. Applying this to equation (7.5), gives us the result,

$$\hbar\omega_{\mu}\psi_n^{\mu} = \sum_{\nu}\left(-\sum_{m\neq n} t_{nm}^{\nu}\psi_m^{\mu+\nu} + \varepsilon_n^{\nu}\psi_n^{\mu+\nu}\right). \tag{7.7}$$

Starting from some value of the wave-function ψ_n^{μ}, we end up traversing a grid in (n, ν)-space connected by Fourier components t_{nm}^{ν} and ε_n^{ν}.

When the Hamiltonian depends harmonically on time, it only "connects" neighbor sites in the (n, ν)-grid as pictured in Figure 7.3. This can be directly realized when calculating,

$$\hbar\omega_{\mu}\psi_n^{\mu} = \sum_{\nu}\left(-\sum_{m=\pm 1} t_{n\,n\pm 1}^{\nu}\psi_{n\pm 1}^{\mu+\nu} + \varepsilon_n^{\nu}\psi_n^{\mu+\nu}\right) \tag{7.8}$$

$$= \sum_{\nu}\left(-t_{n\,n+1}^{\nu}\psi_{n+1}^{\mu+\nu} - t_{n\,n-1}^{\nu}\psi_{n-1}^{\mu+\nu} + \varepsilon_n^{\nu}\psi_n^{\mu+\nu}\right). \tag{7.9}$$

Collecting coefficients into vectors $\boldsymbol{\psi}_n = (\ldots, \psi_n^{-N}, \ldots, \psi_n^{\nu-1}, \psi_n^{\nu}, \psi_n^{\nu+1}, \ldots)$, the above equation can be written as a matrix equation.

$$\hbar\boldsymbol{\omega}^{\dagger}\mathbf{I}\boldsymbol{\psi}_n = -\mathbf{t}_{n\,n+1}\boldsymbol{\psi}_{n+1} - \mathbf{t}_{n\,n-1}\boldsymbol{\psi}_{n-1} + \boldsymbol{\varepsilon}_n\boldsymbol{\psi}_n. \tag{7.10}$$

---

[a]Harmonically means that the parameters only depend on time through harmonic functions of the form, $cos(\Omega\tau + \phi)$.
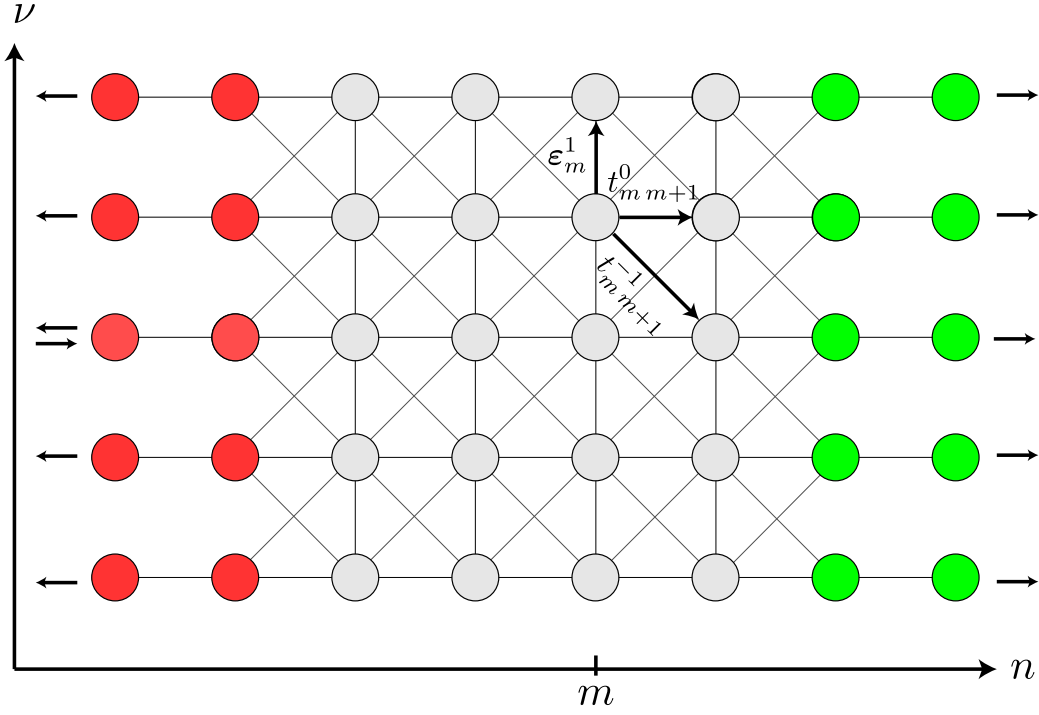
Figure 7.3: (n, ν)-grid when only $H^{\pm 1}, H^0 \neq 0$. Red sites denotes the incoming wavefunction and reflected waves in the left electrode, while the green sites labels the transmitted modes of the right lead.

Here

$$
\mathbf{t}_{n\,n+1} = \begin{pmatrix}
\ddots & \ddots & \ddots & & & \\
 & t^{-1}_{n\,n+1} & t^0_{n\,n+1} & t^1_{n\,n+1} & & \\
 & & t^{-1}_{n\,n+1} & t^0_{n\,n+1} & t^1_{n\,n+1} & \\
 & & & t^{-1}_{n\,n+1} & t^0_{n\,n+1} & t^1_{n\,n+1} \\
 & & & & \ddots & \ddots & \ddots
\end{pmatrix},
\tag{7.11}
$$

and $\mathbf{t}_{n+1,n} = (\mathbf{t}_{n,n+1})^\dagger$. When there is no additional phase arising because of e.g. a magnetic field, we have that $\mathbf{t}_{n+1,n} = (\mathbf{t}_{n,n+1})^\dagger = \mathbf{t}_{n,n+1}$. The energy offset matrix shares the tridiagonal structure,

$$
\varepsilon_n = \begin{pmatrix}
\ddots & \ddots & \ddots & & & \\
 & \varepsilon^{-1}_n & \varepsilon^0_n & \varepsilon^1_n & & \\
 & & \varepsilon^{-1}_n & \varepsilon^0_n & \varepsilon^1_n & \\
 & & & \varepsilon^{-1}_n & \varepsilon^0_n & \varepsilon^1_n \\
 & & & & \ddots & \ddots & \ddots
\end{pmatrix}.
\tag{7.12}
$$

Isolating $\boldsymbol{\psi}_{n+1}$ we get that

$$
\boldsymbol{\psi}_{n+1} = \mathbf{t}^{-1}_{n\,n+1}\left(\varepsilon_n - \hbar\boldsymbol{\omega}^\dagger \mathbf{I}\right)\boldsymbol{\psi}_n - \mathbf{t}^{-1}_{n\,n+1}\mathbf{t}_{n\,n-1}\boldsymbol{\psi}_{n-1}.
\tag{7.13}
$$

Writing this as a matrix equation

$$\begin{pmatrix} \psi_{n+1} \\ \psi_n \end{pmatrix} = \mathbf{T}_n \begin{pmatrix} \psi_n \\ \psi_{n-1} \end{pmatrix}. \tag{7.14}$$

The forward scattering *transfer matrix* looks like,

$$\mathbf{T}_n = \begin{pmatrix} \mathbf{t}_{n\,n+1}^{-1}(\boldsymbol{\varepsilon}_n - \hbar\boldsymbol{\omega}^\dagger\mathbf{I}) & -\mathbf{t}_{n\,n+1}^{-1}\mathbf{t}_{n\,n-1} \\ \mathbf{I} & 0 \end{pmatrix}, \tag{7.15}$$

and the inverse (or backward scattering) transfer matrix is given by,

$$(\mathbf{T}_n)^{-1} = \begin{pmatrix} 0 & \mathbf{I} \\ -\mathbf{t}_{n\,n-1}^{-1}\mathbf{t}_{n\,n+1} & \mathbf{t}_{n\,n-1}^{-1}(\boldsymbol{\varepsilon}_n - \hbar\boldsymbol{\omega}^\dagger\mathbf{I}) \end{pmatrix}. \tag{7.16}$$

So given the wavefunction coefficients at two neighboring sites, we can by repeated use of equation (7.15) solve the wavefunction for any other two given sites. For example

$$\begin{pmatrix} \psi_{m+1} \\ \psi_m \end{pmatrix} = \left\{ \prod_{a=m}^1 \mathbf{T}_a \right\} \begin{pmatrix} \psi_1 \\ \psi_0 \end{pmatrix}. \tag{7.17}$$

Let us return to our transport model. The electrodes will be modeled as semi-infinite tight-binding chains. Consider the two electrode tight-binding sites closest to the quantum pump, which will be occupied by an incoming and several reflected plane electron waves. In the opposing electrode the wavefunction is composed of transmitted plane waves, and since the wavefunction can be propagated from one electrode to the other by successive use of the transfer matrix equation, we can solve for the transmission and reflection coefficients.

The incoming wave coefficients $\mathbf{a}$ and the reflection coefficients $\mathbf{r}$, can be related to the wavefunction coefficients by a linear relation,

$$\begin{pmatrix} \psi_{n+1} \\ \psi_n \end{pmatrix} = \mathbf{O}_L \begin{pmatrix} \mathbf{a} \\ \mathbf{r} \end{pmatrix} = \begin{pmatrix} e^{i\mathbf{k}^T}\mathbf{I} & e^{-i\mathbf{k}^T}\mathbf{I} \\ \mathbf{I} & \mathbf{I} \end{pmatrix} \begin{pmatrix} \mathbf{a} \\ \mathbf{r} \end{pmatrix}. \tag{7.18}$$

Similarly the transmission coefficients $\mathbf{f}$ are also related to the wave-function coefficients in the outgoing leads

$$\begin{pmatrix} \psi_{n+1} \\ \psi_n \end{pmatrix} = \mathbf{O}_R \begin{pmatrix} \mathbf{f} \\ \mathbf{0} \end{pmatrix} = \begin{pmatrix} e^{i\mathbf{k}^T}\mathbf{I} & e^{-i\mathbf{k}^T}\mathbf{I} \\ \mathbf{I} & \mathbf{I} \end{pmatrix} \begin{pmatrix} \mathbf{f} \\ \mathbf{0} \end{pmatrix}. \tag{7.19}$$

It can be shown that the inverse operator to the basis-change operator $\mathbf{O}$ looks like

$$\mathbf{O}^{-1} = \begin{pmatrix} \frac{1}{2\sin\mathbf{k}}\mathbf{I} & 0 \\ 0 & \frac{1}{2\sin\mathbf{k}}\mathbf{I} \end{pmatrix} \begin{pmatrix} \mathbf{I} & -e^{-i\mathbf{k}}\mathbf{I} \\ -\mathbf{I} & e^{i\mathbf{k}}\mathbf{I} \end{pmatrix}. \tag{7.20}$$

7.1.1 A Simple Quantum Pump Example

To demonstrate the use of our method we will - as an example - investigate the very simple quantum pump sketched on Fig. 7.4. The Floquet scattering equation looks like:

$$\begin{pmatrix} \mathbf{a} \\ \mathbf{r} \end{pmatrix} = \mathbf{S} \begin{pmatrix} \mathbf{f} \\ \mathbf{0} \end{pmatrix}, \tag{7.21}$$

$$t_R = t\cos^2(\Omega\tau/2)$$

$$\varepsilon\cos(\Omega\tau + \phi)$$

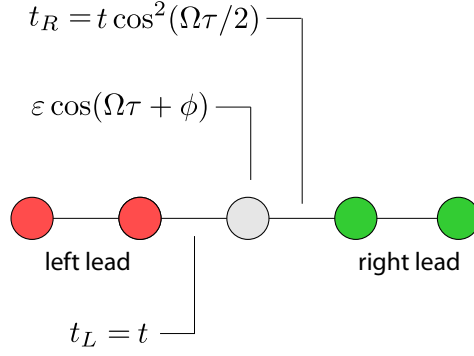left lead   right lead

$$t_L = t$$

Figure 7.4: Simple quantum pump model

where the scattering matrix is the product of two basis-change operators and three transfer matrices:

$$\mathbf{S} = \mathbf{O}_L^{-1}\begin{pmatrix} 0 & \mathbf{I} \\ -\mathbf{t}_{21}^{-1}\mathbf{t}_{23} & \mathbf{t}_{21}^{-1}(\varepsilon_n - \hbar\boldsymbol{\omega}^\dagger\mathbf{I}) \end{pmatrix}\begin{pmatrix} 0 & \mathbf{I} \\ -\mathbf{t}_{32}^{-1}\mathbf{t}_{34} & \mathbf{t}_{32}^{-1}(\varepsilon_n - \hbar\boldsymbol{\omega}^\dagger\mathbf{I}) \end{pmatrix}$$
$$\times\begin{pmatrix} 0 & \mathbf{I} \\ -\mathbf{t}_{43}^{-1}\mathbf{t}_{45} & \mathbf{t}_{43}^{-1}(\varepsilon_n - \hbar\boldsymbol{\omega}^\dagger\mathbf{I}) \end{pmatrix}\mathbf{O}_R. \tag{7.22}$$

Choose a Krönecker delta vector $\mathbf{a} = \boldsymbol{\delta}_{n,0}$, which represents only *a single incoming wave*,

$$\begin{pmatrix} \boldsymbol{\delta}_{n,0} \\ \mathbf{r} \end{pmatrix} = \begin{pmatrix} \mathbf{S}_{11} & \mathbf{S}_{12} \\ \mathbf{S}_{21} & \mathbf{S}_{22} \end{pmatrix}\begin{pmatrix} \mathbf{f} \\ \mathbf{0} \end{pmatrix}. \tag{7.23}$$

We can then find the transmitted wave coefficients, $\mathbf{f} = \mathbf{S}_{11}^{-1}\boldsymbol{\delta}_{n,0}$, and the reflected wave coefficients $\mathbf{r} = \mathbf{S}_{21}\mathbf{f} = \mathbf{S}_{21}\mathbf{S}_{11}^{-1}\boldsymbol{\delta}_{n,0}$.

7.1.2 Pumped Current

The current carried by a single mode $e^{i(kx-\omega_k\tau)}$ is given by,

$$J_k = it_0\langle\psi|n-1\rangle\langle n|\psi\rangle - it_0^*\langle\psi|n\rangle\langle n-1|\psi\rangle = -2\,\mathrm{Im}\{t_0\langle\psi|n-1\rangle\langle n|\psi\rangle\}$$
$$= 2\,\mathrm{Re}(t_0)\sin(ka) + 2\,\mathrm{Im}(t_0)\cos(ka). \tag{7.24}$$

For a transmitted wave composed of several modes k_j each with the weight f_j, the current at site n is given by,

$$J(n) = -2\,\mathrm{Im}\left\{t_0\sum_{j,l}f_j^*f_l e^{-i(k_j(n-1)a-\omega_j\tau)}e^{i(k_l na-\omega_l\tau)}\right\}$$
$$= -2\,\mathrm{Im}\left\{t_0\sum_{j,l}f_j^*f_l e^{i(k_l-k_j)na}e^{ik_j a}e^{i(\omega_j-\omega_l)\tau}\right\}. \tag{7.25}$$

Now, the difference $\omega_l - \omega_j$ is a multiple of the base driving frequency Ω. Integrating over a period $T = 2\pi/\Omega$, only terms with $\omega_l = \omega_j$ contribute. Hence one must have $k_l = k_j$ and

then the averaged current is,

$$\langle J \rangle_T = -2 \operatorname{Im} \left\{ t_0 \sum_j |f_j|^2 e^{ik_j a} \right\} = \sum_j |f_j|^2 J_{k_j}. \tag{7.26}$$

For the slightly more complicated case which have several reflected modes k_j with weight r_j and one incident wave at k_0 with weight 1, the current is given by

$$J(n) = -2 \operatorname{Im}\{ t_0 \langle \psi | n-1 \rangle \langle n | \psi \rangle \}$$

$$= -2 \operatorname{Im} \left\{ t_0 \sum_{j,l} r_j^* r_l e^{i(k_j - k_l)na} e^{-ik_j a} e^{i(\omega_j - \omega_l)\tau} \right\} - 2 \operatorname{Im} \left\{ t_0 e^{ik_0 a} \right\}$$

$$- 2 \operatorname{Im} \left\{ t_0 \sum_j r_j^* e^{i(k_j + k_0)na} e^{-ik_j a} e^{i(\omega_j - \omega_0)\tau} + t_0 \sum_l r_l e^{-i(k_l + k_0)na} e^{ik_0 a} e^{i(\omega_0 - \omega_l)\tau} \right\}.$$

Again integrating over one base period T we obtain,

$$\langle J \rangle_T = J_{k_0} - \sum_j |r_j|^2 J_{k_j}. \tag{7.27}$$

Now, if the two leads are identical, the total current through the device should be conserved, and

$$J_{tot} = J_{k_0} - \sum_j \left\{ |f_j|^2 + |r_j|^2 \right\} J_{k_j} = 0. \tag{7.28}$$

7.1.3 The Band Egde

In the Floquet formulation a periodic Hamiltonian allows for some initial state to absorb or emit a number of modulation quanta of energy $\hbar\Omega$.

Think about what would happen if the time-dependent part of the Hamiltonian was able to excite states with energies outside the electrode energy band. This is most important, when modeling the electrodes as semi-infinite tight-binding chains, which only supports a single band of energies $E \in (-2t_0, 2t_0)$. The answer is rather straightforward. Looking at equation (7.3), it is obvious that only Fourier components ψ_ω within the band survive, and the components of state vectors ψ_ω, which are positioned outside the band, must be removed.

7.2 Symmetry and Quantum Pumping

It is perhaps not obvious how the symmetry of the Hamiltonian will affect the ability of a quantum system to pump particles. Normally one would argue that a time-reversal symmetric Hamiltonian should not be able to sustain a net current. However, Wagner[116] and Kohler, Lehmann, and Hänggi[52] have showed that in a Floquet scattering formalism this reasoning is flawed.

It is the asymmetry of the electronic system near the Fermi energy which drives the pumping. The mechanism is displayed in Figure 7.5, where the symmetry of the Hamiltonian is related to the symmetry of the transmission coefficients. The relevant Hamiltonian symmetry is that of *generalized parity*. This symmetry operation involves a time translation
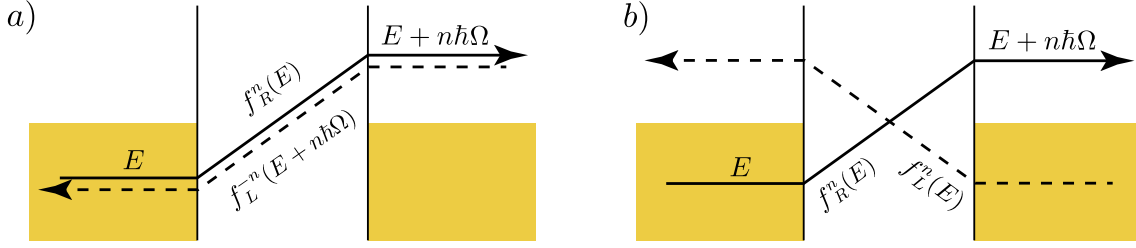
Figure 7.5: Shows the symmetry of transmission coefficients for scattering between tow electrodes based on Kohler, Lehmann, and Hänggi[52]. **a)** The Hamiltonian is time-reversal symmetric, i.e. $H(n,\tau) = H(n,-\tau)$. **b)** The Hamiltonian is symmetric with respect to generalized parity, i.e. $H(n,\tau) = H(-n,\tau+\tau')$.

along with a parity operation $n \to -n$. If this symmetry is broken, a net current may be pumped by the system.

The results of the time reversal symmetry and the generalized symmetry is not directly obvious from our scattering matrix approach. The general rule is that no current can run whenever the scattering matrix is involutory, i.e., $\mathbf{S}^{-1} = \mathbf{S}$. Written in terms of transfer matrices this condition takes the form:

$$\prod_{i=N-1}^{2} \mathbf{T}_i = \prod_{i=2}^{N-1} (\mathbf{T}_i)^{-1}. \tag{7.29}$$

7.3   Two Models

We can apply the above method to a very simple model as pictured on Fig. 7.4. Here we show the results for two (prototypical) example quantum pumps.

7.3.1   A One-Parameter Pump

Here the central dot is coupled weakly to the right lead by a static coupling $t_L = t$ and also weakly to the left lead through the oscillating coupling $t_R = t(1 + \cos(\Omega\tau))$. For small frequencies $\hbar\Omega = 0.001 t_0$ and small couplings $t = 0.01 t_0$ the transmission difference, $f_R(\nu) - f_L(\nu)$, and the resulting current, $I(E) = \rho(f_R - f_L)$, is shown in Figure 7.6. Here we have introduced the density of states of the tight-binding chain, $\rho(E) = 1/(\pi\sqrt{(2t_0)^2 - E^2})$.

The lead electrons constitutes a Fermi sea, where the occupation of each electronic state is determined by the temperature through the Fermi-Dirac distribution. At zero temperature all states below the Fermi energy E_F are fully occupied, while all states above the Fermi energy are completely unoccupied. The total (cumulative) current is a simple sum of the current pumped by states below the Fermi energy, $I_{tot}(E_F) = \sum_{E<E_F} I(E)$.

Note that the system is *not* spatially symmetric, and hence a net current can indeed flow. It is not surprising that a net current only flows at values of E close to the resonance, since this is the only place where the total transmission differs significantly from zero. In this example, the net current is of the order of $\langle I \rangle_T = 10^{-5} t_0/\hbar$.

7.3.2   A Two-Parameter Pump

We can also build a simple two-parameter pump. Assume again that the single orbital is coupled to the two leads with the couplings $t_R = t$ and $t_L = t\cos(\Omega\tau + \phi)$, and then change the resonance energy periodically $\varepsilon(\tau) = \varepsilon\cos(\Omega\tau)$. Again we choose parameters so that
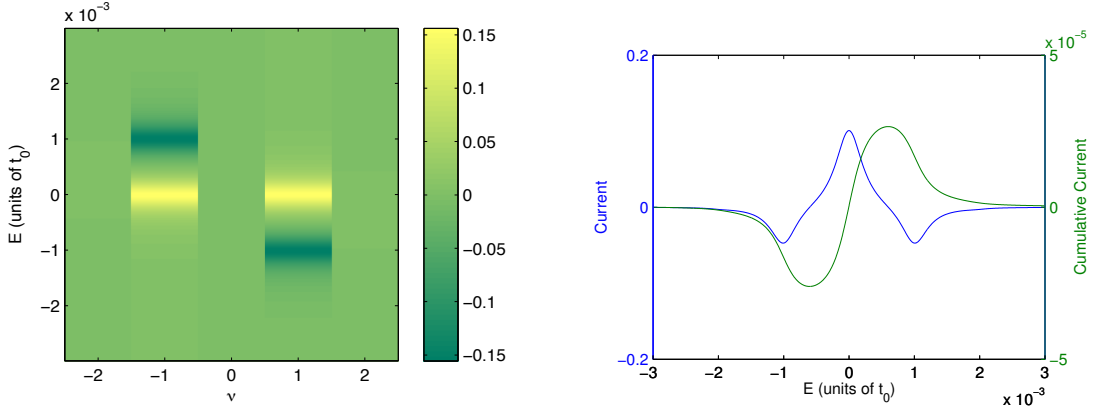
Figure 7.6: A single orbital coupled to two leads through the couplings $t_R = t$ and $t_L = t(1 + \cos(\Omega \tau)$ with parameters $t = 10^{-2}t_0$ and $\hbar\Omega = 10^{-3}t_0$. The left panel shows transmission difference $f_R(\nu) - f_L(\nu)$ as a function of incoming energy E, while the right panel shows the current and the cumulative current.

the oscillation frequency $\hbar\Omega = 10^{-3}t_0$, the tunneling $t = 10^{-2}t_0$ and the resonance energy $\varepsilon = 5 \cdot 10^{-3}t_0$.

For zero phase difference, $\phi = 0$, we showcase the resulting transmission difference and the resulting current in Figure 7.7. Note that the transmission (rather surprisingly) mainly involves very distant side bands, and hence for these parameters, the system behaves highly non-adiabatic.
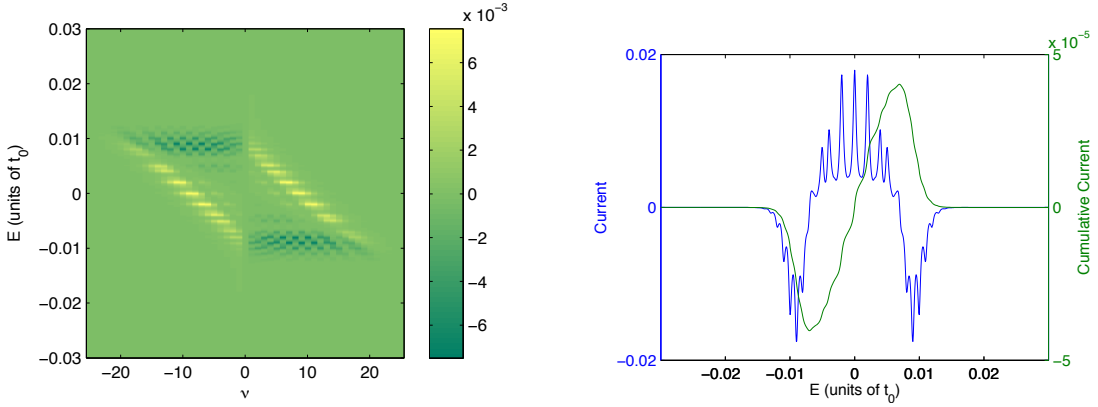
Figure 7.7: A single oscillating orbital $\varepsilon(\tau) = \varepsilon \cos(\Omega \tau)$ coupled to two leads by a static coupling $t_R = t$ and an oscillating coupling $t_L = t \cos(\Omega \tau + \phi)$. Chosen parameters $\hbar\Omega = 10^{-3}t_0$, $\varepsilon = 5 \cdot 10^{-3}t_0$ and $t = 10^{-2}t_0$. The left panel shows transmission difference and the right panel shows current and cumulative current.

7.4   Rate Equation

Let us now turn to the semi-classical electron pump, which we model as a single orbital coupled to two electrodes. Again the orbital on-site energy and the coupling to the electrodes depend periodically on time in a way, which emulates the simple two-parameter pump examined in section 7.3.2. Let $P(\tau)$ be the instantaneous probability for the orbital to be occupied by an electron. Again the leads are modeled as a Fermi sea electrons in the
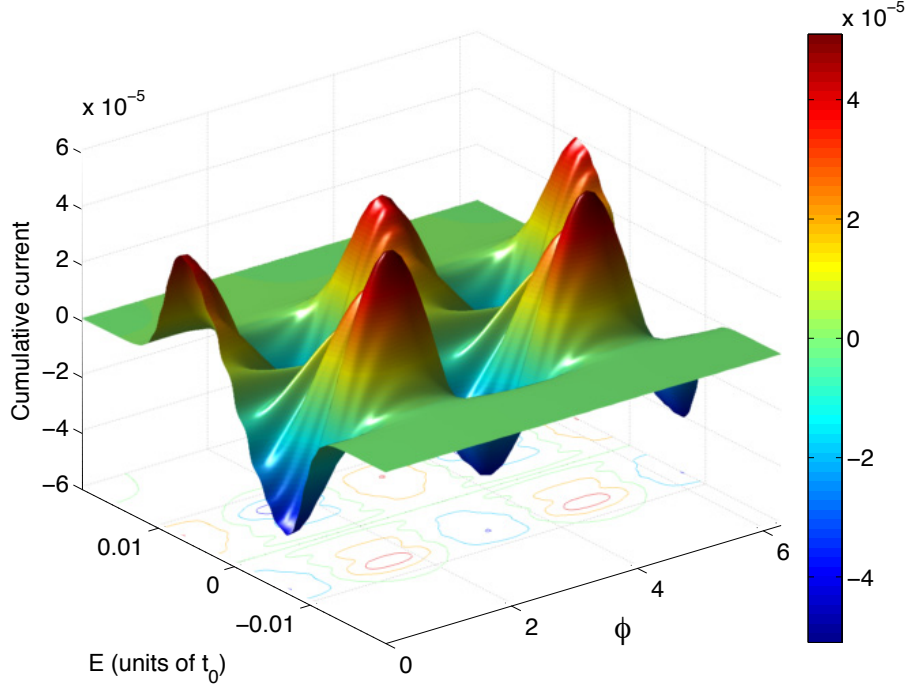
Figure 7.8: Cumulative current calculated by the Floquet scattering method. Current is shown as a function of the Fermi level E and the phase difference ϕ. Note that no electrons are pumped at $E = 0$. The non-zero current extends to about $E = \pm 2\varepsilon = \pm 0.01 t_0$.

zero-temperature limit. When the orbital on-site energy, ε, lies below the Fermi energy, the lead electrons can tunnel onto the orbital, and when the orbital is above the Fermi energy the electrons tunnel out of the orbital.

The rates at which the electrons tunnel to either the right electrode or the left electrode are of course determined by the instantaneous tunneling rates. At any given instant of time the probability for having an electron occupying the orbital changes according to the rate equation:

$$\dot{P}(\tau) = -[\Gamma_L(\tau) + \Gamma_R(\tau)]P(\tau)\theta(\epsilon(\tau)) + [\Gamma_L(\tau) + \Gamma_R(\tau)](1 - P(\tau))\theta(-\epsilon(\tau))$$
$$= -[\Gamma_L(\tau) + \Gamma_R(\tau)]P(\tau) + [\Gamma_L(\tau) + \Gamma_R(\tau)]\theta(-\epsilon(\tau)). \tag{7.30}$$

Here Γ_L and Γ_R determine the rates at which electrons leave (or enter) the left and the right electrode respectively. Note that the Heaviside step functions $\theta(\pm\epsilon(\tau))$ determine whether electrons tunnel onto the single orbital or off the single orbital.

We can actually guess a steady state solution to this equation,

$$P(\tau) = \exp(-F(\tau - \tau_0))(g(\tau - \tau_0) + P(\tau_0)), \tag{7.31}$$

and direct derivation yields that,

$$\dot{P}(\tau) = -f(\tau)P(\tau) + \exp(-F(\tau))\dot{g}(\tau). \tag{7.32}$$
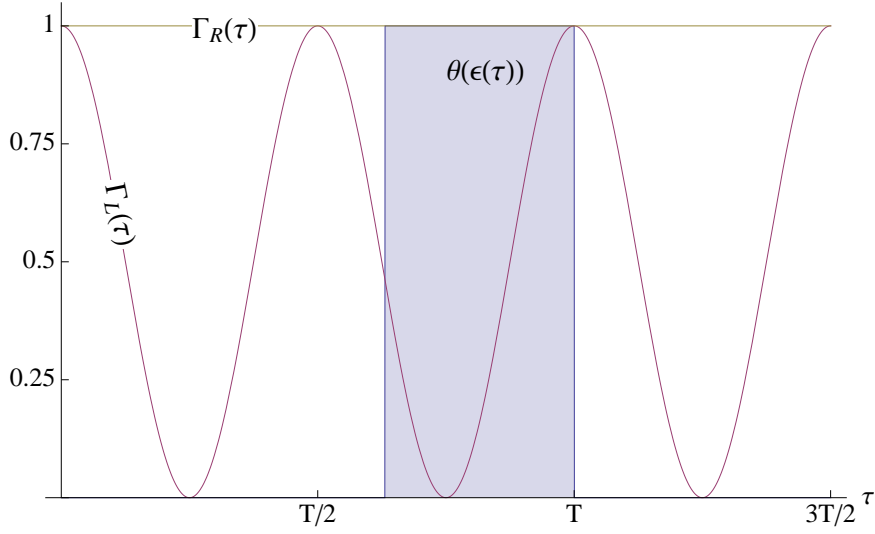
Figure 7.9: Couplings $\Gamma_L(\tau)$, $\Gamma_R(\tau)$ along with $\theta(\epsilon(\tau))$.

Hence identifying

$$F(\tau) = \int_{\tau_0}^{\tau} d\tau' \left[\Gamma_L(t') + \Gamma_R(\tau') \right], \tag{7.33a}$$

$$g(\tau) = \int_{\tau_0}^{\tau} d\tau' \exp(F(\tau')) [\Gamma_L(\tau') + \Gamma_R(\tau')]\theta(-\epsilon(\tau')). \tag{7.33b}$$

Now, the total current flowing between the single orbital, and the right lead is given by the expression

$$\begin{aligned} I(\tau) &= \Gamma_R(\tau)P(\tau)\theta(\epsilon(\tau)) - \Gamma_R(\tau)(1 - P(\tau))\theta(-\epsilon(\tau)) \\ &= \Gamma_R(\tau)P(\tau) - \Gamma_R(\tau)\theta(-\epsilon(\tau)). \end{aligned} \tag{7.34}$$

Now, our toy model will have a single orbital with the on-site chemical potential

$$\epsilon(\tau) = \varepsilon_1 \cos(\Omega\tau + \chi) + \varepsilon_0, \text{ where } \cos(\chi) = -\varepsilon_0/\varepsilon_1. \tag{7.35}$$

On the other hand the two tunneling rates depend on time such that,

$$\Gamma_L(\tau) = \tfrac{1}{2}\Gamma_L \{(\cos(2\Omega\tau + 2\phi) + 1\}, \Gamma_R(\tau) = \Gamma_R \text{ (constant)}. \tag{7.36}$$

In that case for the first period $0 < \tau < 2\pi/\Omega$,

$$\begin{aligned} F(\tau) &= \int_0^{\tau} d\tau' \left[\tfrac{1}{2}\Gamma_L\{(\cos(2\Omega\tau - \phi) + 1\} + \Gamma_R \right] \\ &= \tfrac{1}{2}\Gamma_L \left\{ \frac{\Omega\tau + \cos(\Omega\tau + 2\phi)\sin(\Omega\tau)}{\Omega} \right\} + \Gamma_R\tau. \end{aligned} \tag{7.37}$$

Also $F(2\pi n/\Omega) = \Gamma_L \frac{\pi n}{\Omega} + \Gamma_R \frac{2\pi n}{\Omega}$. Note that $g(\tau)$ is constant in any of the intervals $\Omega\tau \in [2(n\pi - \chi), 2n\pi]$. For $\tau \in [0, 2(\pi - \chi)/\Omega]$ we have

$$g(\tau) = \int_0^\tau d\tau' \exp(F(\tau'))(\tfrac{1}{2}\Gamma_L\{(\cos(\Omega\tau' + 2\phi) + 1\} + \Gamma_R) \tag{7.38}$$

$$= -1 + \exp\left(\tfrac{1}{2}\Gamma_L \frac{\Omega\tau - \tfrac{1}{2}\sin(2\phi) + \tfrac{1}{2}\sin(2\Omega\tau + 2\phi)}{\Omega} + \Gamma_R\tau\right), \tag{7.39}$$

and

$$g(2\pi/\Omega) = g(2(\pi - \chi)/\Omega)$$

$$= -1 + \exp\left(\frac{\Gamma_L(-\tfrac{1}{4}\sin(2\phi) - \tfrac{1}{4}\sin(-2\phi + 4\chi) + (\pi - \chi)) + 2\Gamma_R(\pi - \chi)}{\Omega}\right). \tag{7.40}$$

The constant solution when $P(\tau_0) = P(2\pi n/\Omega + \tau_0)$ is then simply

$$P = \frac{\exp(-F(2\pi/\Omega))g(2\pi/\Omega)}{1 - \exp(-F(2\pi/\Omega))}. \tag{7.41}$$

During one period $T = 2\pi/\Omega$ the time-averaged current is then easily calculated to give,

$$\langle I\rangle = \frac{\Omega}{2\pi}\Gamma_R\left(\int_0^{2\pi/\Omega} d\tau\, P(\tau) - \frac{2(\pi - \chi)}{\Omega}\right)$$

$$= \frac{\Omega}{2\pi}\Gamma_R\int_0^{2\pi/\Omega} d\tau\, \exp(-F(\tau))(g(\tau) + P) - \left(1 - \frac{\chi}{\pi}\right)\Gamma_R. \tag{7.42}$$

The rates can easily be related to the original tight-binding parameters from the Floquet scattering model using the Fermi Golden Rule [14] (assuming a constant density of states $\rho = 1/(2\pi t_0)$),

$$\Gamma_L(\tau) = \frac{2\pi}{\hbar}|\langle i|\hat{H}|f\rangle|^2\rho = \frac{1}{\hbar}\frac{t^2}{t_0}\cos^2(\Omega\tau + \phi). \tag{7.43}$$

Relate the different angles of the two problems, $\phi_{scattering} = \phi_r - \chi/2$, and redefine time to have units of inverse energy $\tau' = \tau/\hbar$. T

7.5 Comparison

The resulting current for two comparable systems is presented in Figures 7.10 - 7.11.

The results look, if not identical, then at least qualitatively very similar. You may note that the scattering calculation produces a current ten times larger than the rate equation. This discrepancy could perhaps be removed if including the broadening of the sharp resonance due to tunneling. But the conclusion is (unfortunately) that for such simple systems "quantum" pumping cannot be distinguished from "classical" pumping. More elaborate systems where quantum interferences plays a role, could however be a promising candidate for finding a distinction between the two.
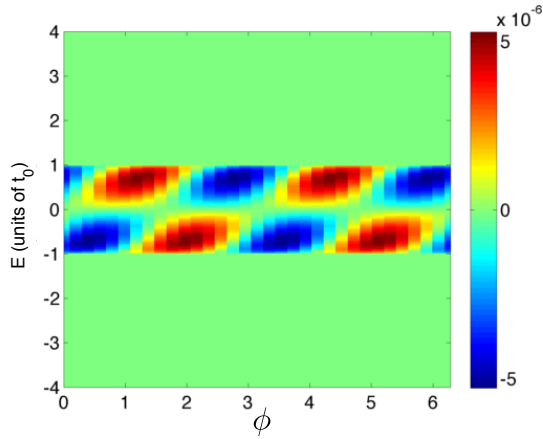
Figure 7.10: Current calculated from a rate equation as a function of phase angle ϕ and Fermi energy E. Note that the scale of ε is unimportant, but here chosen to ease a direct comparison with the scattering results. The rates are given by $\Gamma_L = \Gamma_R = 0.01^2 t_0/\hbar$, and the driving frequency is $\hbar\Omega = 0.001t_0$.
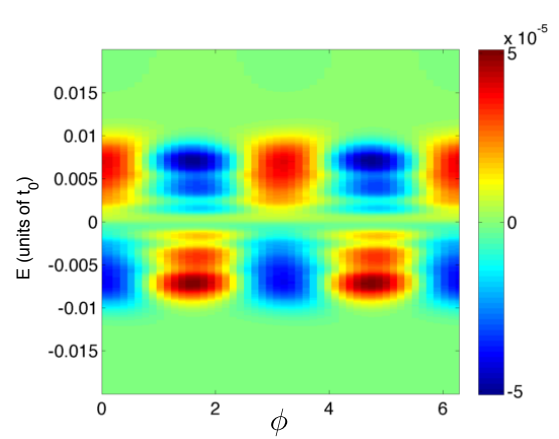

Figure 7.11: Current calculated from a naive Floquet scattering method with $\varepsilon = 0.005t_0$, $t = 0.01t_0$, and driving frequency $\hbar\Omega = 0.001t_0$.

7.6 Conclusions

In conclusion we have investigated pumping of a molecular pump model, and found that coherent quantum pumping is nearly indistinguishable from classical pumping around a resonance. For this purpose we have derived a simple, but effective Floquet scattering approach describing harmonic time-dependent evolution of the electrode scattering states.

I would like to thank J. Thijssen of the TU Delft for our discussions about the theory of molecular quantum pumps.

Resumé

Teoretiske undersøgelser angående enkelt-molekyler

Denne afhandling undersøger organiske molekyler med fokus på anvendelse indenfor molekylær elektronik. Et enkelt molekyle kan, hvis det lykkes at placere molekylet mellem to mikroskopiske elektroder, indgå som en del af et elektronisk kredsløb og i princippet fungere som en lillebitte elektronisk komponent.

For at opnå en tilstrækkelig god beskrivelse af de elektroniske egenskaber for så klejne komponenter må man ty til kvantemekanikken. I denne afhandling undersøger vi plane organiske molekyler, hvor elektronerne i det såkaldte π-system kan beskrives kvantemekanisk med den kemiske Pariser-Parr-Pople (PPP) model. Der findes adskillige numeriske metoder til udføre udregninger med denne PPP model, men stort set ingen analytiske tilgangsmåder.

Vi forsøger at udbedre denne rystende mangel på fornuftige analytiske metoder, ved at forsøge en akut genopliving af Paulings og Rumers valens-bindings-udregninger. Denne *ny-klassicistiske valens-bindings-teori* giver mulighed for med en stærk reduktion i kompleksitet, at udføre en kontrolleret tilnærmelse til den fulde PPP model. Tilnærmelse kan i princippet udføres så præcist at resultatet ikke kan skelnes fra udregninger udført med eksakt diagonalisering. Vi viser ligeledes hvorledes ny-klassicistisk valens-bindings-teori fungerer lige godt, uanset om man inkluderer elektron-elektron vekselvirkningen i udregningerne eller undlader at medtage den.

I den efterfølgende del af afhandlingen vender vi os i stedet mod kvante-transport af elektroner gennem molekylernes π-system. Helt specifikt undersøger vi hvordan elektronerne kan kvante-interferere under deres vej igennem molekylet. Det viser sig at elektron-transporten igennem molekylet kan inddeles i to kvante-interferens-klasser, og for neutrale, alternante kulbrinter udleder vi en simpel regel til at forudsige transportens interferens-klasse. Endvidere erfares det, at hvis der inkorporeres en elektro-statisk gate til at kontrollere molekylets elektrostatiske energi, kan der findes adskillige interessant interferens-fænomener.

Molekylære kontakter med en spin-doublet grundtilstand kan ved meget lave temperaturer undergå en Kondo-overgang, hvor ledningselektronernes spin skærmer molekylets spin i en effektiv mange-partikel singlet-tilstand. Vi viser at kvante-interferens kan overleve denne Kondo-overgang og dermed blive voldsomt forstærket. Endvidere opdager vi, at det er muligt at finde interferens i Kondo-overgangs-temperaturen. Denne effekt forudsætter at spin-triplet tilstande i de nærliggende ladningstilstande kobler stærkt til spin-doublet grundtilstanden. Denne analyse afslører også muligheden for at spredningen af elektroner fra en elektrode til den anden (gennem spin-doublet grundtilstanden) kan forårsage Kondo effekt, hvilket ellers ikke er set indtil videre.

Til sidst beskæftiger vi os også med pumpning af elektroner, hvor en vekselspænding kan rotere et molekyle og dermed i princippet fungerer som en lille kvantemekanisk pumpe. Hovedspørgsmålet er her, om en sådan pumpe opfører sig anderledes end en klassisk pumpe.

For at undersøge den kvantemekaniske pumpning, udvikler vi en simpel ikke-vekselvirkende metode, som vi kalder *simpel Floquet-spredning*, og den semi-klassiske pumpe undersøger vi med en analytisk løsning af de tilhørende rate-ligninger.

Nyd det.

Appendix A

Inverting a Jacobi Matrix

A Jacobi matrix, is a symmetric tridiagonal matrix, of the form

$$T = \begin{pmatrix} a_0 & b_1 & & & \cdots \\ b_1 & a_1 & b_2 & & \\ & b_2 & a_2 & b_3 & \\ & & b_3 & & \\ \vdots & & & & \ddots \end{pmatrix} \tag{A.1}$$

We will only be interested in a single matrix element of the inverse $(T^{-1})_{11}$. For simplicity we will define a sequence of submatrices of T, such that

$$T_i = \begin{pmatrix} a_i & b_{i+1} & & & \cdots \\ b_{i+1} & a_{i+1} & b_{i+2} & & \\ & b_{i+2} & a_{i+2} & b_{i+3} & \\ & & b_{i+3} & & \\ \vdots & & & & \ddots \end{pmatrix} \tag{A.2}$$

If T is invertible the inverse is given by it's adjugate matrix. In the case of the 11 component, the exact formula is,

$$(T^{-1})_{11} = \frac{1}{\det(T_0)} \det T_1 \tag{A.3}$$

Now, using Laplace's equation for the matrix determinant, it is straightforward to show that

$$\det A_i = a_i \det A_{i+1} - b_{i+1}^2 \det A_{i+2} \tag{A.4}$$

Hence we can produce a recursive calculation

$$\frac{\det(A_i)}{\det(A_{i-1})} = \frac{1}{a_{i-1} - b_i^2 \frac{\det(A_{i+1})}{\det(A_i)}} \tag{A.5}$$

Which conclusively shows that

$$(T^{-1})_{11} = \cfrac{1}{a_0 - \cfrac{b_1^2}{a_1 - \cfrac{b_2^2}{a_2 - \cdots}}} \tag{A.6}$$

Appendix B

Numerical Representation of Valence Bond States

In order to construct a full basis set one forms Rumer diagrams, where lattice sites are positioned in a circle and only states with *non-crossing* valence bonds are included.[8,90,105] Similarly, the basis can be built up as the full Krylov subspace basis for a chain of the same size, if starting from a Kekulé state.

The crucial part of the calculation is to choose an effective representation of the valence bond basis. The state can be represented as an integer array, where the entries label the state of each site. Hence entry i must refer to whether the site i is occupied by a spinon, holon, doublon or connected to another site by a valence bond.

Working in base N we use the following table for determining the value entry i.

number	meaning
0i	holon
1i	spinon ($\downarrow$)
2i	spinon ($\uparrow$)
3i	doublon
0j	singlet (0) paired to site j
1j	triplet (1) paired to site j
2j	triplet (2) paired to site j
3j	triplet (3) paired to site j

As an example of this ordering consider the valence bond state

$$|\psi\rangle = \hat{c}_{2\uparrow}^{\dagger}(\hat{c}_{6\uparrow}^{\dagger}\hat{c}_{6\downarrow}^{\dagger})\hat{\chi}_{13}^{0\dagger}\hat{\chi}_{45}^{1\dagger}|vac\rangle. \tag{B.1}$$

In base 6 the corresponding numerical representation reads,

$$|\psi\rangle = (03, 22, 01, 15, 14, 36)_6. \tag{B.2}$$

The states are usually stored in different number basis which renders the naked states unreadable. Consider, e.g., the above state in base 10, where $|\psi\rangle = (3, 14, 1, 11, 10, 21)_{10}$.

You may note that this representation is a little redundant when representing valence bonds. According to the first entry (03) site 1 is connected to site 3 with a singlet valence bond, but the same information is contained in the third entry (01).

Alternatively the valence bond states could be written as a list of pairs of site indices (i, j). Such a representation has the disadvantage that the same state have multiple representations depending on the ordering of the pairs. Applying an operator to a state can easily change the pair ordering, which means that all states must be reordered before they

can be compared to the basis states. Hence the added redundancy of our basis naming scheme means that each state now has a single unique representation, and we do not have to worry about reordering anything.

Another approach orders the sites in a circle and labels the sites according to whether it is a spinon, a holon, a doublon, valence bond paired to the right or valence bond paired to the left. This is a very effective model for the spin-singlet subspace, because this basis automatically incorporates the Rumer basis.[105]

Calculating overlaps and elements of the Hamiltonian is a direct implementation of our convenient pictionary of section 3.5 and the calculation of overlaps in section 3.6.1.

Appendix C

Examples of Kondo Effect in Transport Through Molecules
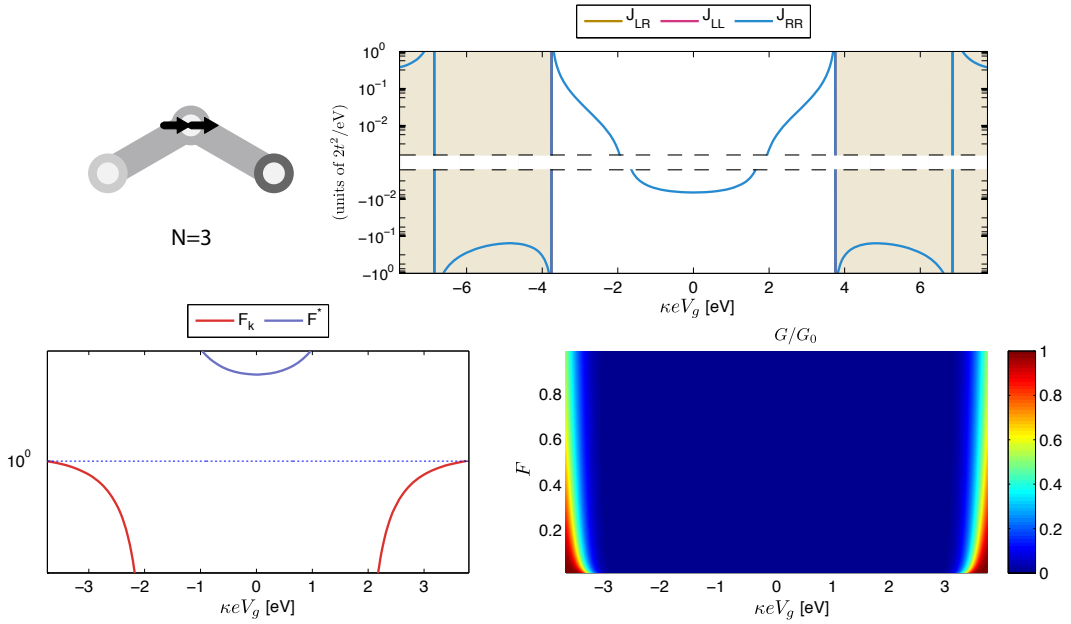
Figure C.1: Asymmetrical triple-dot with $\mu_1 = -\mu_3 = 2$ eV. The asymmetry induces a finite overlap (Feynman-Dyson orbital) between the charge state ground states at the center orbital. This belongs clearly to the singlet-singlet class with AFM Kondo near the Coulomb diamond edges.
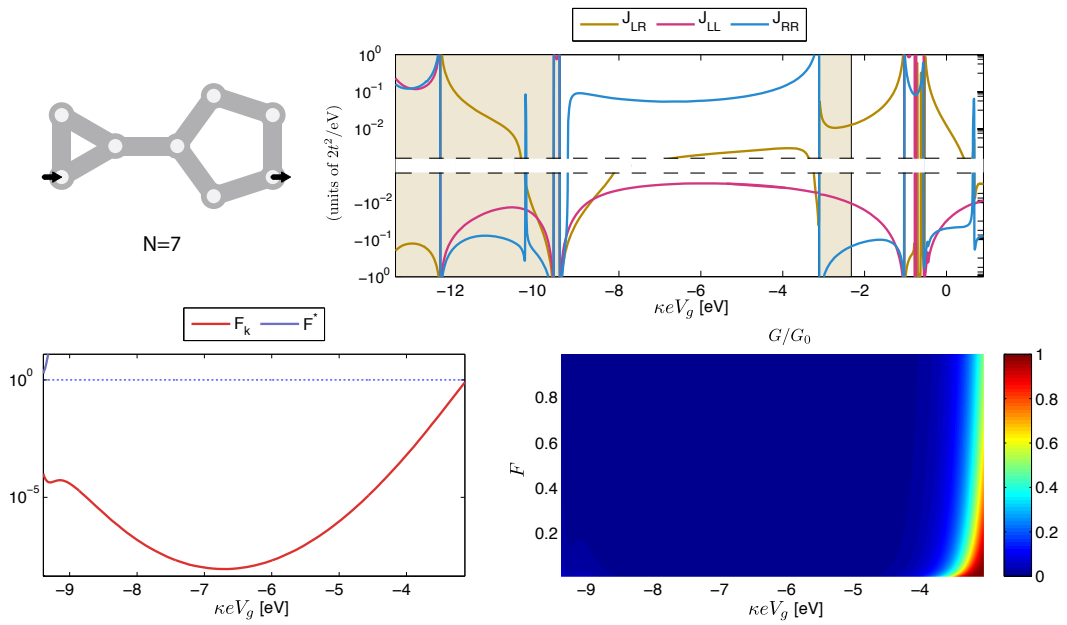
Figure C.2: *Calicene.* The 6-electron charge state have a triplet ground state, which forces all exchange couplings negative in the left part of the diamond. Interestingly the negative couplings does *not* lead to a ferromagnetic Kondo effect, as can be seen from the dimensionless Kondo scaling parameter $T_k < 1$. This is consistent with the scaling equations, and shows that it is not in general true, that negative exchange couplings are not always sufficient in order to create anti-ferromagnetic Kondo effect.

Appendix D

Floquet Scattering Theory for Extended Structures

This is a direct extension of the naive Floquet theory to the investigation of branched structures. Here we describe how to extend the naive Floquet method to both branched structures and structures with dead ends (leafs).

D.1   Branched structures

If the system branches out into a more complex structure with some sites having three or more connected sites, we must refine our transfer matrix approach, In taking the system of
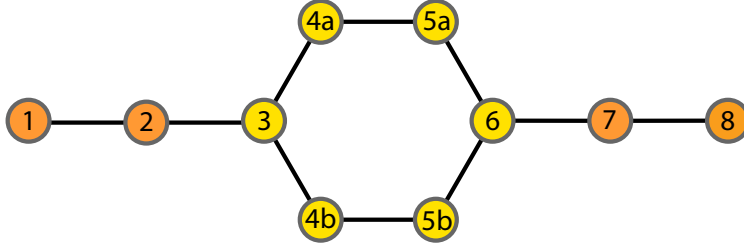
Figure D.1: **Example branched system**

Figure D.1 as a branched system example, then $|3\rangle$ couples to both $|4a\rangle$ and $|4b\rangle$. In that case Schrödinger's equation (7.7)

$$\omega_\mu \psi_3^\mu = \sum_\nu \left(-t_{3,4a}^\nu \psi_{4a}^{\mu+\nu} - t_{3,4b}^\nu \psi_{4b}^{\mu+\nu} - t_{3,2}^\nu \psi_2^{\mu+\nu} + \varepsilon_3^\nu \psi_3^{\mu+\nu} \right) \tag{D.1}$$

Which can be rewritten on transfer matrix form,

$$\mathbf{t}_{3,4a}\psi_{4a} + \mathbf{t}_{3,4b}\psi_{4b} = -\mathbf{t}_{3,2}\psi_2 + (\varepsilon_3 - \omega^\dagger\mathbf{I})\psi_3$$

$$\begin{pmatrix} \mathbf{t}_{3,4a} & \mathbf{t}_{3,4b} & 0 \\ 0 & 0 & 1 \end{pmatrix} \begin{pmatrix} \psi_{4a} \\ \psi_{4b} \\ \psi_3 \end{pmatrix} = \begin{pmatrix} \varepsilon_3 - \omega^\dagger\mathbf{I} & -\mathbf{t}_{3,2} \\ 1 & 0 \end{pmatrix} \begin{pmatrix} \psi_3 \\ \psi_2 \end{pmatrix}. \tag{D.2}$$

Simply applying equation (7.15) gives us that

$$\begin{pmatrix} \mathbf{t}_{4a,5a} & 0 & 0 & 0 \\ 0 & 1 & 0 & 0 \\ 0 & 0 & \mathbf{t}_{4b,5b} & 0 \\ 0 & 0 & 0 & 1 \end{pmatrix} \begin{pmatrix} \psi_{5a} \\ \psi_{4a} \\ \psi_{5b} \\ \psi_{4b} \end{pmatrix} = \begin{pmatrix} \varepsilon_{4a} - \omega^\dagger\mathbf{I} & 0 & -\mathbf{t}_{4a,3} \\ 1 & 0 & 0 \\ 0 & \varepsilon_{4b} - \omega^\dagger\mathbf{I} & -\mathbf{t}_{4b,3} \\ 0 & 1 & 0 \end{pmatrix} \begin{pmatrix} \psi_{4a} \\ \psi_{4b} \\ \psi_3 \end{pmatrix} \tag{D.3}$$

Very similarly one may show that

$$
\begin{pmatrix} \mathbf{t}_{5a,6} & 0 & 0 \\ \mathbf{t}_{5b,6} & 0 & 0 \\ 0 & 1 & 0 \\ 0 & 0 & 1 \end{pmatrix} \begin{pmatrix} \psi_6 \\ \psi_{5a} \\ \psi_{5b} \end{pmatrix} = \begin{pmatrix} \varepsilon_{5a} - \omega^\dagger \mathbf{I} & -\mathbf{t}_{5a,4a} & 0 & 0 \\ 0 & 0 & \varepsilon_{5b} - \omega^\dagger \mathbf{I} & -\mathbf{t}_{5b,4b} \\ 1 & 0 & 0 & 0 \\ 0 & 0 & 1 & 0 \end{pmatrix} \begin{pmatrix} \psi_{5a} \\ \psi_{4a} \\ \psi_{5b} \\ \psi_{4b} \end{pmatrix} \tag{D.4}
$$

And to tie it all back together, we have the equation

$$
\begin{pmatrix} \mathbf{t}_{6,7} & 0 \\ 0 & 1 \end{pmatrix} \begin{pmatrix} \psi_7 \\ \psi_6 \end{pmatrix} = \begin{pmatrix} \varepsilon_6 - \omega^\dagger \mathbf{I} & -\mathbf{t}_{6,5a} & -\mathbf{t}_{6,5b} \\ 1 & 0 & 0 \end{pmatrix} \begin{pmatrix} \psi_6 \\ \psi_{5a} \\ \psi_{5b} \end{pmatrix}. \tag{D.5}
$$

Hence we can now connect $\langle 3|\psi\rangle$ to $\langle 6|\psi\rangle$ by multiplying transfer matrices. In the branched part of the system we can propagate the wavefunction on each branch independently, like

$$
\begin{pmatrix} \mathbf{t}_{4a,5a} & 0 & 0 & 0 \\ 0 & 1 & 0 & 0 \\ 0 & 0 & 1 & 0 \\ 0 & 0 & 0 & 1 \end{pmatrix} \begin{pmatrix} \psi_{a+1} \\ \psi_a \\ \psi_b \\ \psi_{b-1} \end{pmatrix} = \begin{pmatrix} \varepsilon_a - \omega^\dagger \mathbf{I} & -\mathbf{t}_{a,a-1} & 0 & 0 \\ 1 & 0 & 0 & 0 \\ 0 & 0 & 1 & 0 \\ 0 & 0 & 0 & 1 \end{pmatrix} \begin{pmatrix} \psi_a \\ \psi_{a-1} \\ \psi_b \\ \psi_{b-1} \end{pmatrix}. \tag{D.6}
$$

D.2   Tree structures

Similarly we can build a structure with dead ends (or leafs if you prefer). In taking the
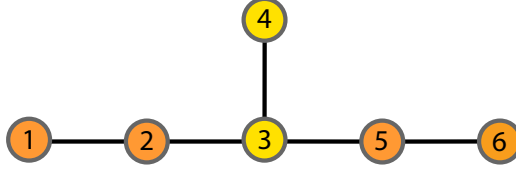
Figure D.2: **Example tree system**

system of Figure D.2 as a leaf system example, then $|4\rangle$ is only coupled to $|3\rangle$. In that case Schrödinger's equation (7.7),

$$
\omega_\mu \psi_3^\mu = \sum_\nu \left(-t_{3,4a}^\nu \psi_{4a}^{\mu+\nu} - t_{3,4b}^\nu \psi_{4b}^{\mu+\nu} - t_{3,2}^\nu \psi_2^{\mu+\nu} + \varepsilon_3^\nu \psi_3^{\mu+\nu} \right). \tag{D.7}
$$

This can be rewritten on transfer matrix form,

$$
\mathbf{t}_{3,4a} \psi_{4a} + \mathbf{t}_{3,4b} \psi_{4b} = -\mathbf{t}_{3,2} \psi_2 + (\varepsilon_3 - \omega^\dagger \mathbf{I}) \psi_3
$$

$$
\begin{pmatrix} \mathbf{t}_{3,4a} & \mathbf{t}_{3,4b} & 0 \\ 0 & 0 & 1 \end{pmatrix} \begin{pmatrix} \psi_{4a} \\ \psi_{4b} \\ \psi_3 \end{pmatrix} = \begin{pmatrix} \varepsilon_3 - \omega^\dagger \mathbf{I} & -\mathbf{t}_{3,2} \\ 1 & 0 \end{pmatrix} \begin{pmatrix} \psi_3 \\ \psi_2 \end{pmatrix}. \tag{D.8}
$$

Simply applying equation (7.15) gives us that

$$
\begin{pmatrix} \mathbf{t}_{4a,5a} & 0 & 0 & 0 \\ 0 & 1 & 0 & 0 \\ 0 & 0 & \mathbf{t}_{4b,5b} & 0 \\ 0 & 0 & 0 & 1 \end{pmatrix} \begin{pmatrix} \psi_{5a} \\ \psi_{4a} \\ \psi_{5b} \\ \psi_{4b} \end{pmatrix} = \begin{pmatrix} \varepsilon_{4a} - \omega^\dagger \mathbf{I} & 0 & -\mathbf{t}_{4a,3} \\ 1 & 0 & 0 \\ 0 & \varepsilon_{4b} - \omega^\dagger \mathbf{I} & -\mathbf{t}_{4b,3} \\ 0 & 1 & 0 \end{pmatrix} \begin{pmatrix} \psi_{4a} \\ \psi_{4b} \\ \psi_3 \end{pmatrix}. \tag{D.9}
$$

Very similarly one may show that

$$
\begin{pmatrix} \mathbf{t}_{5a,6} & 0 & 0 \\ \mathbf{t}_{5b,6} & 0 & 0 \\ 0 & 1 & 0 \\ 0 & 0 & 1 \end{pmatrix} \begin{pmatrix} \psi_6 \\ \psi_{5a} \\ \psi_{5b} \end{pmatrix} = \begin{pmatrix} \varepsilon_{5a} - \omega^\dagger \mathbf{I} & -\mathbf{t}_{5a,4a} & 0 & 0 \\ 0 & 0 & \varepsilon_{5b} - \omega^\dagger \mathbf{I} & -\mathbf{t}_{5b,4b} \\ 1 & 0 & 0 & 0 \\ 0 & 0 & 1 & 0 \end{pmatrix} \begin{pmatrix} \psi_{5a} \\ \psi_{4a} \\ \psi_{5b} \\ \psi_{4b} \end{pmatrix}. \tag{D.10}
$$

And to tie it all back together we have the equation

$$
\begin{pmatrix} \mathbf{t}_{6,7} & 0 \\ 0 & 1 \end{pmatrix} \begin{pmatrix} \psi_7 \\ \psi_6 \end{pmatrix} = \begin{pmatrix} \varepsilon_6 - \omega^\dagger \mathbf{I} & -\mathbf{t}_{6,5a} & -\mathbf{t}_{6,5b} \\ 1 & 0 & 0 \end{pmatrix} \begin{pmatrix} \psi_6 \\ \psi_{5a} \\ \psi_{5b} \end{pmatrix} \tag{D.11}
$$

Hence we can now connect $\langle 3|\psi\rangle$ to $\langle 6|\psi\rangle$ by multiplying transfer matrices. In the branched part of the system we can propagate the wavefunction on each branch independently, like

$$
\begin{pmatrix} \mathbf{t}_{4a,5a} & 0 & 0 & 0 \\ 0 & 1 & 0 & 0 \\ 0 & 0 & 1 & 0 \\ 0 & 0 & 0 & 1 \end{pmatrix} \begin{pmatrix} \psi_{a+1} \\ \psi_a \\ \psi_b \\ \psi_{b-1} \end{pmatrix} = \begin{pmatrix} \varepsilon_a - \omega^\dagger \mathbf{I} & -\mathbf{t}_{a,a-1} & 0 & 0 \\ 1 & 0 & 0 & 0 \\ 0 & 0 & 0 & 1 \\ 0 & 0 & 0 & 1 \end{pmatrix} \begin{pmatrix} \psi_a \\ \psi_{a-1} \\ \psi_b \\ \psi_{b-1} \end{pmatrix}. \tag{D.12}
$$

Bibliography

[1] Amit Agarwal and Diptiman Sen "Nonadiabatic charge pumping in a one-dimensional system of noninteracting electrons by an oscillating potential" in: *Physical Review B* 76.23 (Dec. 2007), p. 235316 DOI: 10.1103/PhysRevB.76.235316 (see p. 86).

[2] S. Andergassen et al. "Charge transport through single molecules, quantum dots and quantum wires." in: *Nanotechnology* 21.27 (July 2010), p. 272001 DOI: 10.1088/0957-4484/21/27/272001 (see p. 1).

[3] P. W. Anderson "A poor man's derivation of scaling laws for the Kondo problem" in: *Journal of Physics C: Solid State Physics* 3 (1970), pp. 2436–2441 DOI: 10.1088/0022-3719/3/12/008 (see p. 76).

[4] Liliana Arrachea "Green-function approach to transport phenomena in quantum pumps" in: *Physical Review B* 72.12 (Sept. 2005), p. 125349 DOI: 10.1103/PhysRevB.72.125349 (see p. 86).

[5] Assa Auerbach *Interacting Electrons and Quantum Magnetism* Springer-Verlag New York, Inc., 1994 (see pp. 21, 22, 25).

[6] Roi Baer and Daniel Neuhauser "Phase coherent electronics: A molecular switch based on quantum interference" in: *Journal of the American Chemical Society* 124 (2002), pp. 4200–4201 DOI: 10.1021/ja016605s (see p. 51).

[7] P. P. Baruselli et al. "Ferromagnetic Kondo Effect in a Triple Quantum Dot System" in: *Physical Review Letters* 111.4 (July 2013), p. 047201 DOI: 10.1103/PhysRevLett.111.047201 (see p. 81).

[8] K.S.D. Beach and Anders W. Sandvik "Some formal results for the valence bond basis" in: *Nuclear Physics B* 750.3 (Aug. 2006), pp. 142–178 DOI: 10.1016/j.nuclphysb.2006.05.032 (see pp. 28, 29, 32, 103).

[9] Georg Begemann "Quantum interference phenomena in transport through molecules and multiple quantum dots" PhD thesis Universität Regensburg, 2009 (see pp. 8, 71).

[10] Georg Begemann et al. "Symmetry fingerprints of a benzene single-electron transistor: Interplay between Coulomb interaction and orbital symmetry" in: *Physical Review B* 77.20 (May 2008), p. 201406 DOI: 10.1103/PhysRevB.77.201406 (see pp. 50, 71).

[11] Niels Henrik David Bohr "On the Constitution of Atoms and Molecules." in: *Philosophical Magazine* 2.151 (1913) (see p. 5).

[12] Max Born and Robert Oppenheimer "Zur Quantentheorie der Molekeln" in: *Annalen der Physik* 84 (1927), pp. 457–484 DOI: 10.1002/andp.19273892002 (see p. 9).

[13] P. W. Brouwer "Scattering approach to parametric pumping" in: *Physical Review B* 58.16 (1998), pp. 10135–10138 DOI: 10.1103/PhysRevB.58.R10135 (see p. 86).

[14] Henrik Bruus and Karsten Flensberg *Many-Body Quantum Theory in Condensed Matter Physics* 1st ed. Oxford University Press, 2004 (see pp. 6, 9, 47, 50, 74, 75, 96).

[15] Robert J. Bursill, Christopher Castleton, and William Barford "Optimal parametrisation of the Pariser – Parr – Pople Model for benzene and biphenyl" in: *Chemical Physics Letters* 294.4-5 (1998), pp. 305–313 DOI: 10.1016/S0009-2614(98)00903-8 (see p. 13).

[16] M. Büttiker and R. Landauer "Traversal Time for Tunneling" in: *Physical Review Letters* 49.23 (1982), pp. 1739–1742 DOI: 10.1103/PhysRevLett.49.1739 (see p. 86).

[17] M. Büttiker and R. Landauer "Traversal time for tunneling" in: *Physica Scripta* 49.23 (1985), pp. 1739–1742 DOI: 10.1088/0031-8949/32/4/031 (see p. 86).

[18] M. Büttiker, A. Prêtre, and H. Thomas "Dynamic conductance and the scattering matrix of small conductors" in: *Physical Review Letters* 70.26 (1993), pp. 4114–4117 DOI: 10.1103/PhysRevLett.70.4114 (see p. 86).

[19] C. Caroli et al. "Direct calculation of the tunneling current" in: *J. Phys. C: Solid State Phys.* 4 (1971), p. 916 DOI: 10.1088/0022-3719/4/8/018 (see p. 62).

[20] R. Lloyd Carroll and Christopher B. Gorman "The Genesis of Molecular Electronics" in: *Angewandte Chemie (International ed. in English)* 41 (2002), pp. 4378–4400 DOI: 10.1002/1521-3773(20021202)41:23<4378::AID-ANIE4378>3.0.CO;2-A (see p. 1).

[21] Doron Cohen "Classical and quantum pumping in closed systems" in: *Solid State Communications* 133 (2006), pp. 583–588 (see p. 86).

[22] Doron Cohen "Quantum Pumping and dissipation: From closed to open systems" in: *Physical Review B* 68 (2003), 201303(R) DOI: 10.1103/PhysRevB.68.201303 (see p. 86).

[23] D. L. Cooper, J. Gerratt, and M. Raimondi "Modern valence bond theory" in: *Advances in Chemical Physics: Ab Initio Methods in Quantum Chemistry* 69 (1987), pp. 87–100 DOI: 10.1002/9780470142943.ch6 (see p. 22).

[24] (a) C. A. Coulson and G. S. Rushbrooke "Note on the method of molecular orbitals" in: *Mathematical Proceedings of the Cambridge Philosophical Society* 36.02 (Oct. 2008), p. 193 DOI: 10.1017/S0305004100017163; (b) A. D. McLachlan "The pairing of electronic states in alternant hydrocarbons" in: *Molecular Physics* 2 (1959), p. 271 DOI: 10.1080/00268975900100261; (c) A. D. McLachlan "Electrons and holes in alternant hydrocarbons" in: *Molecular Physics* 4 (1961), p. 49 DOI: 10.1080/00268976100100061 see p. 54.

[25] S. M. Cronenwett "A Tunable Kondo Effect in Quantum Dots" in: *Science* 281.5376 (July 1998), pp. 540–544 DOI: 10.1126/science.281.5376.540 (see p. 73).

[26] J. Cullum and R. Willoughby *Lanczos Algorithm for Large Symmetric Eigenvalue Computations, Vol. 1 Theory* Birkhauser, Boston, 1985 (see p. 16).

[27] Mousumi Das "Low-lying excitations of poly-fused thiophene within Pariser-Parr-Pople model: A density matrix renormalization group study." in: *The Journal of chemical physics* 132.19 (May 2010), p. 194107 DOI: 10.1063/1.3425882 (see p. 13).

[28] O. Donati "An Experiment on Electron Interference" in: *American Journal of Physics* 41.5 (1973), p. 639 DOI: 10.1119/1.1987321 (see p. 51).

[29] I. R. Ducasse, T. E. Miller, and Z. G. Soos "Correlated states in finite polyenes: Exact PPP results" in: *The Journal of Chemical Physics* 76.8 (1982), p. 4094 DOI: 10.1063/1.443484 (see pp. 13, 14).

[30] A. L. Fetter and J. D. Walecka *Quantum Theory of Many-particle Systems* Dover Books on Physics Dover Publications, 2003 (see p. 55).

[31] Inga Fischer-Hjalmars and M. Sundbom "Semi-empirical Parameters in pi-Electron Systems III. Heteroatomic Molecules Containing Nitrogen" in: *Acta chem. scand.* 22 (1968), pp. 607–627 DOI: 10.3891/acta.chem.scand.22-0607 (see p. 13).

[32] Qiang Fu, Jinlong Yang, and Xue-Bin Wang "On the electronic structures and electron affinities of the m-benzoquinone (BQ) diradical and the o-, p-BQ molecules: a synergetic photoelectron spectroscopic and theoretical study." in: *The journal of physical chemistry. A* 115.15 (Apr. 2011), pp. 3201–7 DOI: 10.1021/jp1120542 (see p. 13).

[33] L. J. Geerligs et al. "Frequency-locked turnstile device for single electrons" in: *Physical Review Letters* 64.22 (1990), pp. 2691–2694 DOI: 10.1103/PhysRevLett.64.2691 (see p. 86).

[34] D. Goldhaber-Gordon et al. "From the Kondo Regime to the Mixed-Valence Regime in a Single-Electron Transistor" in: *Phys. Rev. Lett.* 81.23 (Dec. 1998), pp. 5225–5228 DOI: 10.1103/PhysRevLett.81.5225 (see pp. 73, 79).

[35] D. Goldhaber-Gordon et al. "The Kondo effect in a single-electron transistor" in: *Materials Science and Engineering B* 84.1-2 (2001), pp. 17–21 DOI: 10.1038/34373 (see p. 73).

[36] Gene H. Golub and Charles F. van Loan *Matrix Computations* 3rd ed. Baltimore and London: The Johns Hopkins University Press, 1996 (see p. 16).

[37] Constant M. Guédon et al. "Observation of quantum interference in molecular charge transport." in: *Nature Nanotechnology* 7.5 (May 2012), pp. 305–9 DOI: 10.1038/nnano.2012.37 (see p. 52).

[38] R. Hanson et al. "Spins in few-electron quantum dots" in: *Reviews of Modern Physics* 79.4 (2007), p. 1217 DOI: 10.1103/RevModPhys.79.1217 (see pp. 1, 43).

[39] Roger Haydock and Ronald L. Te "Accuracy of the recursion method" in: *Physical Review B* 49.16 (1994), p. 10845 DOI: 10.1103/PhysRevB.49.10845 (see p. 17).

[40] Hubert B. Heersche et al. "In situ imaging of electromigration-induced nanogap formation by transmission electron microscopy" in: *Applied Physics Letters* 91.7 (2007), p. 072107 DOI: 10.1063/1.2767149 (see pp. 1, 43).

[41] Werner Heisenberg "Zur Theorie des Ferromagnetismus." in: *Zeitschrift für Physik* 4 (1928), pp. 619–636 DOI: 10.1007/BF01328601 (see p. 22).

[42] Walter Heitler and Fritz London "Wechselwirkung neutraler Atome und homöopolare Bindung nach der Quantenmechanik" in: *Zeitschrift für Physik* 472.1927 (1927), pp. 1–19 DOI: 10.1007/BF01397394 (see pp. 7, 21).

[43] Alex C. Hewson *The Kondo Problem to Heavy Fermions* Cambridge Studies in Magnetism Cambridge University Press, 1997 (see p. 73).

[44] Ivan Hubac and Stephen Wilson *Brillouin-Wigner Methods for Many-Body Systems* 1st ed. Springer-Verlag New York, Inc., 2010 DOI: 10.1007/978-90-481-3373-4 (see p. 25).

[45] (a) Erich Hückel "Quantentheoretische Beiträge zum Benzolproblem" in: *Zeits. f. Physik* 70.3-4 (1931), p. 204 DOI: 10.1007/BF01339530; (b) Erich Hückel "Quanstentheoretische Beiträge zum Benzolproblem" in: *Zeits. f. Physik* 72.5-6 (1931), p. 310 DOI: 10.1007/BF01341953; (c) Erich Hückel "Quantentheoretische Beiträge zum Problem der aromatischen und ungesättigten Verbindungen. III" in: *Zeits. f. Physik* 76.9-10 (1932), p. 628 DOI: 10.1007/BF01341936 see p. 21.

[46] H. Jensen and P. N. Skancke "Semi-empirical Parameters in pi-Electron Systems V. The Carbonyl Group" in: *Acta chem. scand.* 22 (1968), pp. 2899–2909 DOI: 10.3891/acta.chem.scand.22-2899 (see p. 13).

[47] C. Joachim, J. K. Gimzewski, and A. Aviram "Electronics using hybrid-molecular and mono-molecular devices." in: *Nature* 408.6812 (Nov. 2000), pp. 541–8 DOI: 10.1038/35046000 (see pp. 1, 43).

[48] Thomas Juffmann et al. "Real-time single-molecule imaging of quantum interference." in: *Nature nanotechnology* 7.5 (May 2012), pp. 297–300 DOI: 10.1038/nnano.2012.34 (see p. 51).

[49] O. Karlström et al. "Increasing thermoelectric performance using coherent transport" in: *Physical Review B* 84.11 (Sept. 2011), p. 113415 DOI: 10.1103/PhysRevB.84.113415 (see pp. 1, 51).

[50] S. H. Ke, W. Yang, and H. U. Baranger "Quantum-Interference-Controlled Molecular Electronics" in: *Nano letters* 8 (2008), pp. 3257–3261 DOI: 10.1021/nl8016175 (see pp. 51, 57, 61).

[51] Douglas J. Klein and Nenad Trinasjstic "Valence-Bond Theory and Chemical Structure" in: *Journal of Chemical Education* 67.8 (1990), pp. 633–637 DOI: 10.1021/ed067p633 (see p. 21).

[52] S. Kohler, J. Lehmann, and P. Hänggi "Driven quantum transport on the nanoscale" in: *Physics Reports* 406.6 (Feb. 2005), pp. 379–443 DOI: 10.1016/j.physrep.2004.11.002 (see pp. 91, 92).

[53] Leo P. Kouwenhoven et al. "Electron transport in quantum dots." in: *Proceedings of the Advanced Study Institute on Mesoscopic Electron Transport* Kluwer 1997 (see p. 44).

[54] Andrey V. Kretinin, Hadas Shtrikman, and Diana Mahalu "Universal line shape of the Kondo zero-bias anomaly in a quantum dot" in: *Physical Review B* 85.20 (May 2012), p. 201301 DOI: 10.1103/PhysRevB.85.201301 (see p. 79).

[55] C. Lanczos "An iteration method for the solution of the eigenvalue problem of linear differential and integral operators" in: *Journal of Research of the National Bureau of Standards* 45.4 (Oct. 1950), p. 255 DOI: 10.6028/jres.045.026 (see p. 15).

[56] Rolf Landauer "Spatial Variation of Currents and Fields Due to Localized Scatterers in Metallic Conduction" in: *IBM Journal of Research and Development* 1.3 (1957), pp. 223–231 DOI: 10.1147/rd.13.0223 (see p. 62).

[57] M Leijnse et al. "Interaction-induced negative differential resistance in asymmetric molecular junctions" in: *The Journal of Chemical Physics* 134.10 (2011), pages DOI: http://dx.doi.org/10.1063/1.3560474 (see p. 50).

[58] Gilbert N. Lewis "The atom and the molecule." in: *Journal of the American Chemical Society* 1448.1913 (1916), pp. 762–785 DOI: 10.1021/ja02261a002 (see p. 7).

[59] Elliott H. Lieb "Two Theorems of the Hubbard model" in: *Physical Review Letters* 62.10 (1989) DOI: 10.1103/PhysRevLett.62.1201 (see p. 27).

[60] Elliott H. Lieb and Daniel Mattis "Ordering Energy Levels of Interacting Spin Systems" in: *Journal of Mathematical Physics* 3.4 (1962), p. 749 DOI: 10.1063/1.1724276 (see p. 27).

[61] H. Q. Lin and J. E. Gubernatis "Exact diagonalization methods for quantum systems" in: *Computers in Physics* 7.4 (1993), p. 400 (see p. 14).

[62] Daniel A. Lovey and Rodolfo H. Romero "Quantum interference through gated single-molecule junctions" in: *Chemical Physics Letters* 530 (Mar. 2012), pp. 86–92 DOI: 10.1016/j.cplett.2012.01.068 (see pp. 51, 53).

[63] Valerio Magnasco *Molecular Quantum Mechanics* First edit John Wiley & Sons, 2009 (see pp. 7, 21).

[64] Troels Markussen, Robert Stadler, and Kristian S Thygesen "The relation between structure and quantum interference in single molecule junctions." in: *Nano letters* 10.10 (Oct. 2010), pp. 4260–5 DOI: 10.1021/nl101688a (see pp. 52, 62).

[65] Christian A. Martin, Roel H. M. Smit, and Herre S. J. van der Zant "A Nanoelectromechanical Single-Atom Switch" in: *Nano letters* 9.8 (2009), pp. 2940–2945 DOI: 10.1021/nl901355y (see pp. 1, 43).

[66] Christian A. Martin et al. "Lithographic mechanical break junctions for single-molecule measurements in vacuum: possibilities and limitations" in: *New Journal of Physics* 10.6 (June 2008), p. 065008 DOI: 10.1088/1367-2630/10/6/065008 (see pp. 1, 43).

[67] Noboru Mataga and Kitisuke Nishimoto "Electronic Structure and Spectra of Nitrogen Heterocycles" in: *Zeitschrift für Physikalische Chemie* (1957), pp. 140–157 DOI: 10.1524/zpch.1957.13.3_4.140 (see p. 12).

[68] D. Natelson et al. "Anomalous gate dependence of the Kondo effect in single-molecule transistors" in: *Physica B: Condensed Matter* 403.5-9 (Apr. 2008), pp. 1526–1528 DOI: 10.1016/j.physb.2007.10.179 (see p. 73).

[69] P. Nozieres "A "Fermi-liquid" description of the Kondo problem at low temperatures" in: *Journal of Low Temperature Physics* 17.1 (1974), pp. 31–42 DOI: 10.1007/BF00654541 (see p. 77).

[70] P. Nozieres "Kondo effect for spin 1/2 impurity a minimal effector scaling approach" in: *Le Journal de Physique* 39 (1978), 1117ff DOI: 10.1051/jphys:0197800390100111700 (see p. 79).

[71] Takahide Numata et al. "Kondo effects in a triangular triple quantum dot: Numerical renormalization group study in the whole region of the electron filling" in: *Physical Review B* 80.15 (Oct. 2009), p. 155330 DOI: 10.1103/PhysRevB.80.155330 (see p. 81).

[72]   J. Nygård, D. H. Cobden, and P. E. Lindelof "Kondo physics in carbon nanotubes"
       in: *Nature* 408.6810 (2000), pp. 342–346 DOI: 10.1038/35042545 (see p. 73).

[73]   K. Ohno "Some remarks on the Pariser-Parr-Pople method" in: *Theoretica Chimica
       Acta* 227 (1964), pp. 219–227 DOI: 10.1007/BF00528281 (see p. 12).

[74]   (a) Edgar A. Osorio et al. "Electronic excitations of a single molecule contacted
       in a three-terminal configuration." in: *Nano letters* 7.11 (Nov. 2007), pp. 3336–42
       DOI: 10.1021/nl0715802; (b) E a Osorio et al. "Single-molecule transport in three-
       terminal devices." in: *Journal of physics. Condensed matter : an Institute of Physics
       journal* 20.37 (Sept. 2008), p. 374121 DOI: 10.1088/0953-8984/20/37/374121
       see pp. 46, 73.

[75]   C. C. Paige "Accuracy and effectiveness of the Lanczos algorithm for the symmetric
       eigenproblem" in: *Linear algebra and its applications* 34 (1980), pp. 235–258 DOI:
       10.1016/0024-3795(80)90167-6 (see p. 16).

[76]   Rudolph Pariser and Robert G. Parr "A Semi-Empirical Theory of the Electronic
       Spectra and Electronic Structure of Complex Unsaturated Molecules. II" in: *The
       Journal of Chemical Physics* 21.5 (1953), p. 767 DOI: 10.1063/1.1699030 (see
       pp. 1, 11).

[77]   Wolfgang Pauli "Über den Zusammenhang des Abschlusses der Elektronen- gruppen
       im Atom mit der Komplexstruktur der Spektren." in: *Zeitschrift für Physik* 31
       (1925), p. 725 DOI: 10.1007/BF02980631 (see p. 6).

[78]   Linus Pauling "The Calculation of Matrix Elements for Lewis Electronic Structures
       of Molecules" in: *The Journal of Chemical Physics* 1.4 (1933), p. 280 DOI: 10.
       1063/1.1749284 (see p. 21).

[79]   Linus Pauling "The nature of the chemical bond. Application og results obtained
       from the quantum mechanics and from a theory of paramagnetic susceptibility to
       the structure of molecules" in: *J. Am. Chem. Soc.* 53 (1931), pp. 1367–1400 DOI:
       10.1021/ja01355a027 (see pp. 8, 9).

[80]   Linus Pauling and G. W. Wheland "The Nature of the Chemical Bond. V. The
       Quantum-Mechanical Calculation of the Resonance Energy of Benzene and Naph-
       thalene and the Hydrocarbon Free Radicals" in: *The Journal of Chemical Physics*
       1.6 (1933), p. 362 DOI: 10.1063/1.1749304 (see pp. 21, 35, 36).

[81]   Kim Georg Lind Pedersen *Poor Man's Scaling for the Nonequilibrium Kondo Problem
       and Antiferromagnetic Correlations in Optical Lattice* tech. rep. University of
       Copenhagen, 2009 (see p. 76).

[82]   (a) R. E. Peierls *Quantum Theory of Solids* Clarendon, Oxford, 1955, p. 108;
       (b) Hans Fröhlich "On the Theory of Superconductivity: The One-Dimensional Case"
       in: *Proceedings of the Royal Society A: Mathematical, Physical and Engineering
       Sciences* 223 (1954), p. 296 DOI: 10.1098/rspa.1954.0116; (c) Tom Kennedy and
       Elliott H. Lieb "Proof of the Peierls instability in one dimension." in: *Physical Review
       Letters* 59.12 (Sept. 1987), pp. 1309–1312 DOI: 10.1103/PhysRevLett.59.1309
       see p. 13.

[83]   John. A. Pople "Electron interaction in unsaturated hydrocarbons" in: *Transactions
       of the Faraday Society* 49 (1953), p. 1375 DOI: 10.1039/tf9534901375 (see pp. 1,
       11).

[84] H. Pothier et al. "Single-electron pump based on charging effects" in: *EPL (Europhysics Letters)* 17 (1992), p. 249 DOI: 10.1209/0295-5075/17/3/011 (see p. 86).

[85] Ferry Prins et al. "Room-temperature gating of molecular junctions using few-layer graphene nanogap electrodes." in: *Nano letters* 11.11 (Nov. 2011), pp. 4607–11 DOI: 10.1021/nl202065x (see pp. 1, 43).

[86] M. Pustilnik "Kondo effect in nanostructures" in: *Physica Status Solidi (a)* 203.6 (May 2006), pp. 1137–1147 DOI: 10.1002/pssa.200566191 (see p. 73).

[87] Vincent Rabache et al. "Direct observation of large quantum interference effect in anthraquinone solid-state junctions." in: *Journal of the American Chemical Society* 135.28 (July 2013), pp. 10218–21 DOI: 10.1021/ja403577u (see p. 52).

[88] A. Rosch et al. "Nonequilibrium Transport through a Kondo Dot in a Magnetic Field: Perturbation Theory and Poor Man's Scaling" in: *Physical Review Letters* 90.7 (Feb. 2003), p. 76804 DOI: 10.1103/PhysRevLett.90.076804 (see p. 76).

[89] A. Rosch et al. "The Kondo effect in Non-Equilibrium Quantum Dots: Perturbative Renormalization Group" in: *J. Phys. Soc. Japan* 74 (2005), pp. 118–126 DOI: DOI:10.1143/JPSJ.74.118 (see pp. 76, 78).

[90] G. Rumer, E. Teller, and H. Weyl "Eine fur die Valenztheorie geeignete Basis der binaren Vektorinvarianten" in: *Nachr. Ges. Wiss. Göttingen Math. Phys. Kl.* (1932), pp. 499–504 (see pp. 34, 103).

[91] P. Sautet and C. Joachim "Electronic interference produced by a benzene embedded in a polyacetylene chain" in: *Chemical Physics Letters* 153.6 (Dec. 1988), pp. 511–516 DOI: 10.1016/0009-2614(88)85252-7 (see p. 58).

[92] J. R. Schrieffer and P. A. Wolff "Relation between the anderson and kondo hamiltonians" in: *Physical Review* 149.2 (1966), pp. 491–492 DOI: 10.1103/PhysRev.149.491 (see p. 74).

[93] Erwin Schrödinger "Quantisierung als Eigenwertproblem von E. Schrödinger" in: *Annalen der Physik* (1926), pp. 361–377 (see p. 5).

[94] M. Schüler et al. "Optimal Hubbard Models for Materials with Nonlocal Coulomb Interactions: Graphene, Silicene, and Benzene" in: *Physical Review Letters* 111.3 (July 2013), p. 036601 DOI: 10.1103/PhysRevLett.111.036601 arXiv: arXiv:1302.1437v1 (see p. 18).

[95] G. Scott et al. "Universal scaling of nonequilibrium transport in the Kondo regime of single molecule devices" in: *Physical Review B* 79.16 (Apr. 2009), p. 165413 DOI: 10.1103/PhysRevB.79.165413 (see p. 73).

[96] Johannes S. Seldenthuis et al. "An all-electric single-molecule motor." in: *ACS nano* 4.11 (Nov. 2010), pp. 6681–6 DOI: 10.1021/nn1021499 (see pp. 3, 85).

[97] Sason S. Shaik and Phillipe C. Hiberty *A Chemist's Guide to Valence Bond Theory* New Jersey: Wiley-Interscience, 2008 (see p. 21).

[98] T. Siro and A. Harju "Exact diagonalization of the Hubbard model on graphics processing units" in: *Computer Physics Communications* 183.9 (Sept. 2012), pp. 1884–1889 DOI: 10.1016/j.cpc.2012.04.006 (see p. 15).

[99] A. Skancke and P. N. Skancke "Semi-empirical Parameters in pi-Electron Systems VIII. Sulphur-containing Heteroaromatic Systems" in: *Acta chem. scand.* 24 (1970), pp. 23–32 DOI: `10.3891/acta.chem.scand.24-0023` (see p. 13).

[100] J. C. Slater "Directed valence in polyatomic molecules" in: *Physical Review* 729.1930 (1931) DOI: `10.1103/PhysRev.37.481` (see p. 21).

[101] J. C. Slater "The Theory of Complex Spectra" in: *Physical Review* 3 (1929) DOI: `10.1103/PhysRev.34.1293` (see p. 6).

[102] David W. Small and Martin Head-Gordon "Post-modern valence bond theory for strongly correlated electron spins." in: *Physical chemistry chemical physics : PCCP* 13.43 (Nov. 2011), pp. 19285–97 DOI: `10.1039/c1cp21832h` (see p. 22).

[103] Gemma C. Solomon et al. "Quantum interference in acyclic systems: conductance of cross-conjugated molecules." in: *Journal of the American Chemical Society* 130.51 (Dec. 2008), pp. 17301–8 DOI: `10.1021/ja8044053` (see pp. 51, 63).

[104] Gemma C. Solomon et al. "When "small" terms matter: Coupled interference features in the transport properties of cross-conjugated molecules." in: *Beilstein Journal of Nanotechnology* 2 (Jan. 2011), pp. 862–71 DOI: `10.3762/bjnano.2.95` (see p. 51).

[105] Z. G. Soos and S. Ramasesha "Valence-bond theory of linear Hubbard and Pariser-Parr-Pople models" in: *Physical Review B* 29.10 (1984) DOI: `10.1103/PhysRevB.29.5410` (see pp. 29, 103, 104).

[106] Jozef Spalek "t-J model then and now: A personal perspective from the pioneering times" in: *Arxiv* cond-mat.s (June 2007) arXiv: `0706.4236v1` (see p. 21).

[107] Robert Stadler and Troels Markussen "Controlling the transmission line shape of molecular t-stubs and potential thermoelectric applications." in: *The Journal of chemical physics* 135.15 (Oct. 2011), p. 154109 DOI: `10.1063/1.3653790` (see p. 51).

[108] Charles A. Stafford, David M. Cardamone, and Sumit Mazumdar "The quantum interference effect transistor." in: *Nanotechnology* 18.42 (Oct. 2007), p. 424014 DOI: `10.1088/0957-4484/18/42/424014` (see pp. 1, 51).

[109] M. Switkes et al. "An adiabatic quantum electron pump" in: *Science* 283.5409 (1999), p. 1905 DOI: `10.1126/science.283.5409.1905` (see p. 86).

[110] Tomofumi Tada and Kazunari Yoshizawa "Quantum transport effects in nanosized graphite sheets." in: *Chemphyschem : a European journal of chemical physics and physical chemistry* 3.12 (Dec. 2002), pp. 1035–7 DOI: `10.1002/cphc.200290006` (see p. 53).

[111] Tomofumi Tada and Kazunari Yoshizawa "Quantum Transport Effects in Nanosized Graphite Sheets. II. Enhanced Transport Effects by Heteroatoms" in: *The Journal of Physical Chemistry B* 107.34 (Aug. 2003), pp. 8789–8793 DOI: `10.1021/jp021739t` (see p. 53).

[112] Tomofumi Tada et al. "Oscillation of conductance in molecular junctions of carbon ladder compounds." in: *Journal of the American Chemical Society* 126.43 (Nov. 2004), pp. 14182–9 DOI: `10.1021/ja031736+` (see p. 53).

[113] D. J. Thouless "Quantization of particle transport" in: *Physical Review B* 27.10 (1983), p. 6083 DOI: `10.1103/PhysRevB.27.6083` (see p. 85).

[114] Piotr Trocha and Józef Barnaś "Large enhancement of thermoelectric effects in a double quantum dot system due to interference and Coulomb correlation phenomena" in: *Physical Review B* 85.8 (Feb. 2012), p. 085408 DOI: 10.1103/PhysRevB.85.085408 (see p. 51).

[115] M. G. Vavilov, L. Dicarlo, and C. M. Marcus "Photovoltaic and rectification currents in quantum dots" in: *Physical Review B* 71.24 (June 2004), p. 241309 DOI: 10.1103/PhysRevB.71.241309 (see p. 86).

[116] M. Wagner "Probing Pauli blocking factors in quantum pumps with broken time-reversal symmetry" in: *Physical Review Letters* 85.1 (2000), pp. 174–177 DOI: 10.1103/PhysRevLett.85.174 (see p. 91).

[117] K. G. Wilson "The renormalization group: Critical phenomena and the Kondo problem" in: *Reviews of Modern Physics* 47.4 (1975), pp. 773–840 DOI: 10.1103/RevModPhys.47.773 (see pp. 77, 80).

[118] S. Yoo, B. Domercq, and B. Kippelen "Efficient thin-film organic solar cells based on pentacene/C[sub 60] heterojunctions" in: *Applied Physics Letters* 85.22 (2004), p. 5427 DOI: 10.1063/1.1829777 (see p. 1).

[119] Kazunari Yoshizawa, Tomofumi Tada, and Aleksandar Staykov "Orbital views of the electron transport in molecular devices." in: *Journal of the American Chemical Society* 130.29 (July 2008), pp. 9406–13 DOI: 10.1021/ja800638t (see p. 51).

[120] Herre S. J. van der Zant et al. "Molecular three-terminal devices: fabrication and measurements" in: *Faraday Discussions* 131 (2006), p. 347 DOI: 10.1039/b506240n (see pp. 1, 43).